Foreword

This thesis has been prepared in fulfilment of the requirements for a Ph.D. at the University of Sultan MoulaySlimane, BeniMellal, Morocco, under the direction of Professor Dr.Khalil El-Hami.

Dedication

To my parents

To all my family

To all those who are dear to me

Acknowledgements

First of all, I would like to thank my university supervisor, Prof. Dr. Khalil El-Hami, for support at every point along the way, including reading over all my work and providing valuable insight and feedback (a big task), who without him, this work could not have been completed. Thank you for sharing your knowledge, and for always remaining positive and showing interest in my work.
During these three years, he was able to provide me with his knowledge, his kindness, his humor, his extreme patience, his great availability and especially his flawless supervision from the beginning to the end of this thesis.
I would like to thank all the members of the jury for letting me benefit from their expertise by agreeing to judge this work and devote time to review this manuscript.
A huge thank you to my friends at the Laboratory who believe in me and help me move forward and be who I am. For this and for all the moments shared, I wish to express my affection deeper at: A. Elmoutarajji, Z. Kbiri, M. Eddya and B. Tbib.
I thank my wife F.Abouharim, for the patience and the support, which she showed during all the duration of this thesis, all my family especially my parents.I would like to comply with the traditional thanks, hoping not to forget anyone. Knowing the lost thing in advance, I will therefore begin by apologizing to those whom I accidentally forgot to mention here, and if their direct or indirect contribution is not in this page, let them know that I will not miss to remember it.

General Introduction

Nanoparticles today represent a major technological and economic issue. They allow very promising innovations in many fundamental areas such asthat: health, energy or industry.

In this work we are interested in the potential contribution of MWCNT in the field of thermal and electrical transfers. More systematic use of inexhaustible sources energy (solar, wind, geothermal, etc.) is not enough to meet the energy challenge of future generations. All solutions must be explored and the path to savingsynergy is an important contribution to develop.Thermal transfers, very common in the industrial and technological world (engine coolant, lubricating oils, heat transfer fluids from solar panels and heat exchangers. . .) often use liquids with very low heat conductivity. The CNTs, on the other hand, have the highest thermal conductivities available but do not allow easy thermal contacts. The surface condition of nanoparticles within the host fluid is another important parameter to consider in order identifying the real influence of nanoparticles on the physical properties of the nanofluid.

So we chose the MWCNT / Glycerol system which requires no chemical surface treatment and allows homogeneous and stable suspensions to be produced without the use of disruptive chemical additives. It is therefore to be hoped that MWCNTs will give Glycerol a fraction of its important thermal and electrical conductivity.

From a thermal point of view, single-walled or multi-walled CNTs suspended in a base liquid, are likely to bring very significant gains in thermal performance thanks to their very high thermal conductivity. Several experimental studies have confirmed that the improvement of the thermal conductivity of nanofluids based on carbon nanotubes, under certain conditions, is much higher compared to nanofluids based on metallic nanoparticles or oxides [1.2.3]. This is explained on the one hand by the nature of carbon, but also by the shape of the nanoparticles, which put in suspensions behave like thermal nano-bridges likely to lead energy quickly from one point to another (Figure 1) via the network made up of nanotubes, this network being linked to the nanotube concentration and the number of nano-bridges.

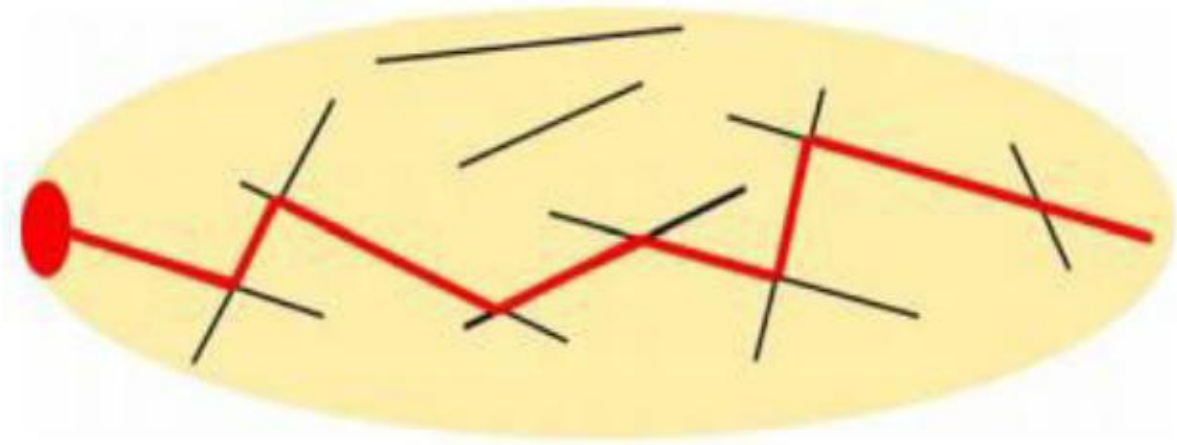

Figure 1: Diagram of the creation of a network of thermal bridges (red line) created by a dispersion of nanofibers (black line) in a fluid (Beige) which allows the propagation of a hot spot (red oval) [4]

The behavior of CNTs in dispersion is governed by two types of interaction: electrostatic interactions (attractants or repellents) between the particles themselves, and hydrodynamic interactions between the particles and the base liquid. Some interactions are opposed while others accumulate. In addition, the CNTs are distinguished by their high aspect ratio and their specific surface, which results in strong attractive forces of the Van Der Walls type [5] which can cause the regrouping and the arrangement of particles in aggregates. The main difficulty with this type then nanofluid is dispersed homogeneously in time the NTC.

The suspension of CNTs is generally accompanied by mechanical processes which consist in applying a strong mechanical action using a rotary or ultrasonic agitator, making it possible to break up the agglomerates and ensure the dispersion of the particles in the solution. Thus, it is important to master these mechanical actions in order to ensure good dispersion of the CNTs without reducing and / or modifying their structures and therefore their thermal properties.In this context, the work of this PhD thesis, carried out at the Sultan MoulaySlimane University, Laboratory of Nanosciences and Modelling Polydisciplinary Faculty of Khouribgha FPK under the supervision of Professor Dr. Khalil EL-HAMI where the objective was to propose an innovative nanofluid MWCNT/Glycerol potentially interesting in terms of improving thermal and electrical conductivity and also anticorrosive for industrial applications.The study of the thermal properties of nanofluids raises the delicate problem of the influence of convection on the determination of the effective thermal conductivity of the liquid. In order to determine the real properties of the system, we have adapted the thermal characterization method 3ω frequently used with insulating solids to the case of liquids. This method has the

advantage of allowing thermal excitations sufficiently weak tomake the influence of convection almost negligible. The detailed description of this method and the evaluation of its main limitations are the subject of the chapter 2, in this chapter that illustratesthe results of the numerical study which consists in determining the thermal conductivity of our base fluid by the hot wire method and comparing it with those obtained experimentally by the 3ω method, electrical conductivity and thermal conductivity of MWCNT/Glycerol nanofluids were measured at different volumes fractions ($0.0025\% \leq \Phi \leq 0.01\%$) and temperatures ($20°C \leq \Theta \leq 40$ °C),the results obtained are compared and discussed in relation to existing classical modelsafter beginning with a bibliographic study on the Glycerol andCNT which is the subject of thechapter 1.This research mainly concerns the study of the real effects of concentration of MWCNT nanoparticles on the thermal, electrical and rheological properties of Glycerol-based nanofluids. The study of the rheological properties and density of nanofluids is the subject of the chapter 3, in this part a new correlation was proposed to represent the experimental data for the dynamic viscosity of MWCNT/Glycerol nanofluids.In the fourth chapter, we present the novel nano-system of Glycerol/$Er_2P_4O_{13}$/MWCNT that is was studied for the application in energy storage, extensive experimental of electrical conductivity and resistivity of Glycerol containing Erbium and MWCNT particles with various concentrations in the dilute regime was evaluated. The electrical conductivity and resistivity of MWCNT/$Er_2P_4O_{13}$/ Glycerol as a function of temperature have being studied, the surface of samples were been observed by scanning electron microscope (SEM) and the characterization by FT-IR were performed to determine the band of absorption, Glycerol shows excellent anti-corrosive properties. Finally, the objective of the last chapter is to obtain a semiconductor material based on Glycerol nanofluid prepared by various volumetric fraction Φ=0.004%, 0.005% and 0.01% of MWCNT. The materials have been characterized by UV-visible spectroscopy carried in the range 200- 1000 cm^{-1}. We report the results of FTIR in the range 400–4000 cm^{-1} to study the attachment of carbon nanotubes on Glycerol and to confirm the presence of carbon nanotubes inside of Glycerol. The experimental results show clearly that the gap energy ≤ 3.5 eV. The electrical conductivity and resistivity of MWCNT/Glycerol as a function of temperature have being studied.

Résumé de la thèse de doctorat

Les nanoparticules représentent aujourd'hui un enjeu technologique et économique majeur. Ils permettent des innovations très prometteuses dans de nombreux domaines fondamentaux tels que : la santé, l'énergie ou l'industrie.

Dans ce travail, nous nous intéressons à la contribution potentielle des MWCNT dans le domaine des transferts thermiques et électriques. Une exploitation plus systématique des sources d'énergie inépuisables (solaire, éolienne, géothermique, etc.) ne suffit pas pour relever le défi énergétique des générations futures. Toutes les solutions doivent être explorées et la voie des économies d'énergie est une contribution importante à développer. Les transferts thermiques, très courants dans le monde industriel et technologique (liquide de refroidissement moteur, huiles lubrifiantes, fluides caloporteurs des panneaux solaires et des échangeurs de chaleur, ...) utilisent souvent des liquides très peu conducteurs de la chaleur, par contre, les NTC présentent les plus grandes conductivités thermiques mais ne permettent pas des contacts thermiques aisés. L'état de surface des nanoparticules au sein du fluide hôte est un autre paramètre important à prendre en compte afin d'identifier l'influence réelle des nanoparticules sur les propriétés physiques du nanofluide.

Nous avons donc choisi le système MWCNT / Glycérol qui ne nécessite aucun traitement chimique de surface et permet de produire des suspensions homogènes et stables sans utilisation d'additifs chimiques perturbateurs. Il est donc à espérer que les MWCNT donneront au Glycérol une fraction de son importante conductivité thermique et électrique.

La suspension des NTC s'accompagne généralement de procédés mécaniques qui consistent à appliquer une forte action mécanique à l'aide d'un agitateur rotatif ou ultrasonique, permettant de briser les agglomérats et d'assurer la dispersion des particules dans la solution. Ainsi, il est important de maîtriser ces actions mécaniques afin d'assurer une bonne dispersion des NTC sans réduire et / ou modifier leurs structures et donc leurs propriétés thermiques. Dans ce contexte, les travaux de cette thèse de doctorat, réalisés à l'Université Sultan Moulay Slimane, Laboratoire de Nanosciences et Modélisation Faculté Polydisciplinaire de Khouribgha FPK sous la direction du Professeur Dr Khalil EL-HAMI où l'objectif de l'étude était de proposer un nanofluide innovant MWCNT/Glycérol potentiellement intéressant en termes d'amélioration de la conductivité thermique et électrique et également anticorrosif pour les applications industrielles. L'étude des propriétés thermiques des nanofluides pose le problème délicat de l'influence de la convection sur la détermination de la conductivité thermique effective du liquide. Afin de déterminer les propriétés réelles du système, nous avons adapté

la méthode de caractérisation thermique 3ω fréquemment utilisée avec les solides isolants. Cette méthode présente l'intérêt de permettre des excitations thermiques suffisamment faibles pour rendre l'influence de la convection presque négligeable. La description détaillée de cette méthode et l'évaluation de ses principales limites font l'objet du chapitre 2. Dans ce chapitre qui illustre les résultats de l'étude numérique qui consiste à déterminer la conductivité thermique de notre fluide de base par la méthode du fil chaud et la comparer à celles obtenues expérimentalement par la méthode 3ω, la conductivité électrique et la conductivité thermique des nanofluides MWCNT / Glycérol ont été mesurés à différentes fractions de volumes (0,0025% ≤Φ ≤ 0,01%) et températures (20 ° C ≤Θ ≤ 40 ° C), les résultats obtenus sont comparés et discutés face à des modèles classiques existants après avoir débuté par une étude bibliographique sur le Glycérol et le MWCNT qui fait l'objet du chapitre 1. Ce travail de recherche concerne principalement l'étude des effets réels de concentration de nanoparticules de MWCNT sur les propriétés thermiques, électriques et rhéologiques des nanofluides à base de glycérol. L'étude des propriétés rhéologiques des nanofluides fait l'objet du chapitre 3,dans cette partie un nouveau modèlea été proposé pour représenter les données expérimentales de la viscosité dynamique des nanofluides MWCNT / Glycérol. Dans le quatrième chapitre, nous présentons le nouveau nano-système de Glycerol / $Er_2P_4O_{13}$ / MWCNT qui a été étudié pour l'application au stockage d'énergie. Une expérience approfondie de la conductivité électrique et de la résistivité du Glycérol contenant des particules d'erbium et de MWCNT avec diverses concentrations dans le régime dilué a été évaluée. La conductivité électrique et la résistivité du MWCNT / $Er_2P_4O_{13}$ / Glycérol en fonction de la température ont été étudiées. La surface des échantillons a été observée au microscope électronique à balayage (MEB) et la caractérisation par FT-IR a été réalisée pour déterminer la bande d'absorption. Le Glycérol présente d'excellentes propriétés anticorrosives.

Enfin, l'objectif du dernier chapitre est d'obtenir un matériau semi-conducteur à base de nanofluide de Glycérol préparé par différentes fractions volumétriques Φ = 0,004%, 0,005% et 0,01% de MWCNT. Les matériaux ont été caractérisés par spectroscopie UV-visible portée dans la gamme 200-1000 cm^{-1}. Nous rapportons les résultats du FTIR dans l'intervalle 400–4000 cm^{-1} pour étudier l'attachement de nanotubes de carbone sur le Glycérol et pour confirmer la présence de nanotubes de carbone à l'intérieur du Glycérol. Les résultats expérimentaux montrent clairement que l'énergie de gap ≤ 3,5 eV. La conductivité électrique et la résistivité du MWCNT / Glycérol en fonction de la température ont été étudiées.

Table of contents

List of figures

List of tables

CHAPTER I:

Review on Glycerol and Carbon Nanotubes

INTRODUCTION

The basic heat transfer fluids often used in cooling or heating applications have very low thermal conductivities which sometimes limit their heat transfer capacity. The use of nanofluids, particles of nanometric size with very high thermal conductivity suspended in a heat transfer fluid, is likely to bring very significant gains in thermal performance. Of a lot of research has been carried out on this new generation of fluids in order to provide a better understanding of the physical mechanisms involved in the use of nanofluids, and thus to develop more efficient heat transfer liquids.

This chapter is divided into two main parts. The first part presents a study description of Glycerol considered as basic fluid.

The second part focuses on the analysis of the thermophysical properties of carbon nanotubes and their methods of synthesis. Glycerol (1,2,3-propanetriol or glycerin), an organic molecule isolated by heating fats in the presence of ash (to produce soap) as early as 2800 BC[1], is an industrial chemical with tens of applications (Figure 1). Since the late 1940s, and following the discovery of synthetic surfactants, Glycerol has been produced from epichlorohydrin obtained from propylene (and thus from fossil oil) as large chemical companies forecasted a glycerol shortage and initiated its synthetic production [2]. Today, however, glycerol plants are closing and others are opening that use glycerol as a raw material (including for the production of epichlorohydrin itself)[3] as a result of the large surplus of Glycerol that is formed as a byproduct (10% in weight) in manufacturing biodiesel fuel by transesterification of seed oils with methanol. To illustrate the trend, the global glycerol market was 800 000 tons in 2005 with 400 000 tons from biodiesel in comparison to 60 000 tons only in 2001[4]. Over the last decade, biodiesel has emerged as a viable fuel and as a fossil diesel additive to replace sulfur, whose content is being progressively lowered according to tighter environmental legislation. Until the recent increases in petroleum prices, high production costs made biofuels unprofitable without government subsidies. However, the increasing production of biodiesel is not artificially sustained and is predicted to spread and increase, as biodiesel provides sufficient advantages to merit subsidy. [5] Besides the closure of production plants, industry reacted to this situation by starting research to find new applications of glycerol as a low-cost feedstock for functional derivatives either for mass consumption, such as additives for concrete [6], or as a precursor of valued fine chemicals.

Petroleum has been the major resource for the production of fuels and chemicals for decades. Since the energy crisis in the 1970s and the environmental problems linked to global warming, the mentalities and the policies engaged have changed the situation. All of these

facts lead to the search for alternative and renewable resources in the short term. In this context, the transformation of biomass is part of the solutions allowing to at least partially solving these problems.

I. 1 Overview of Glycerol

I. 1. 1 Properties of Glycerol

Glycerol (1, 2, 3-propanetriol, Figure 1.1) is a colorless, odorless, viscous liquid with a sweet taste, derived from both natural and petrochemical feedstocks. The name glycerol is derived from the Greek word for ‘‘sweet,’’ glykys, and the terms glycerin, glycerine, and glycerol tend to be used interchangeably in the literature. On the other hand, the expressions glycerin or glycerine generally refers to a commercial solution of glycerol in water of which the principal component is glycerol. Crude glycerol is 70–80% pure and is often concentrated and purified prior to commercial sale to 95.5–99% purity.

Figure 1.1: (a) Structure of Glycerol, (b) Representation" ball and stick"

Glycerol is one of the most versatile and valuable chemical substances known to man. In the modern era, it was identified in 1779, by Swedish chemist Carl W Scheele, who discovered a new transparent, syrupy liquid by heating olive oil with litharge (PbO, used in lead glazes on ceramics). It is completely soluble in water and alcohols, is slightly soluble in many common solvents such as ether and dioxane, but is insoluble in hydrocarbons. In its pure anhydrous condition, glycerol has a specific gravity of 1.261 g/mL, a melting point of 18.2 °C and a boiling point of 290 °C under normal atmospheric pressure, accompanied by decomposition. At low temperatures, glycerol may form crystals which melt at 17.9 °C. Overall, it possesses a unique combination of physical and chemical properties (table 1.1), which are utilized in many thousands of commercial products [8].Indeed, glycerol has over 1500 known end uses, including applications as an ingredient or processing aid in cosmetics,

Table 1.1: Physicochemical properties of Glycerol at 20°C.

Chemical formula	C3H5(OH)3
Molecular mass	92.09382 g/mol
Density	1.261 g/mL
Viscosity	1.49 Pa.s
Melting point	18.2 °C
Boiling point	290 °C
Thermal conductivity	0.285 W/m.k

The development of the bio-diesel market (which generates abundant quantities of glycerol), the new environmental concerns of consumers and the rarefaction in the long term oil have boosted the last ten years research on this material first vegetable.

Glycerol is widely used in many industries with classic applications in the sectors food, cosmetics or even pharmaceutical. It also constitutes an important platform molecule of the oleaginous biorefinery which offers large number of potential derivatives in the vegetable chemistry sector.

I. 1. 2 Glycerol applications

The more or less purified Glycerol is used in a large number of industrial sectors. It is commonly used in food, cosmetic and even pharmaceutical applications. It is used in particular for its emollient properties and as a wetting agent.

In cosmetics, glycerol is often used as a hydrating agent, solvent and lubricant; glycerin is thus a humectants which protects the epidermis, softens the skin and makes it suppler and more extensible. It is used in the formulation of toothpastes, moisturizers and hair products.

In drugs, it acts as moisturizer that improves oiliness and lubrication of pharmaceutical preparations. It is used for example in the preparation of medicated syrups.

As a food ingredient, it is used for its sugar taste, to retain moisture and as a solvent.

Glycerol and its derivatives are also used in various industrial applications: plasticizer, formulation of lubricants, synthesis of resins and explosives (nitroglycerin), solvent for dyes and inks, formulation of antifreeze fluids, surfactants (derivatives of mono- and triglyceridesethoxylates or sulfates).

Traditional applications of glycerol, either directly as an additive or as a raw material, range from its use as a food, tobacco and drugs additive to the synthesis of trinitroglycerine, alkyd resins and polyurethanes (Figure 2) [13]. Currently, the amount of glycerol that goes annually

into technical applications is around 160 000 tons and is expected to grow at an annual rate of 2.8%. [7]

Glycerol is also increasingly used as a substitute for propylene glycol. As one of the major raw materials for the manufacture of polyols for flexible foams, and to a lesser extent rigid polyurethane foams, glycerol is the initiator to which propylene oxide and ethylene oxide is added. Glycerol is widely used in alkyd resins and regenerated cellulose as a softener and plasticizer to impart flexibility, pliability and toughness in surface coatings and paints.

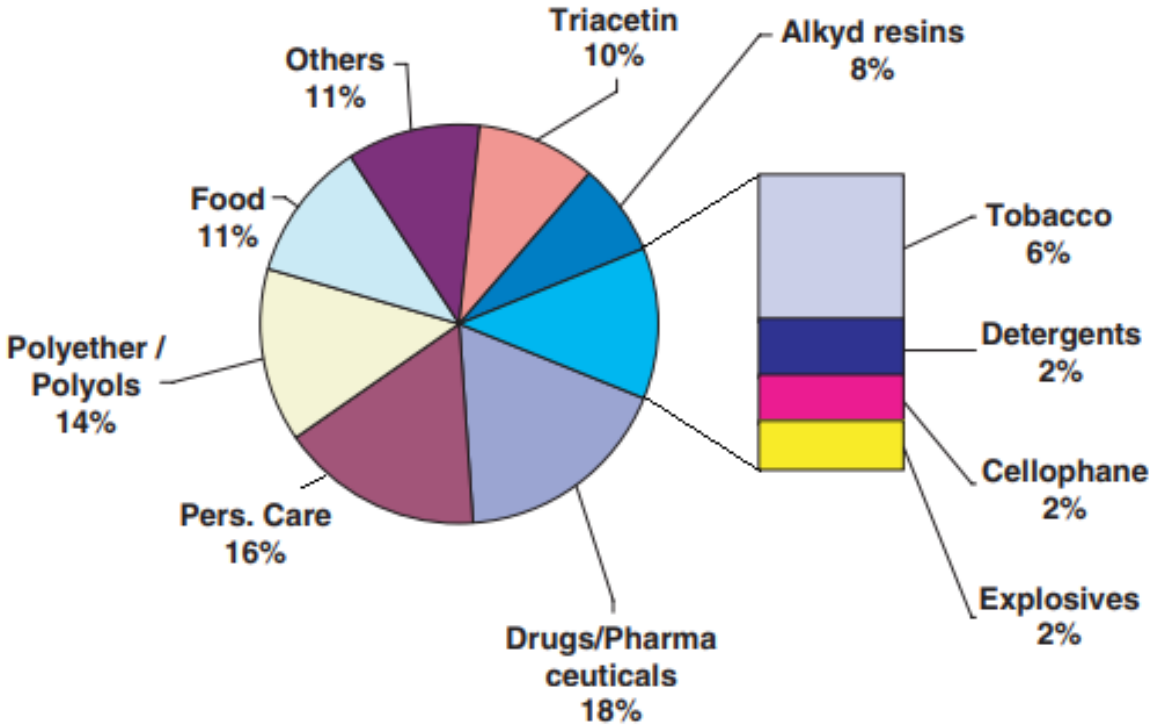

Figure 1.2: Market for Glycerol (volumes and industrial uses).
(Source: Novaol, May 2002.)

I. 1. 3 Production of Glycerol

Until 1949, glycerol was obtained as a co-product during the processing of vegetable and animal fatty acids and oils; hereinafter we will name Glycerol or natural Glycerin, the molecule obtained as a by-product of transesterification, saponification, etc. When fatty oils (triglycerides) are saponified during soap making, glycerol is recovered as a by-product. The first glycerol synthesis process was applied in 1949. This process is developed from propylene which can be chlorinated to allyl chloride with a high yield, the latter goes through different stages to obtain glycerol in fine (Figure 1.3). [10].

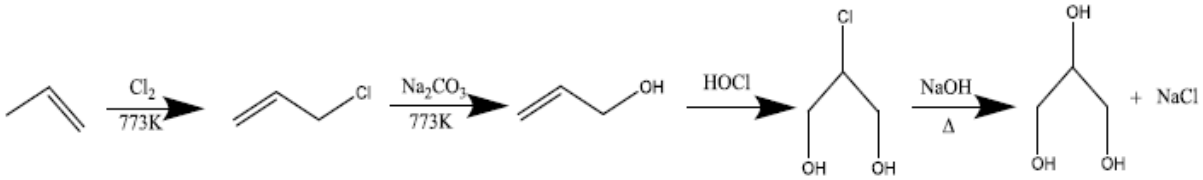

Figure 1.3: Transformation of propylene into Glycerol according to the Solvay process via epichlorohydrin.

Natural glycerol is thus nowadays mainly obtained from the triglycerides present in vegetable oils and in animal fats by transesterification, saponification and hydrolysis.

Figure 1.4 shows the production of Glycerol obtained as a co-product from different processes. The share from biodiesel production has increased over time while those from other sectors have remained stable

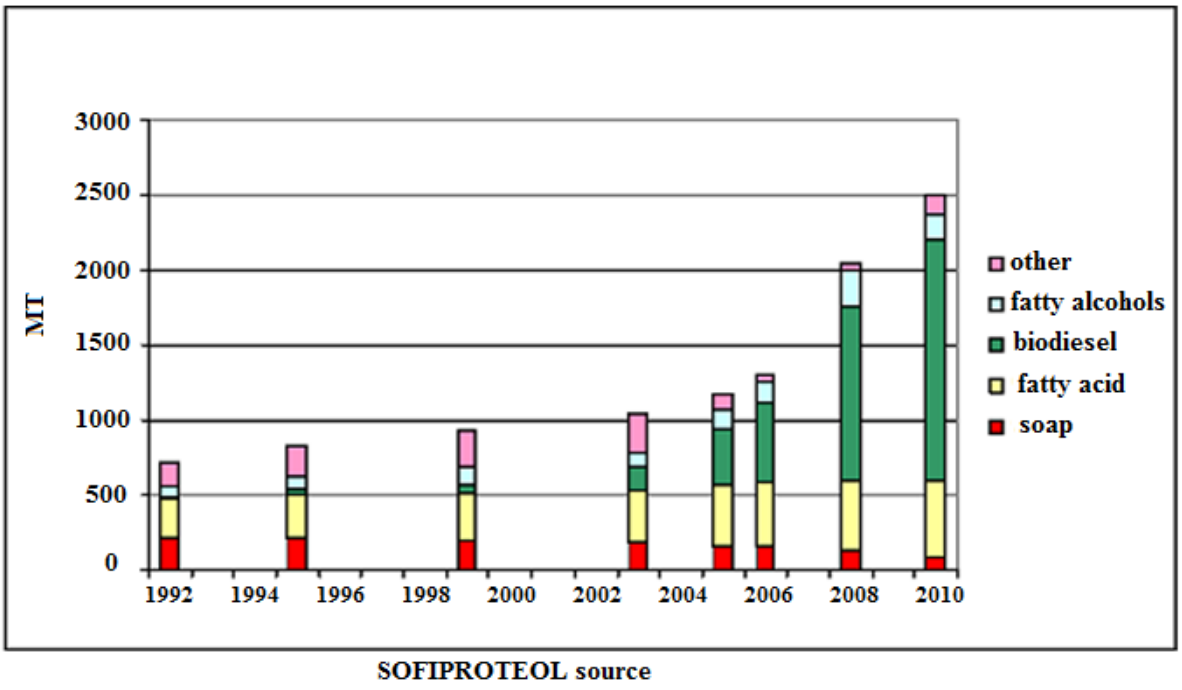

Figure 1.4: Different sources of Glycerol production over time.

The production of biodiesel consists in obtaining fatty methyl esters (biodiesel) by reacting triglycerides with an alcohol (e.g., methanol) in the presence of a basic catalyst mainly in homogeneous phase such as NaOH or KOH. During the transesterification process, 1 mole of triglyceride produces 3 moles of biodiesel (ester) and 1 mole of Glycerol. On this basis, every batch of biodiesel produces approximately 10 wt% of Glycerol Figure 1.5 shows the above reaction.

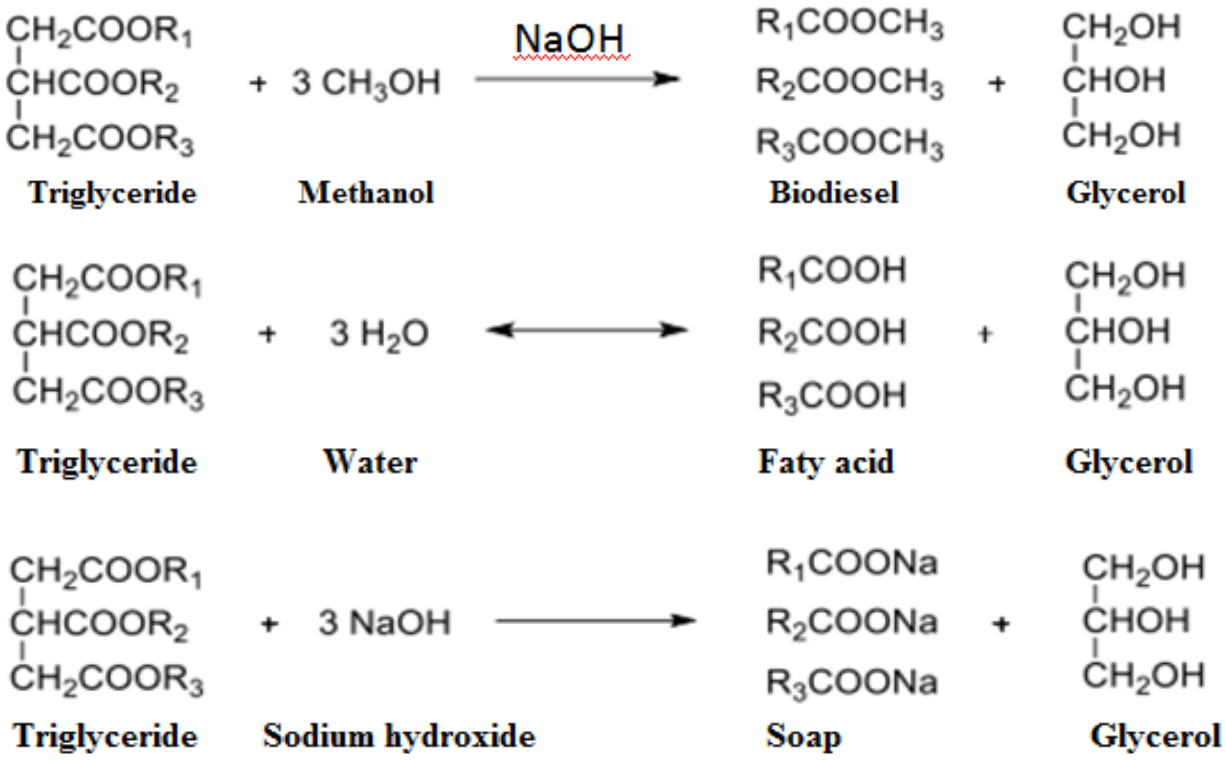

Figure 1.5: Transesterification, hydrolysis and Saponification of triglycerides to obtain Glycerol

The Glycerol side stream typically contains a mixture of Glycerol, methanol, water, inorganic salts (catalyst residue), free fatty acids, unreacted mono-, di-, and triglycerides, methyl esters, and a variety of other ‘‘matter organic non-glycerol’’ (MONG) in varying proportions. The methanol is typically stripped from this stream and reused, leaving crude glycerol after neutralization. In its raw state crude glycerol has a high salt and free fatty acid content and a substantial color (yellow to dark brown). Consequently, crude Glycerol has few direct uses currently; global biodiesel production tends to continue to increase significantly and is expected to reach around 42 billion liters in 2019 as shown in Figure 1.6. This therefore mechanically generates an increase in the quantities of Glycerol

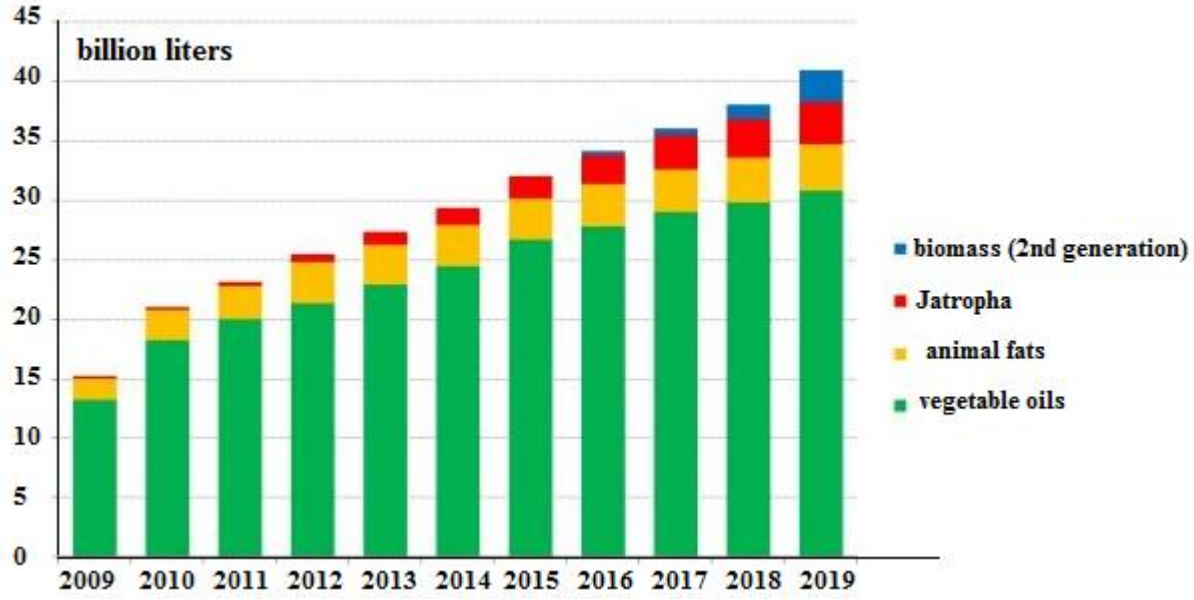

Figure 1.6: Global production of Glycerol from the commodity (planetoscope source)

The transesterification process is the reaction of a triglyceride (fat/oil) with an alcohol such as methanol and base such as potassium or sodium hydroxide (forming sodium or potassium methoxide with methanol as catalyst for the process), resulting in a methyl ester biodiesel stream and a glycerin side stream to form esters and glycerol. A triglyceride has a glycerin molecule as its base with three long chain fatty acids attached. The characteristics of the fat are determined by the nature of the fatty acids attached to the glycerin. The nature of the fatty acids can in turn affect the characteristics of the biodiesel. This reaction is generally effected in a two-stage mixer settler unit. Transesterification takes place in a mixing section, while the subsequent settling section allows for separation of methyl esters as the light phase from glycerin water as the heavy phase. A subsequent countercurrent washing step for the methyl ester removes minute by-product components and gives a biodiesel “ready for use” after the final drying step. The surplus methanol contained in the glycerin water is removed in a rectification column, which assures for methanol the required quality to be reused in the process. For further glycerin water purification, additional steps of chemical treatment, evaporation, distillation and bleaching may follow optionally.

In Figure 1.**7**, the classical main process phases and raw materials and products as well are given.

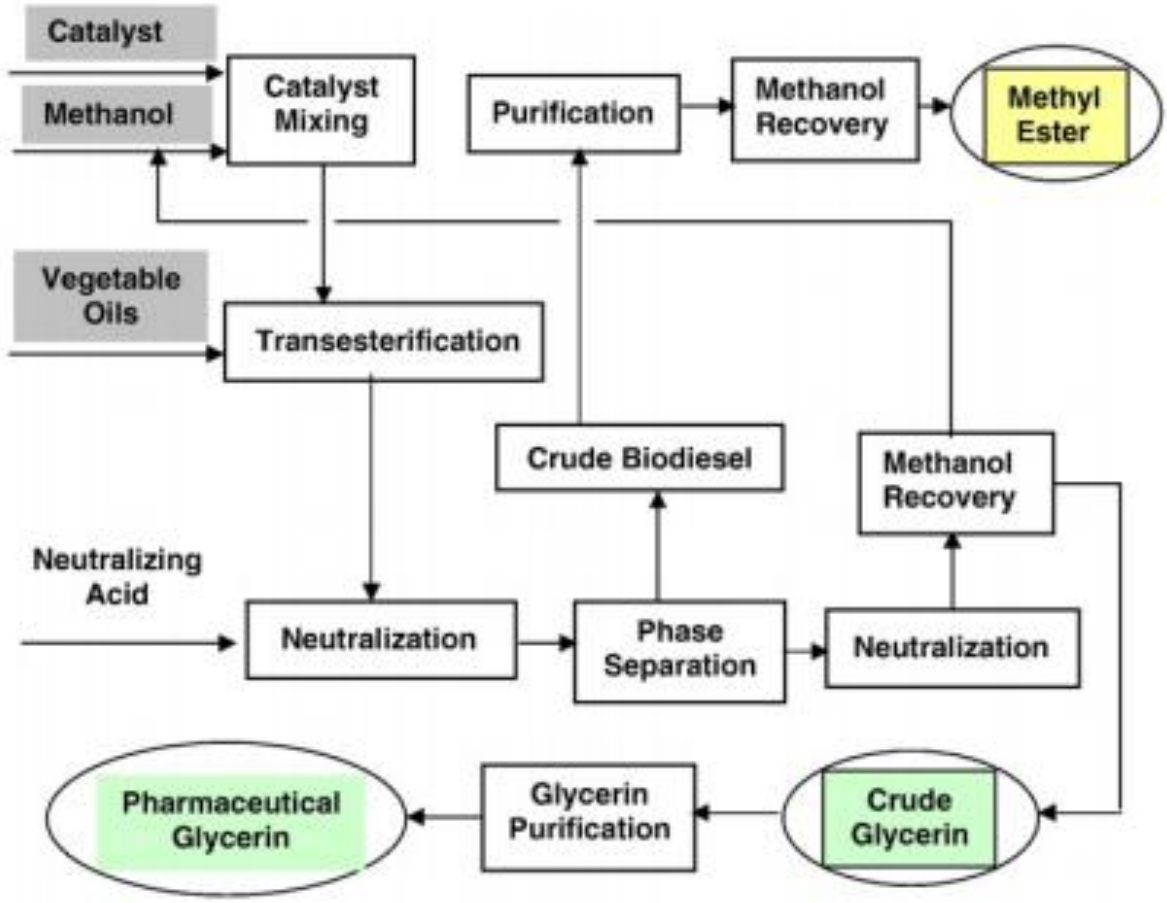

Figure 1.7: Main classical phases of the Glycerol production process [9]

Glycerol can be produced from fats and oils through three reactions: hydrolysis, transesterification and saponification. Figure 1.8 represents schematic diagram of the Glycerol and biodiesel process.

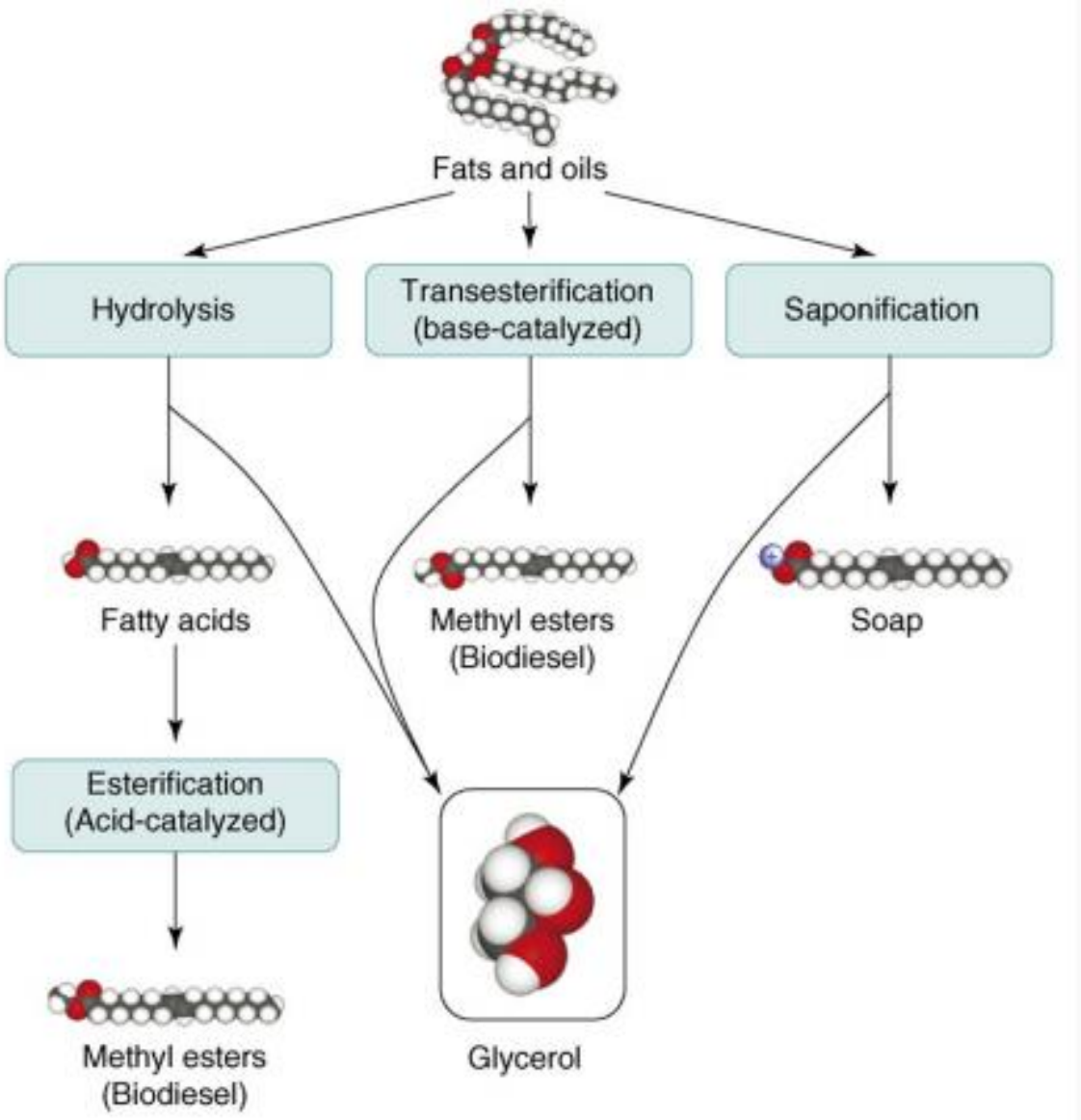

Figure 1.8: Schematic diagram of the Glycerol and biodiesel process [9]

I. 1. 4 Glycerol purification

The Glycerol side stream typically contains a mixture of glycerin, methanol, water, inorganic salts (catalyst residue) free fatty acids, unreacted mono-, di-, and triglycerides, methyl esters, and a variety of other matter organic non-glycerol in varying quantities. The methanol is typically stripped from this stream and reused, leaving behind, after neutralization, what is known as crude glycerin. Removing all the contaminating glycerin as well as other water-soluble impurities such as free fatty acids and salts of free fatty acids is either slow or expensive and always reduces the overall yield of biodiesel. In raw form, crude glycerin has high salt and free fatty acid content and substantial color (yellow to dark brown). Consequently, crude glycerin has few direct uses due to the presence of the salts and other species, and its fuel value is also marginal. The biodiesel industry generates millions of tons

of crude glycerin waste each year, and the amount produced is growing rapidly along with the dramatic growth of biodiesel production. One initial step common to all glycerin purification processes is that fat, soap and other organic impurities need to be chemically separated and removed by filtration and/or centrifugation. Final purification is typically completed using vacuum distillation followed by activated carbon bleaching for large operations or ion exchange followed by flash drying to remove water for smaller capacity plants. Vacuum distillation is very expensive in terms of capital cost and energy consumption and cannot always be carried out continuously and is accompanied by considerable losses of glycerol. In order to separate Glycerol from higher boiling point impurities the mixture needs to be additionally subjected to severe thermal stresses conducting to losses of glycerin due to decomposition. Because of the high salt content, ion exchange is not economically practical, unless it is used to polish a diluted low salt content glycerol-in-water solution. As per such technology the schematic diagram can be those presented in Figure 1.9

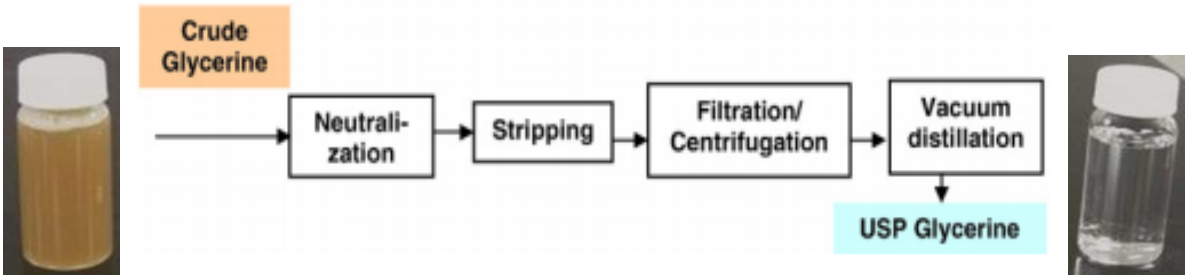

Figure 1.9: Common steps to obtain pure Glycerol

I. 1. 5 Glycerol recovery

Glycerol is an inevitable byproduct generated during both bioethanol and biodiesel production processes, and the tremendous growth of these industries has led to a dramatic decrease in crude Glycerol prices over the past few years [9] . During biodiesel production, the transesterification of fats and oils with an alcohol results in 10 lbs of crude Glycerol for every 100 lbs of biodiesel produced.

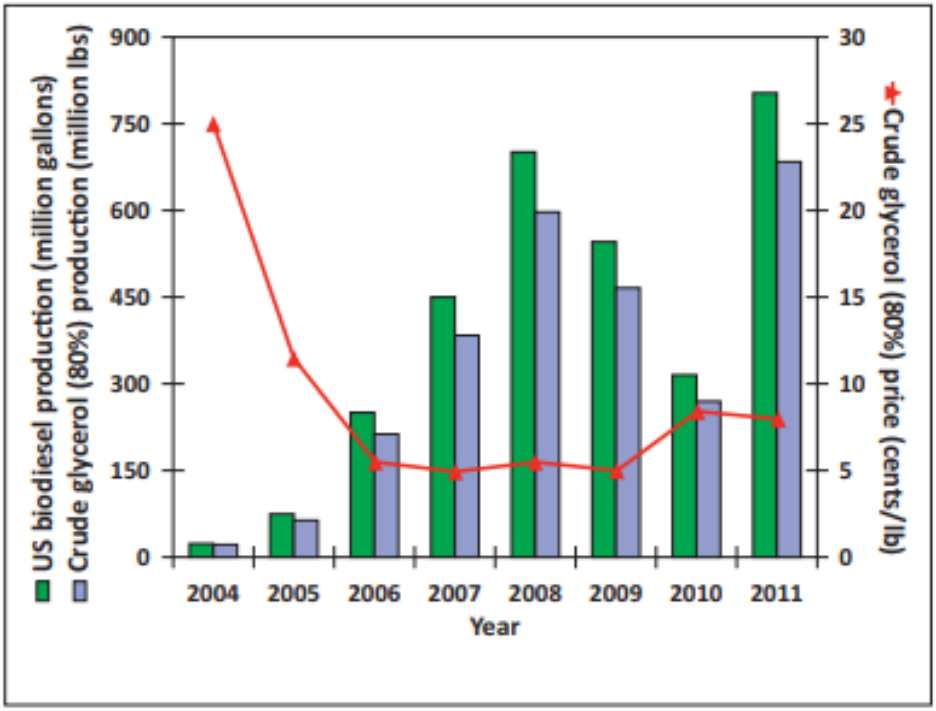

Figure 1.10: US biodiesel production and crude Glycerol price [11]

The evolution of the market price of Glycerol is closely linked to the production of biodiesel as shown in Figure 1.10 [11]. According to this reference, the value of crude Glycerol was divided by 5 between 2004 and 2009. Since then, it has tended to rise and stabilize around 176 Euros per ton (8 cents/lb). This unrefined raw glycerol at the end of the biodiesel production process is composed of 80% by weight of Glycerol, water and impurities such as methanol, ash, unreacted triglycerides and MONG (matter organic non-glycerol) [12]. Today, metals are distinguished from other materials by a set of advantageous properties such as good ductility, high tensile strength, and resistance to high temperatures, good electrical and thermal conductivity, great ease of processing, etc. Their drawbacks are their instability in contact with air and water, which reduces their resistance to corrosion and wear, ie their durability. However, in order to perform their function better during the expected service life, appropriate corrosion protection techniques are employed. The use of new corrosion resistant materials has been the subject of a great deal of research in recent years.

From an economic point of view corrosion is of prime importance. For example, it is estimated that each year a quarter of steel production is destroyed by corrosion, which corresponds to approximately 150 million tons/year or even 5 tons/second. These losses could be greater if there was no corrosion protection.

I. 2 Carbon nanotubes overview

I. 2. 1 Historical

One of the most abundant chemicals, carbon is the basis of almost all of the essential components of life, such as DNA, proteins and oils. However, it only exists in two pure forms in its natural state: graphite and diamond as shown in figure (1.11)

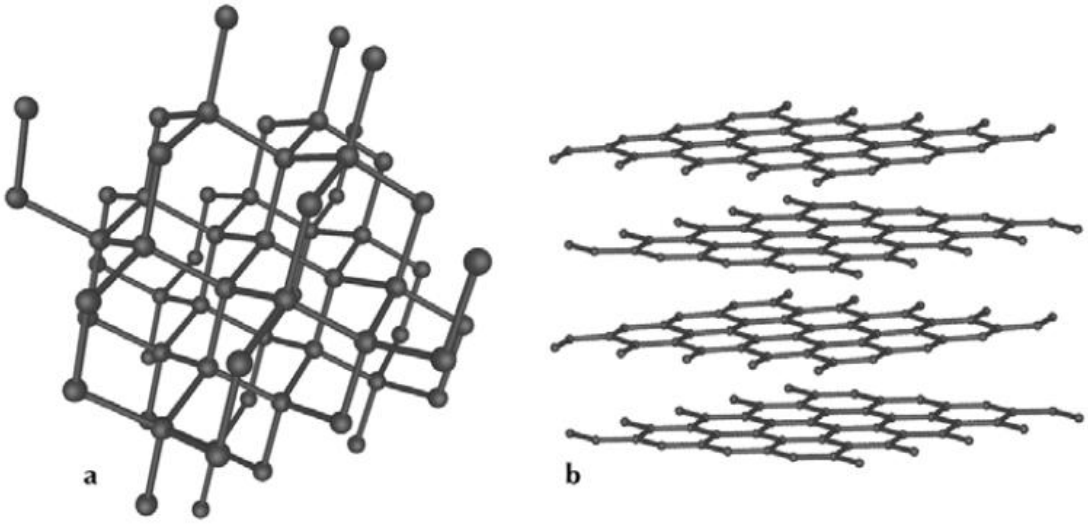

Figure 1.11: Schematic representation of the atomic structure of diamond (a) and graphite (b) [14]

Graphite is the thermodynamically stable form of carbon, made up of parallel stacks of graphene sheets. The latter, each separated by a distance of 0.336 nm, are made up of two-dimensional hexagonal arrays of sp^2 hybridizing carbon atoms. The whole is maintained by weak interactions of the Van der Waals type. Diamond, made up of sp^3 hybridizing carbon atoms, has a face-centered cubic crystallographic structure.

I. 2. 2 Structure of carbon nanotubes

Since their discovery, carbon nanotubes (CNTs) have aroused great scientific interest as much fundamental as applied because of their remarkable thermal, mechanical, electrical and optical properties.

A carbon nanotube is a crystal structure of carbon close to the fullerenes.

Structurally, we can see the nanotube as a graphene sheet (Monolayer of carbon atoms arranged in a honeycomb structure) wound on itself forming a hollow cylinder closed at its ends by half-fullerenes or more complex structures (Figure1.12). This material is characterized by its significant aspect ratio (ratio between its length and its diameter) generated by its dimensions. Indeed, the diameter of a nanotube is nanometric, while its length is micrometric; it can thus be considered as a one-dimensional nanomaterial.

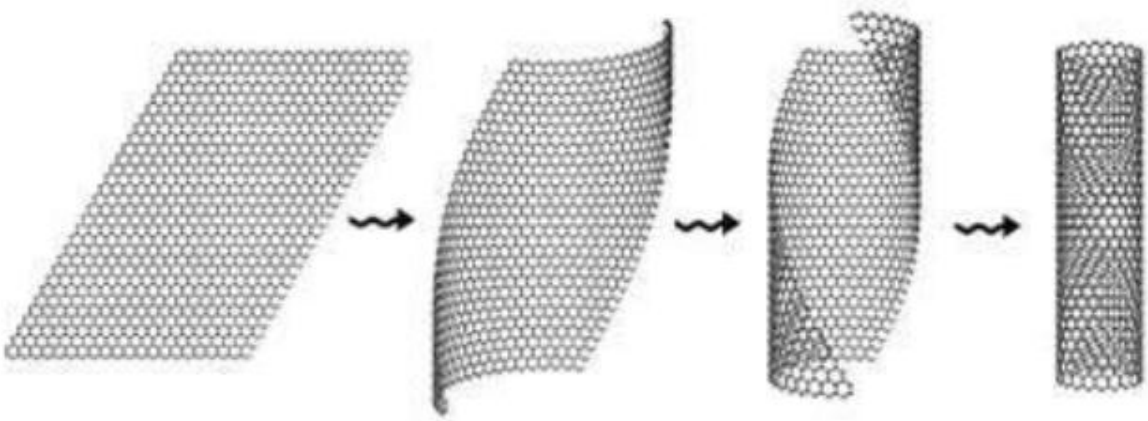

Figure 1.12: Example of winding a graphene sheet to form a tube [14]

Carbon nanotubes were first highlighted in 1991 by Iijima [15]. Carbon nanotubes are composed of carbon atoms, they are chemically inert and have a one-dimensional super elastic structure, electrochemical piezoelectric properties and high thermal conductivity.

The carbon nanotubes are synthesized mainly either by ablation by electric arc [15] which is a reliable but complex technique and which is carried out at 6000°C, or by laser ablation by vaporization of graphite, the synthesis is then carried out at 1200°C, or again by CCVD (chemical catalytic vapor deposition). This last method, the most chemical, consists in growing nanotubes by catalytic decomposition of a hydrocarbon, generally ethane or ethylene on a catalyst supported iron base, this at temperatures around 700°C and in a reducing medium. This method can lead to significant yields of nanotubes, but requires a subsequent purification step to rid it of the residual metallic catalyst.

A carbon nanotube can be made up of a single layer of graphene folded over itself called a single-walled nanotube (single-walled, SWCNT) or of a winding of several layers of graphene called multi-walled nanotubes (multi-walled, MWCNT) (Figure 1.13.a). Double-walled or double-walled nanotubes (double-walled, DWCNT) are a special case between MWCNT and SWCNT (Figure 1.13.b)

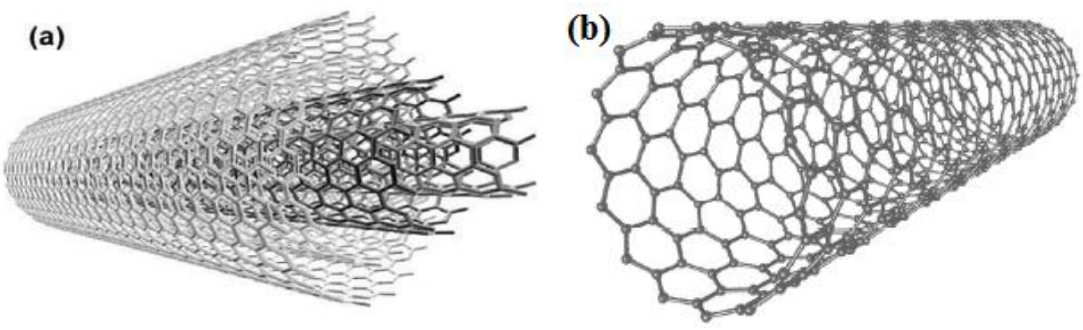

Figure 1.13: (a) MWCNT multi-walled nanotubes and (b) SWCNT single-walled nanotubes [16]

I. 2. 2.1 Single-walled carbon nanotubes

The structure of a single-sheet nanotube is represented by a graphene sheet in a honeycomb-like structure wound on itself (Figure1.14). The cylinder junction points determine the helicity of the nanotube which leads to a chiral, zig-zag or armchair structure**.**

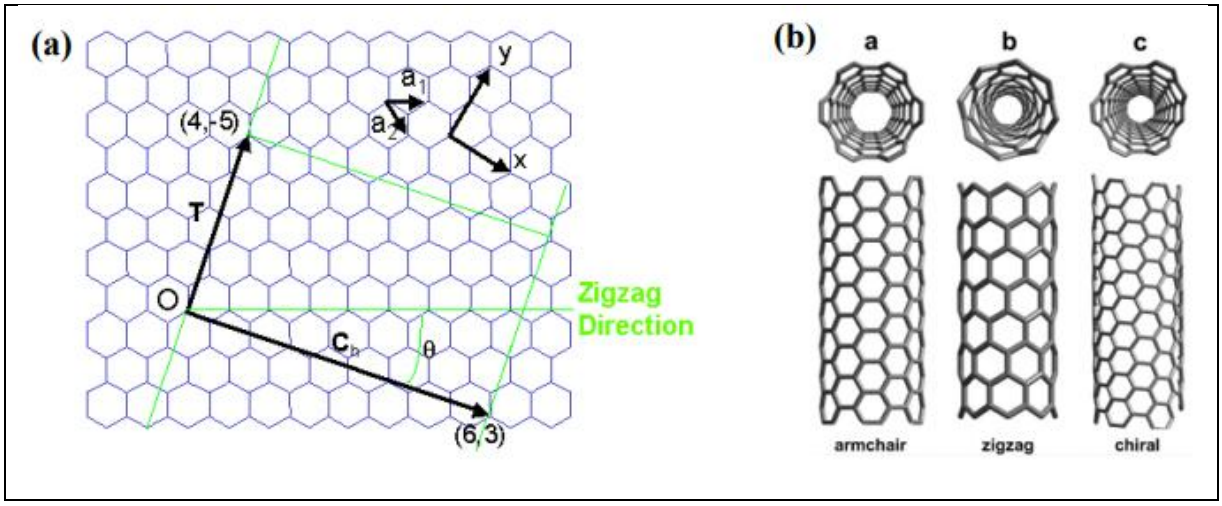

Figure 1.14: Schematic representations of (a) rolling of a graphene sheet, and (b) three types of carbon nanotubes [17].

Helicity

The geometry of a CNT is determined by its diameter and its helicity [18]. The latter depends on the winding conditions of the graphene sheet. This winding is done according to the chiral vector $\overrightarrow{C_h}$ defined such that:

$$\overrightarrow{C_h} = n\overrightarrow{a_1} + m\overrightarrow{a_2} \qquad (1.1)$$

Where a_1 and a_2 represent two directing vectors defined by their Cartesian coordinates (x, y), and n, m are scalars [19]. The translation vector T connects two identical sites along the axis of the tube and orthogonally to the vector C_h. The angle of chirality θ corresponds to the angle between the chiral vector and the zigzag direction (Figure 1.14). Next the value of the scalars n and m, three types of winding [20] of the graphene sheet can be obtained, which consequently leads to three different CNTs:

- If m = 0, the structure of the CNT is of the zigzag type, which corresponds to θ = 0 °;
- If m = n, the CNT is of the "armchair" type, which corresponds to θ = 30 °;
- in all other cases, the CNT is chiral, and 0 <θ <30 °.

These differences in helicity influence the electrical properties of nanotubes. Nanotubes of the "chair" type behave like semiconductors, while nanotubes of the "zig-zag" type behave like

metals. A single-sheet carbon nanotube generally has a diameter between 1 and 10 nm and its length can reach several micrometers.

I. 2. 2. 2 Multiwalled carbon nanotubes

The multi-sheet carbon nanotubes are available in two different structures. The first consists of a concentric entanglement of single-wall nanotubes of increasing diameters (Figure 1.12 a). The second consists of a winding of a graphene sheet, which in section gives a spiral or a roll of parchment. A multi-sheet carbon nanotube can have a diameter of up to a hundred nanometers. Their electrical conductivity is very high (6 $W.cm^{-1}.K^{-1} < \sigma < 20$ $W.cm^{-1}.K^{-1}$) but lower than that of single-walled carbon nanotubes due to Van der Waals type interactions between the different sheets.

I. 2. 3 Synthesis pathways for carbon nanotubes (CNTs)

There are mainly three ways of producing CNTs, which can be classified into two main categories, which will be detailed below:

- Synthesis at very high temperatures: by electric arc (discharge arc, AD) or by laser ablation (LA).
- Synthesis at medium temperatures: by catalytic chemical vapor deposition (CCVD).

I. 2. 3. 1 Electric arc technique (AD)

The electric arc technique was initially used for the synthesis of fullerenes, and then it was modified to produce CNTs [21]. This method consists in the discharge of an electric arc between two graphite electrodes at very high temperatures in an environment containing an inert gas (He, Ar ...) (Figure 1.15). For the synthesis of MWCNT, the electrodes used are made of pure graphite [22], while for the SWCNT; the graphite anode also contains a metal acting as a catalyst [23].

At the start, the two electrodes touch each other finely to generate an electric arc. Then, the growth of CNTs results from the formation of an electric arc, when a current DC (density) 150 A / cm^2 and a voltage set at ~ 20 V are applied between the two electrodes. Once the arc is produced, the electrodes separate by a distance on the order of a millimeter. Thus, the length of the positive electrode decreases following its evaporation. However, the distance between the anode and the cathode is kept constant. Due to the high current densities, the temperature of the reaction zone (plasma created) can quickly reach very high temperatures up to 3000 ° C. Therefore, it is necessary to cool the enclosure with water and maintain the constant pressure [24].

This manufacturing process is very inexpensive. However, the process is so complex that in the end the CNT samples obtained are contaminated with impurities and it there is no precise control over the length and diameter of CNTs [25]. To eliminate these contaminants, thorough purifications are necessary but they damage the NTC and the yields obtained are ultimately relatively low.

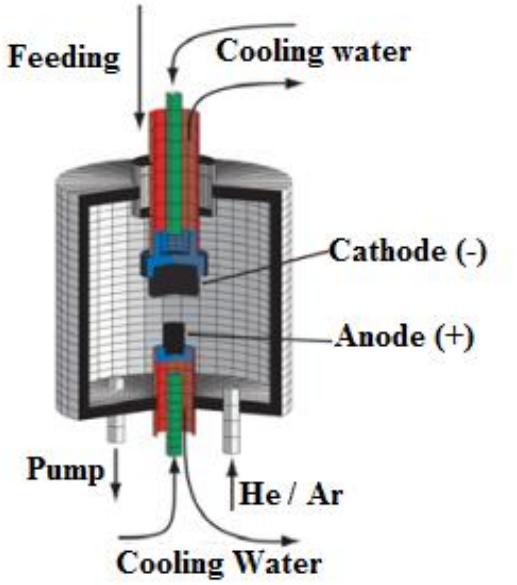

Figure 1.15: Diagram of an electric arc type device used for the growth of CNTs [24]:
(*During the reaction, the cathode is moved down to keep the distance between it and the anode that will be evaporated constant*)

I. 2. 3. 2 Laser ablation technique

Laser ablation is another way of synthesizing CNTs, which is based on the vaporization of a graphite disc, a carbon source, by laser irradiation (Figure 1.16). First, the solid graphite disc is placed in the center of a quartz tube heated to 1200 ° C. Then, an inert gas is injected into the enclosure and simultaneously a laser beam uniformly scans the surface of the graphite target. Under the gas flow, the CNTs produced are directed
from hot areas to cooler areas and collected at the bottom of the tube. As in the case of synthesis by electric arc, the MWCNTs are synthesized starting from a target in pure graphite, while it is necessary to use a metallic catalyst mixed with the target in graphite for SWCNT. The yield and the quality of the samples obtained with this process are better, compared to the case of the electric arc. However, this technique is quite expensive and its yield remains low.

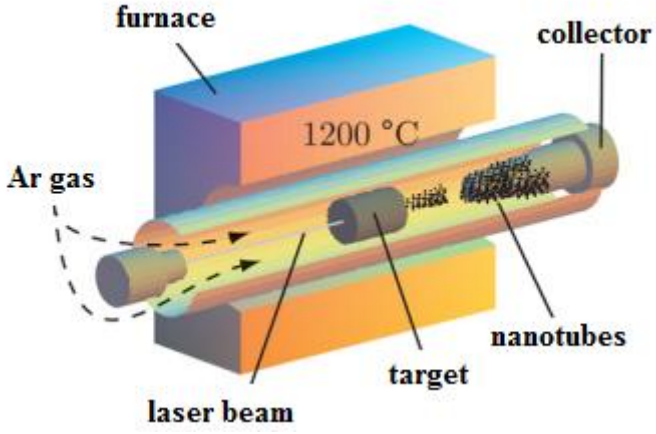

Figure 1.16: Diagram of a laser ablation device [24].

I. 2. 3. 3 Chemical vapor deposition technique (CCVD)

The synthesis of CNTs by the chemical vapor deposition method CCVD was used for the first time by Endo et al. [26]. This technique consists of breaking down a gas stream containing a carbon source (e.g., hydrocarbon $\mathbf{C_nH_m}$, such as acetylene ($\mathbf{C_2H_2}$) or methane ($\mathbf{CH_4}$),) in the presence of metal such as Fe, Ni or Co catalysts in an oven brought to a temperature higher than 700 ° C. The nanotubes then form on the catalyst pads. [27]. Many parameters (temperature, treatment time, composition of the gas flow, gas flow rate, nature and composition of the catalyst, etc.) play on the nature of the CNTs formed. One of advantages of this method is that nanotubes are formed continuously. In addition, the CCVD technique as shown in Figure 1.17, differs from the other two methods (called high temperature) with many benefits, including better control conditions operating and experimental parameters, ease of implementation and low cost. The synthesis of CNTs by CCVD has considerable advantages over other methods. The experimental conditions are more easily modulated, which has direct consequences on the structure and properties of CNTs. For example, a change in temperature results in a change in diameter of the CNTs. Another important parameter concerns the duration of synthesis: in fact an increase in the latter amounts to providing the system with more carbon sources, which results in an increase in the length of the CNTs. The CCVD method compared to the channels previous synthesis offers more comfort and makes it easier to adjust the length and diameter of the CNTs by modifying the nature of the catalyst.

Finally, this technique turns out to be reliable for the production in large quantities of CNTs, which can reach several grams [28] and the lower level of impurities make this process more suitable for industrialization. Furthermore, it is important to note that the CNTs produced by CVD can be directly used for various applications and this without any prior purification. The

latter is in principle necessary to remove residues of catalysts or amorphous carbon. CVD is mainly used to obtain aligned MWNTs [29] with specific intrinsic properties, and more rarely SWNTs [30]. Thus, several companies market MWNTs produced by CCVD such as Future Carbon, Arkema, Nanocyl, and Hyperion Catalysis International. Carbon Nanotechnology also offers SWNT products by a CCVD method known as high pressure catalytic decomposition of carbon monoxide [31].

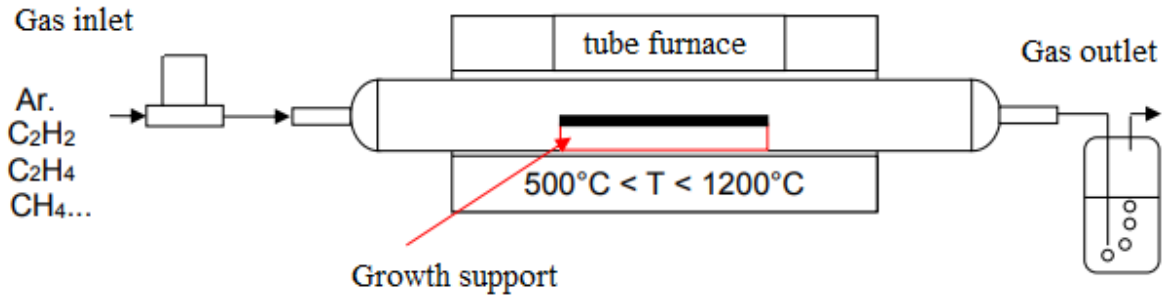

Figure 1. 17: Schematic diagram of the CNT growth process by CVD [31].

The images below represent MWNTs prepared in the MSSMAT laboratory from Paris central school to make MWNTs and which observed with a scanning electron microscope (SEM).

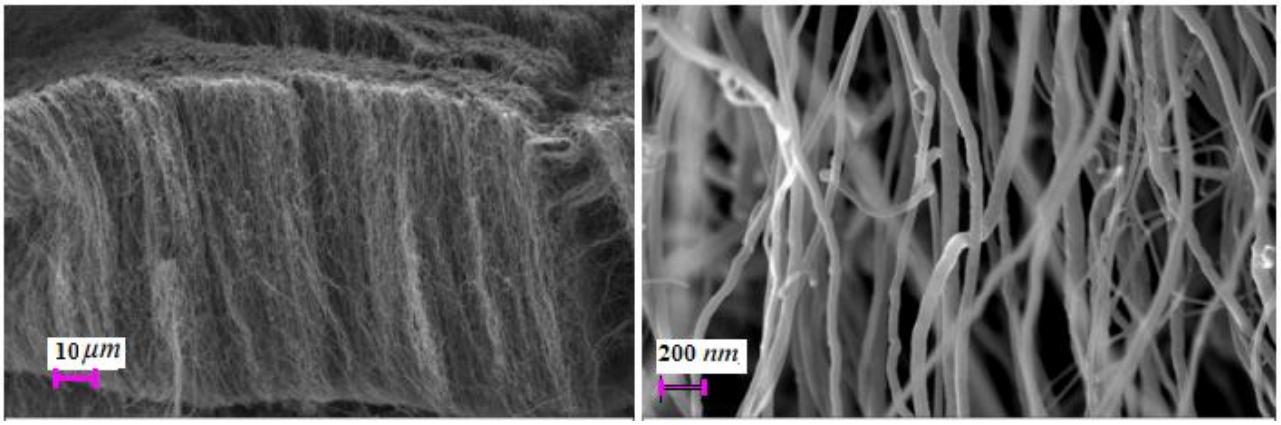

Figure 1.18: SEM photos of MWCNT synthesized by CCVD method in the MSSMAT laboratory (L ≈ 120 µm, d ≈ 50 nm)

I. 2. 4 Properties of carbon nanotubes

Carbon nanotubes are unique in their dimensions because with a diameter (d) on the order of a nanometer and a length (L) of several microns they have a high aspect factor a = L/d. Beyond these geometric characteristics, nanotubes have electrical, thermal, mechanical properties impressive. The properties of MWNTs are less good than those of SWNTs. In the case of MWNTs, it is the last sheet which will be decisive for the overall properties of the CNT. Table 1.2 summarizes the theoretical and experimental characteristics of the CNTs compared for illustrative purposes with graphite carbon.

Table 1.2: Experimental and theoretical properties of MWCNT. [32]

properties	MWCNT	Graphite
Specific gravity	1.8 g/cm^3(theoretical)	2.26 g/cm^3
Young's modulus	~ 0.3-1 TPa	1 TPa(in-plane)
Resistivity	5-50 μΩ.cm	50 μΩ.cm (in-plane)
Thermal conductivity	3000 W.m^{-1}.K^{-1}(theoretical)	3000W.m^{-1}.K^{-1} (in-plane)

Shortly after the discovery of CNTs in 1991, numerous theoretical studies [33] demonstrated that they have a high electrical conductivity [34-35]. Indeed, the modeling of the energy bands [36] confirms one of the characteristics surprising CNTs: their metallic or semiconductor behavior, depending on their diameter and helicity. Thus, the electrical resistance of a CNT has been estimated from calculations [37] at ~ 6.5 kΩ. When the CNTs are in contact, the resistance increases and can reach ~ 6.5 MΩ. Due to the anisotropic electronic properties of Graphene, the mobility of electrons is high in the plane direction.

The thermal conductivity of CNTs along the axis of the tube seems to be the highest among all the materials known to date, and in particular diamond [38]. This remarkable intrinsic property of CNTs can be explained by the rigidity created by the links, and by the one-dimensional structure of the tube which limits diffusion phenomena [39]. Due to their analogy to Graphene, CNTs are stable up to very high temperatures (4000 K, graphite melting point). The thermal conductivity of SWNTs was calculated by simulation of molecular dynamics [40] equal to K_{SWNT} = 6000 W/mK, which is much higher than the conductivity of the diamond. Ajumdar et al. have experimentally measured that of MWNTs equal to K_{MWNT} = 3075 W/mK at room temperature [41].

CNTs have a high tensile strength due to their graphene-based structure. The cylindrical shape of a CNT gives it more structural stability, even under stress [42]. Considering a cluster of CNTs as a uniform material, the Young's modulus (E) of the CNTs exceeds 1 TPa. This value has been verified for SWNTs by Robertson et al. from empirical models [43]. Other theoretical studies have shown that the value of Young's modulus should drop for CNTs with very small diameters (≤ 4 Å). Such a result is physically intuitive because the increase in the curvature deformation implies a weakening of the C-C bonds, and this therefore appears at the level of mechanical properties [44]. A value as high as E = 1.8 TPa has also been measured experimentally [45] for MWNTs interlaced by Ebbesen et al.

I. 2. 4. 1 Mechanical properties

The mechanical properties of the fibers are evaluated in tension using a Zwick Z2.5 apparatus (Figure 1.19). This device makes it possible to plot the stress curve as a function of the deformation and thus to go back to the breaking strength and the Young's modulus of the CNT. The tensile experiment consists of measuring the elongation and the force applied to the CNT until it breaks for a displacement speed of 1 mm / min.

Figure 1.19: Photograph of the Zwick Z2.5 traction device. [46]

In order to overcome variations in the geometry of the various nanotubes tested, in particular the diameter, the elongation and the force are converted into strain (1.2) and stress (1.3) by the following equations:

$$\boldsymbol{\varepsilon} = \frac{\boldsymbol{l}-\boldsymbol{l_0}}{\boldsymbol{l_0}} \qquad (1.2)$$

$$\boldsymbol{\sigma} = \frac{\boldsymbol{F}.\boldsymbol{l}}{\boldsymbol{S}.\boldsymbol{l_n}} \qquad (1.3)$$

With $\boldsymbol{l}$ the length at time t in mm, $\boldsymbol{l_0}$the initial length in mm, **σ** the stress in MPa, **F** the force at time t in N, **S** the section of the nanotube in mm^2 and $\boldsymbol{l_n}$ the length at breakage in mm.

From the stress versus strain curve (Figure 1.20), it is possible to extract various data characterizing the mechanical behavior of a fiber. First, in the elastic domain, the stress is proportional to the strain satisfying Hooke's law and the coefficient of proportionality thus corresponds to the Young's modulus (E) of the nanotube, characterizing its stiffness. From a certain deformation the fiber passes into a plastic domain which means that the deformation is irreversible. The fiber continues to deform until it is stressed limit called breaking stress (σ). This type of measurement makes it possible to extract information characterizing the mechanical behavior of the nanotube such as:

- The breaking stress in (MPa) noted σ, which characterizes the load maximum that the nanotube can withstand;

- Young's modulus (GPa) noted E, which reflects the stiffness of the nanotube;
- The Strain noted ε, which corresponds to the elongation of the nanotube before breaking.

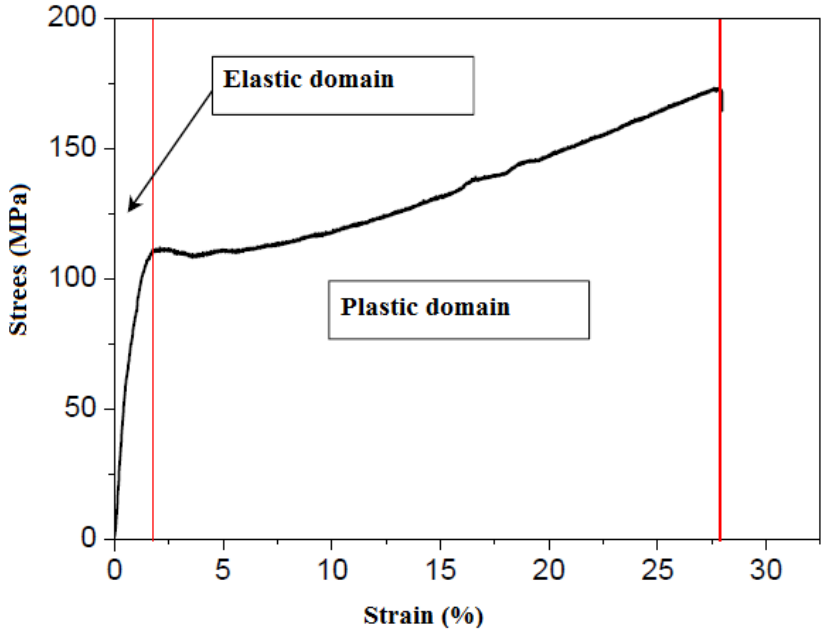

Figure 1.20: Evolution of the stress σ as a function of the strain ε.

Table 1.3 shows the mechanical properties of MWCNT carbon nanotubes obtained by the wet process in a coagulating bath. The first observation is the great variability of Young's modulus and breaking stress from fiber to fiber.

For CNTs, the breaking stress and Young's modulus vary from 0.15 to 1 GPa and from 2 to 120 GPa respectively.

Table 1.3: Mechanical properties of NTC obtained by the wet process.

	σ(GPa)	E(GPa)	ε(%)	Reference
MWCNT/EG	0,15	69	3	[47]
DWCNT/HSO_3Cl	1	120	1,4	[48]
SWCNT/Water	/	2	4,5	[49]

Regarding the MWCNTs obtained by the dry process, the mechanical properties also vary from one study to another as shown in Table 1.4.The breaking stress and Young's modulus vary from 0.345 to 1.170 and from 17.6 to 275GPa respectively.

Table 1.4: Mechanical properties of NTC obtained by the dry process.

CVD method	σ (GPa)	E (GPa)	ε (%)	Reference
MWCNT	0,85	275	2,21	[50]
MWCNT	0,564	74	0,75	[51]
MWCNT	1,170	53,5	2,4	[52]
MWCNT	0,345	17,6	3	[53]
MWCNT	0,35	25	2,2	[54]
MWCNT	1,1	56	2,3	[55]

The authors explain the phenomenon of variability of mechanical properties by the fact that a long CNT will wrap around the fiber a greater number of times during its development thus increasing the stress transfer with the other CNTs.

In conclusion, as shown in Table 1.5, the fibers obtained by the dry process make it possible to obtain a better Young's modulus which generates an increase in the number of contacts between the CNTs allowing better transfer of stresses despite a breaking stress slightly lower.

Table 1.5: Summary of the mechanical properties of fibers obtained by the dry and wet process.

	σ (GPa)	E (GPa)	ε (%)
Wet process	0.15 - 4.4	7.3 - 120	1.4 - 13
Dry process	0.278 - 3.3	6.5 – 330	0.75 - 9.1

I. 2. 4. 2 Electrical and thermal properties

The carbon constituting the CNTs is sp^2 hybridized, that is, there is a combination of the 2s orbital with the $2p_x$ and $2p_y$ orbitals leading to three sp^2 hybrid orbitals as well as a natural $2p_z$ orbital. This results in the formation of three σ bonds and a delocalized π bond with mobile electrons, which implies a high conductivity along the CNT axis. Experimental measurements, by contacting the NTC at its ends, showed a low electrical resistivity along the axis of the NTC of $2.6x10^{-7}\Omega.m$ at 300 K for SWNTs [56] and $9.5x10^{-5}$ to $5.3x10^{-8}\Omega.m$ for MWNTs with a current density of the order of 10^{10} A/cm^2 [57] [58]. CNTs therefore have an electrical resistivity close to that of copper ($1.7x10^{-8}\Omega.m$), as well as a much lower density varying around 2 g/cm^3 depending on the diameter and the number of walls [59] , making them potential candidates for applications requiring a light material and good electrical conduction. However, it is important to take into account the nanotube shaping processes to obtain conductive materials or devices comprising several CNTs, because these materials

have a lower conductivity compared to individual nanotubes, which is often linked to contact resistances [60].

Regarding the thermal properties of CNTs, a simulation revealed a thermal conductivity of up to 6600 W/m.K for an individual SWCNT [61]. Experiments, on individual CNTs, yielded conductivities of 3500 [62] and 200-3000 W/m.K [63] [64] at 300 K for SWCNT and MWCNT respectively. Furthermore, it has been shown that the conductivity

individual NTC is much higher than that of a set of aligned CNTs due to the contact resistances between them, since the thermal conductivity has increased from 3000 W/m.K for a single NTC to around 400 W/m.K for a set of NTC [63].

CONCLUSION 1

In this first chapter, we have given a general description of Glycerol considered as the basic fluid of CNTs and its thermophysical properties. Carbon nanotubes are exceptional charges: on the one hand for their highly anisotropic geometries of several microns in length for a diameter of a few nanometers and on the other hand because they have thermal and electrical properties and a mechanical behavior worthy of metals. These characteristics make CNT ideal loads for energy transfer.

To this end, the following chapter describes in detail the various experimental devices and methods used, for the characterization of the main thermo-physical properties of nanofluids based Glycerol (thermal conductivity, dynamic viscosity, density), and electrical properties.

References

[1] J. A. Hunt, Pharm. J. 263, 985.1999.
[2] Frost & Sullivan: "R&D Creating New Avenues for Glycerol" (August 4, 2006), available online at https://www.frost.com/prod/servlet/market-insight-top.pag?docid = 77264824.
[3] M. McCoy, Chem. Eng. News 2006, 84(6), 7; b) M. McCoy, Chem. Eng. News 2006, 84(2), 32.
[4] McCoy M: Glycerin surplus. Chem Eng News, 84:7, 2006.
[5] J. Hill, E.Nelson, D.Tilman, S. Polasky, D. Tiffany, Proc. Natl. Acad. Sci. USA, 103, 11 206. 2006.
[6] R. Ciriminna, C. Della Pina, W. Kesber, WO2006051574, 2004.
[7] J. Bonnardeaux, Glycerin Overview, Report for the Western Australia Department of Agriculture and Food. http://www.agric.wa.gov.au/content/sust/biofuel/glycerinoverview.pdf. November 2006.
[8] CRC Handbook of Chemistry and Physics, 87th edn., Boca Raton (FL): 2006.
[9] Yazdani, S.S. and Gonzalez, R. Anaerobic fermentation of glycerol: a path to economic viability for the biofuels industry. Curr.Opin.Biotechnol. 18, 213–219, 2007.
[10] G. Knothe, J. Krahl, and J. Van Gerpen, "Preface to the First Edition," in The Biodiesel Handbook (Second Edition), Elsevier, p. vii, 2010.
[11] J.M.ClomburgandR.Gonzalez,"Anaerobicfermentationofglycerol:aplatform for renewable fuels and chemicals," *Trends Biotechnol.*, vol. 31, no. 1, pp. 20–28, Jan.2013.
[12] E. Skrzyńska, S. Zaid, J.-S.Girardon, M. Capron, and F. Dumeignil, "Catalytic behaviour of four different supported noble metals in the crude glycerol oxidation," *Appl. Catal. Gen.*, vol. 499, pp. 89–100, Jun.2015.
[13] R. Ciriminna, M. Pagliaro, Adv. Synth. Catal, 345, 383. As the dehydrate calcium salt, ketomalonate is a potent hypoglycemic agent commercialized in diabetes therapy while in generalketomalonic acid is a versatile synthon for organic chemistry. 2003.
[14] TeissierA., Synthèse de matériaux à base de pentoxyde de niobium et de nanotubesde carbone pour la limitation optique dans l'infrarouge, Thèse Doctorat, Université deStrasbourg 2009.
[15] Helical microtubules of graphitic carbon, S. Ijima, Nature, 354,1991.
[16] LandoisP., synthesis, functionalization and environmental impact of nanotubes carbon, doctoral thesis, University of Toulouse, 2008.
[17] R. Saito, G. Dresselhaus, M.S. DresselhausPhysical properties of carbon nanotubes London and Imperial College Press, London 1998.
[18] Qian, D.; Wagner, G. J.; Liu, W. K.; Yu, M.-F.; Ruoff, R. S., Mechanics of carbon nanotubes. Applied Mechanics Reviews, 55 (6), 495-533, 2002.
[19] Hamada, N.; Sawada, S.-i.; Oshiyama, A., New one-dimensional conductors: Graphitic microtubules. Physical Review Letters, 68 (10), 1579. 1992.
[20] Charlier, J. C.; Blase, X.; Roche, S., Electronic and transport properties of nanotubes. Reviews of Modern Physics, 79 (2), 677-732. 2007.
[21] TaylorR., The Chemistry of fullerenes, Advanced Series of Fullerenes, 4,1995.
[22] Ebbesen, Hiura H., Fujita J., Ochiai Y., Matsui S., Tanigaki K., Patterns in the bulk growth of carbon nanotubes, Chem. Phys. Lett., 209, 83–90, 1993.
[23] Iijima S., IchihashiT., Single-shell carbon nanotubes of 1-nm diameter, Nature, 363/6430, 603–605, 1993.
[24] Miko, C., Synthesis, characterization and macroscopic manipulation of carbon nanotubes. PhD Thesis, EPFL Lausanne, Switzerland. 2005.
[25] Ajayan P. M., Ebbesen T. W., Nanometer-size tubes of carbon, Rep. Prog. Phys, 60, 1025–1062. 1997.
[26] Endo M., Takeuchi K., Kobort K., Takahashi K., Pyrolytic carbon nanotubes from vapor grown carbon fibers, Carbon 33, 873-881, 1995.
[27] Teo, K. B. K.; Singh, C.; Manish, C.; Milne, W. I., Catalytic Synthesis of Carbon Nanotubes and Nanofibers. In Encyclopedia of Nanoscience and Nanotechnology, Nalwa, H. S., Ed. American Scientific Publishers: Los Angeles, Vol. 10, pp 1-22, 2003.

[28] Mukhopadhyay, K.; Koshio, A.; Sugai, T.; Tanaka, N.; Shinohara, H.; Konya, Z.; Nagy, J. B., Bulk production of quasi-aligned carbon nanotube bundles by the catalytic chemical vapour deposition (CCVD) method. Chemical Physics Letters, 303 (1-2), 117-124, 1999.
[29] Fan, S.; Chapline, M. G.; Franklin, N. R.; Tombler, T. W.; Cassell, A. M.; Dai, H., Self-Oriented Regular Arrays of Carbon Nanotubes and Their Field Emission Properties. Science, 283 (5401), 512-514, 1999.
[30] Hafner, J. H.; Bronikowski, M. J.; Azamian, B. R.; Nikolaev, P.; Rinzler, A. G.; Colbert, D. T.; Smith, K. A.; Smalley, R. E., Catalytic growth of single-wall carbon nanotubes from metal particles. Chemical Physics Letters, 296 (1- 2), 195-202, 1998.
[31] Moniruzzaman M, Winey KI. Macromolecules ,39:5194-205, 2006.
[32] Xie XL, Mai YW, Zhou XP. Materials Science and Engineering ,89-112,2005.
[33] Novikov, D. S., Transport in Nanoscale Systems. PhD Thesis, Massachusetts Institute of Technology, USA, 2003.
[34] Dresselhaus, M. S.; Dresselhaus, G.; Saito, R., Physics of carbon nanotubes, 33 (7), 883-891, Carbon 1995.
[35] Dekker, C., Carbon Nanotubes as Molecular Quantum Wires. Physics Today, 52 (5), 22-28, 1999.
[36] Biercuk, M. J.; Ilani, S.; Marcus, C. M.; McEuen, P. L., Electrical transport in single-wall carbon nanotubes. In Carbon Nanotubes, Springer-Verlag Berlin: Berlin, Vol. 111, pp 455-493, 2008.
[37] Yao, Z.; Kane, C. L.; Dekker, C., High-Field Electrical Transport in Single-Wall Carbon Nanotubes. Physical Review Letters, 84 (13), 2941, 2000.
[38] Yamamoto, T.; Watanabe, K.; Hernandez, E. R., Mechanical properties, thermal stability and heat transport in carbon nanotubes. Carbon Nanotubes, 111, 165-194, 2008.
[39] Tomanek, D.; Jorio, A.; Dresselhaus, M. S.; Dresselhaus, G., Introduction to the important and exciting aspects of carbon-nanotube science and technology. In Carbon Nanotubes, Springer-Verlag Berlin: Berlin, Vol. 111, pp 1-12, 2008.
[40] Berber, S.; Kwon, Y. K.; Tomanek, D., Unusually high thermal conductivity of carbon nanotubes. Physical Review Letters, 84 (20), 4613-4616, 2000.
[41] Kim, P.; Shi, L.; Majumdar, A.; McEuen, P. L., Thermal transport measurements of individual multiwalled nanotubes. Phys. Rev. Lett. 8721 (21), 4, 2001.
[42] Tomanek, D.; Jorio, A.; Dresselhaus, M. S.; Dresselhaus, G., Introduction to the important and exciting aspects of carbon-nanotube science and technology. In Carbon Nanotubes, Springer-Verlag Berlin: Berlin, Vol. 111, pp 1-12, 2008.
[43] Robertson, D. H.; Brenner, D. W.; Mintmire, J. W., Energetics of nanoscale graphitic tubules. Physical Review B, 45 (21), 12592, 1992.
[44] Yamamoto, T.; Watanabe, K.; Hernandez, E. R., Mechanical properties, thermal stability and heat transport in carbon nanotubes. In Carbon Nanotubes, SpringerVerlag Berlin: Berlin, Vol. 111, pp 165-194, 2008.
[45] Treacy, M. M. J.; Ebbesen, T. W.; Gibson, J. M., Exceptionally high Young's modulus observed for individual carbon nanotubes. Nature, 381 (6584), 678-680. 1996.
[46] Nicolas D. Fibers obtained from carbon nanotubes vertically aligned: elaboration and properties, doctoral thesis, University paris-sud, 2014.
[47] S. Zhang, K. K. K. Koziol, I. a Kinloch, and A. H. Windle, "Macroscopic fibers of well-aligned carbon nanotubes by wet spinning.," *Small*, vol. 4, no. 8, pp.1217–22, Aug. 2008.
[48] N. Behabtu, C. C. Young, D. E. Tsentalovich, O. Kleinerman, X. Wang, A. W. K. Ma, E. A. Bengio, R. F. terWaarbeek, J. J. de Jong, R. E. Hoogerwerf, S.B. Fairchild, J. B. Ferguson, B. Maruyama, J. Kono, Y. Talmon, Y. Cohen, M.J. Otto, and M. Pasquali, "Strong, light, multifunctional fibers of carbonnanotubes with ultrahigh conductivity" *Science*, vol. 339, no. 6116, pp. 182–6, 2013.
[49] J. Steinmetz, M. Glerup, M. Paillet, P. Bernier, and M. Holzinger, "Production of pure nanotube fibers using a modified wet-spinning method," *Carbon*, vol.43, no. 11, pp. 2397–2429, Sep. 2005.
[50] X. Zhang, Q. Li, Y. Tu, Y. Li, J. Y. Coulter, L. Zheng, Y. Zhao, Q. Jia, D. E.Peterson, and Y. Zhu, "Strong carbon-nanotube fibers spun from long carbon nanotube arrays.," *Small*, vol. 3, no. 2, pp. 244–8, Feb. 2007.
[51] X. Zhang, K. Jiang, C. Feng, P. Liu, L. Zhang, J. Kong, T. Zhang, Q. Li, and S. Fan, "Spinning and Processing Continuous Yarns from 4-Inch Wafer Scale Super-Aligned Carbon Nanotube Arrays," *Adv. Mater.*, vol. 18, no. 12, pp.1505–1510, Jun. 2006.

[52] J. Jia, J. Zhao, G. Xu, J. Di, Z. Yong, Y. Tao, C. Fang, Z. Zhang, X. Zhang, L.Zheng, and Q. Li, "A comparison of the mechanical properties of fibers spun from different carbon nanotubes," *Carbon*, vol. 49, no. 4, pp. 1333–1339, Apr.2011.
[53] A. Ghemes, J. Muramatsu, Y. Minami, M. Okada, Y. Inoue, and H. Mimura, "High Performance Carbon Nanotube Fibers Spun from Long Multi-Walled Carbon Nanotubes," vol. 3, no. 1, pp. 2011–2013, 2012.
[54] S. Zhang, L. Zhu, M. L. Minus, H. G. Chae, S. Jagannathan, C.-P.Wong, J.Kowalik, L. B. Roberson, and S. Kumar, "Solid-state spun fibers and yarns from 1-mm long carbon nanotube forests synthesized by water-assisted chemical vapor deposition," *J. Mater.Sci.*, vol. 43, no. 13, pp. 4356–4362, Apr.2008.
[55] K. Liu, Y. Sun, R. Zhou, H. Zhu, J. Wang, L. Liu, S. Fan, and K. Jiang, "Carbon nanotube yarns with high tensile strength made by a twisting and shrinking method.," *Nanotechnology*, vol. 21, no. 4, p. 045708, Jan. 2010.
[56] E. Pop, D. Mann, Q. Wang, K. Goodson, and H. Dai, "Thermal conductance ofan individual single-wall carbon nanotube above room temperature.," *NanoLett.*, vol. 6, no. 1, pp. 96–100, 2006.
[57] P. R. Bandaru, "Electrical Properties and Applications of Carbon Nanotube Structures," *J. Nanosci.Nanotechnol.*, vol. 7, no. 4, pp. 1239–1267, Apr. 2007.
[58] B. Q. Wei, R. Vajtai, and P. M. Ajayan, "Reliability and current carryingcapacity of carbon nanotubes," *Appl. Phys. Lett.*, vol. 79, no. 8, pp. 1172–1174, 2001.
[59] C. Laurent, E. Flahaut, and A. Peigney, "The weight and density of carbon nanotubes versus the number of walls and diameter," *Carbon*, vol. 48, no. 10, pp. 2994–2996, Aug. 2010.
[60] F. Grillard, C. Jaillet, C. Zakri, P. Miaudet, A. Derre, A. Korzhenko, P. Gaillard, and P. Poulin, "Conductivity and percolation of nanotube based polymer composites in extensional deformations," *Polymer (Guildf).*, vol. 53, no. 1, pp. 183–187, Jan. 2012.
[61] S. Berber, Y. Kwon, and D. Tomanek, "Unusually high thermal conductivity of carbon nanotubes," *Phys. Rev. Lett.*, vol. 84, no. 20, pp. 4613–4616, May 2000.
[62] E. Pop, D. Mann, Q. Wang, K. Goodson, and H. Dai, "Thermal conductance of an individual single-wall carbon nanotube above room temperature.," *NanoLett.*, vol. 6, no. 1, pp. 96–100, 2006.
[63] P. Kim, L. Shi, a. Majumdar, and P. McEuen, "Thermal Transport Measurements of Individual Multiwalled Nanotubes," *Phys. Rev. Lett.*, vol. 87, no. 21, p. 215502, Oct. 2001.
[64] J. Yang, Y. Yang, S. W. Waltermire, T. Gutu, A. a Zinn, T. T. Xu, Y. Chen, and D. Li, "Measurement of the intrinsic thermal conductivity of a multiwalled carbon nanotube and its contact thermal resistance with the substrate.,"*Small*, vol. 7, no. 16, pp. 2334–2340, Aug. 2011.

CHAPTER II:

NUMERICAL AND EXPERIMENTAL STUDIES ON THE EFFECT OF MULTIWALL CARBON NANOTUBE (MWCNT) CONCENTRATION ON THERMAL AND ELECTRICAL PROPERTIES OF GLYCEROL NANOFLUID

INTRODUCTION

Heat transfer, very common in the industrial and technological world (liquid engine cooling, lubricating oils, heat transfer fluids from solar panels and heat exchangers...) often use liquids with very low conductive heat. Metals have the highest thermal conductivities available but do not allow easy thermal contacts. Conventional fluids such as Glycerol have poor thermal properties that restrict the heat transfer performance compared to most of the solids. Many techniques are available in order to increase heat transfer rates and reduce the size of heat transfer equipment [1]. Thermal conductivity is one of the thermophysical properties of nanofluid and depends on several parameters such as thermal conductivities of the base fluid and the nanoparticles, the volume fraction, the shape and kind of the nanoparticles, the surface area, and the temperature [2]. The key idea is to exploit the solid particles with very high thermal conductivity that can be several hundreds of times greater than all of the conventional fluids combined. A few years ago solid particles of millimeter and micrometer in size were suspended in the conventional fluids to improved thermal behavior but some serious problems emerged by use of these types of fluids. For example, poor stability of the suspension and high erosion and pressure drop in pipelines and equipment. With the advent of nanotechnology, nanoparticles in size between 1 nm and 100 nm were replaced instead of particles in order of millimeter and micrometer. This type of fluid is called nanofluid [3]. The stability and heat transfer rate of nanofluids are extraordinarily higher than those of suspensions containing particles in the size of millimeter or even micrometer. Among the various nanoparticles, carbon nanotubes (MWCNTs) due to their very excellent thermal conductivity and large aspect ratio are a good choice to prepare nanofluids [4]. Preparation of stable suspension, the surfactant addition is an effective way to enhance the therefore in the dispersibility of MWCNTs [6]. However, surfactant molecules attaching on the surfaces of MWCNT may increase the thermal resistance between the MWCNT and the base fluid [7], which limits the enhancement of the effective thermal conductivity. Raykar et al. investigated the effect of temperature and Brownian motion on the enhancement of effective thermal conductivity of carbon nanotube based nanofluids [5]. Their experiments revealed that the Brownian motion has a significant effect on the effective thermal conductivity. Also, they observed that the enhancement of effective thermal conductivity in dilute nanofluids is higher [8]. in this chapter that illustrates the results of the numerical study which consists in determining the thermal conductivity of our base fluid by the hot wire method and comparing it with those obtained experimentally by the 3ω method validated by classical models.

II. 1 Numerical study on the thermal conductivity of Glycerol

II. 1. 1 Different experimental method

II. 1. 1. 1 Measurement techniques

Different methods of measuring thermal conductivity are generally used, the hot wire method in transient mode being the most commonly used among the identified works. Other measurement methods can be used, like the 3ω method As such; it will be used in this work and presented in a detailed way in this chapter, stationary methods using a temperature difference between two plates or two cylinders (Benard cell) and optical methods based on the variation of the refractive index as a function of temperature. The methods for measuring the conductivity of nanofluids are listed exhaustively in the publication by Paul et al. [35]. The reader can freely refer to it.

We collected (Figure 2.1) a classification of principal measurement techniques available today, there are essentially methods called transient method from steady-state methods.

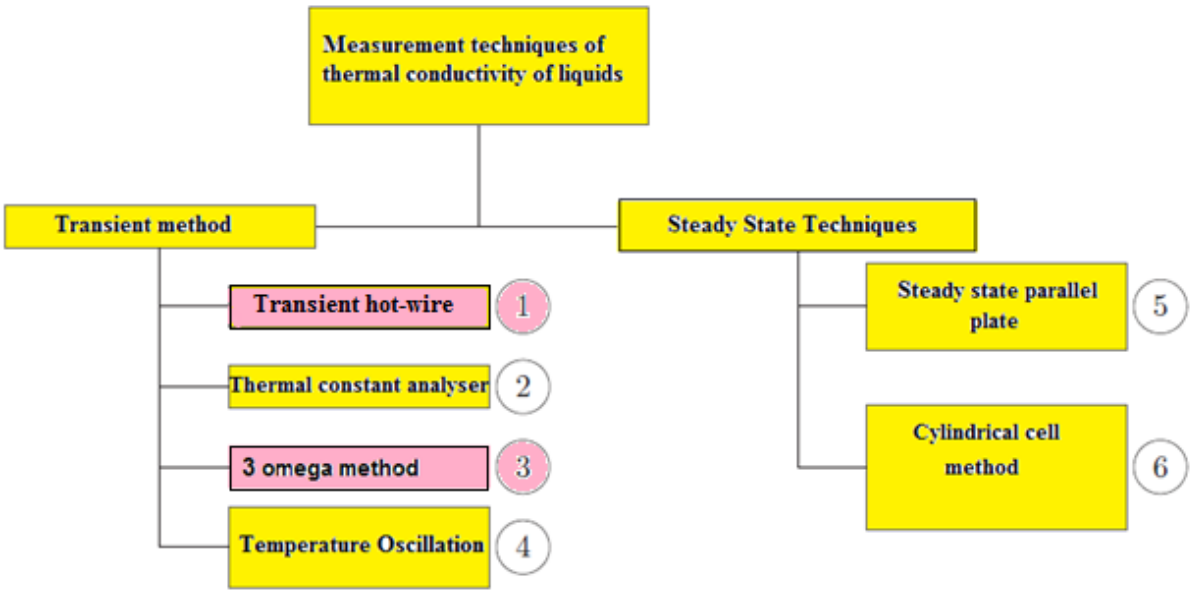

Figure 2. 1: Different thermal conductivity measurement techniques for nanofluids [35].
(*The number indicates the pre-eminence of the method in a classification based on number of publications*)

II. 1. 1. 2 Transient methods

Transient methods use the "brutal" generation of heat in the sample to be characterized using the Joule effect produced in a heating line, generally metallic, placed in thermal contact with the sample. We then measure the rapid temporal variation ΔT (t) of the temperature of the heating line which results from this brief thermal excitation, via the variation of its electrical resistance ΔR (t).

Transient methods have the following advantages:

- They are much faster (a few minutes at most) than steady-state methods (up to a few hours), thus making it possible to limit the influence of convection on the measurements;
- They determine both the thermal conductivity and specific heat of the medium to be characterized;
- The heating line can be used both as a heat excitation source and as a thermometer, thus eliminating the delicate problems of relative placement of the sensor and the heat source. This property even makes it possible to envisage, in certain very favorable cases, absolute measurements which theoretically do not require calibration of the device;
- The quantities which contain the information are electrical, which greatly facilitates the design of the instrumental device, of its interfacing;
- No special preparation of the sample is necessary;
- The thermal conductivity ranges can be significant: from 0.01W/m.K to 100W/m.K.

Obviously these methods also have some drawbacks, which are few in number:

- The heating line must have a very small radius a_1 (10µm to 25µm) which can complicate the installation of the wire and its handling;
- The length L of the wire should preferably check the relationship $L / a_1 \gg 1$ in order to limit errors due to edge effects from electrical contacts and convection. This constraint is not easy to realize when we have to characterize very small samples.
- The medium to be characterized must be insulating so that the electric current i(t) which crosses the heating wire does not also cross part of the fluid. In general, a very thin Teflon or kapton insulating sheath is used. These two materials have the advantage of being fairly good thermal conductors and of introducing very small errors in the determination of the thermal characteristics of the probed fluid.

We briefly describe three of the six methods recalled in Figure 2.1. We limit voluntarily to transient methods because they are systematically used in recent publications.

THW method

THW (Transient Hot Wire) uses a very fine platinum wire which plunges into the fluid to be characterized. A constant electric current is suddenly put in circulation in the wire,

causing there by Joule effect the release of a constant thermal energy which heats the surrounding fluid. This principle is used to measure the conductivity thermal. The experience lasts a maximum of 10 to 200 seconds, so it is very fast. The platinum wire serves both as a source of thermal energy and as a temperature sensor.

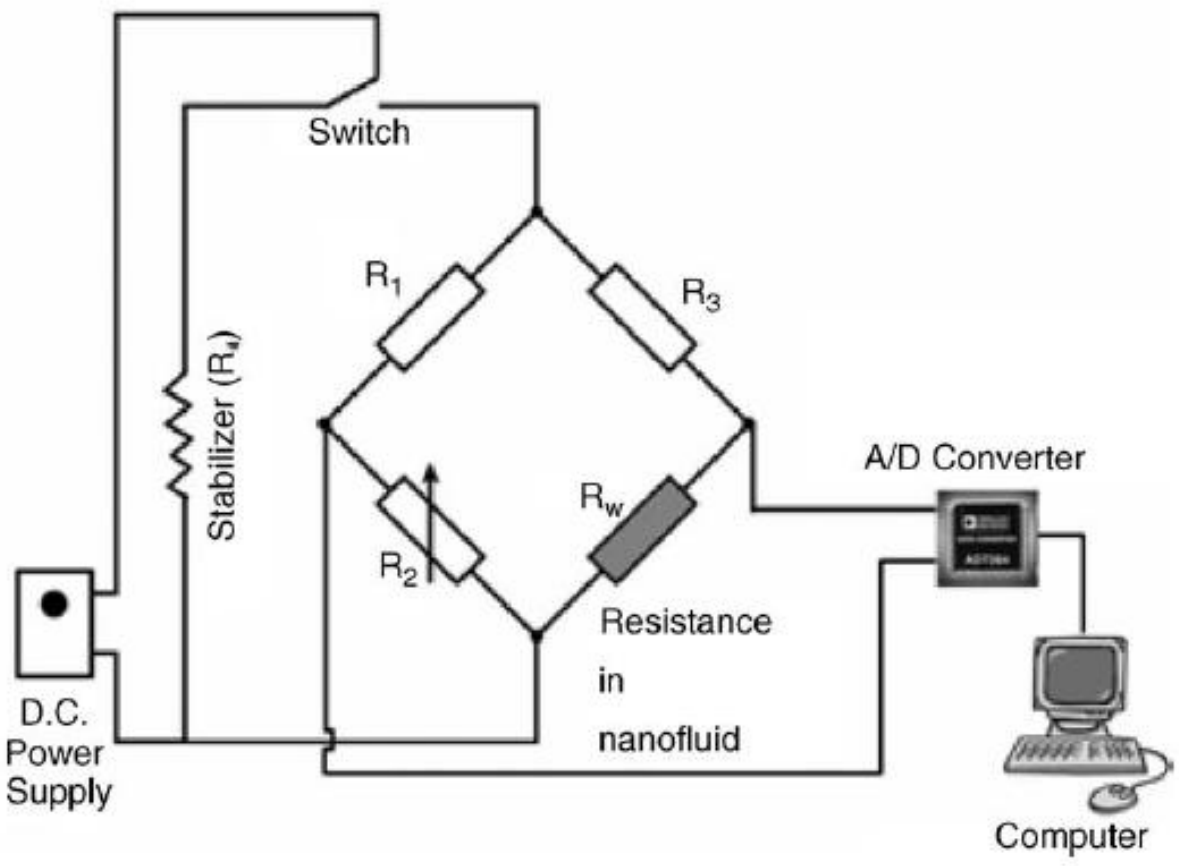

Figure 2. 2: Schematic of transient hot-wire experimental setup [35].

This method follows the theory of the hot line developed by Carslaw and Jaeger [36] and the temperature variation ΔT (a_1, t) of the wire of radius a_1 is given as a good approximation by the relation:

$$\Delta T\,(a_1, t) \approx \frac{\dot{q}DC}{4\pi K} ln \frac{4\alpha t}{{a_1}^2} - \frac{\dot{q}DC\gamma}{4\pi K} \qquad (2.1)$$

With **K** the thermal conductivity of the fluid, $\boldsymbol{\alpha}$ its thermal diffusivity, $\dot{\boldsymbol{q}}$**DC** the linear power released by the Joule effect in the platinum wire and $\boldsymbol{\gamma}$ the Euler constant.

We can easily determine the thermal conductivity **K** of the medium in which the wire dips using (2.1) from the recording of the instantaneous temperature of the heating wire, provided

that we know precisely the linear thermal power $\dot{q}$**DC**.

By measuring the temperature of the heating wire at two instants t_a and $t_b > t_a$ separated by a suitable time interval, we simply obtain the thermal conductivity of the medium by the relation:

$$K = \frac{\dot{q}_{DC}}{4\pi} \frac{\ln\left(\frac{t_b}{t_a}\right)}{\Delta T_b - \Delta T_a} \qquad (2.2)$$

We will note that in semi-logarithmic representation (figure 2.3), the points **a** and **b** used for the calculation of K are located on the linear part of the curve. This greatly facilitates the choice of points **a** and **b** suitable for the calculation of K from the experimental results.

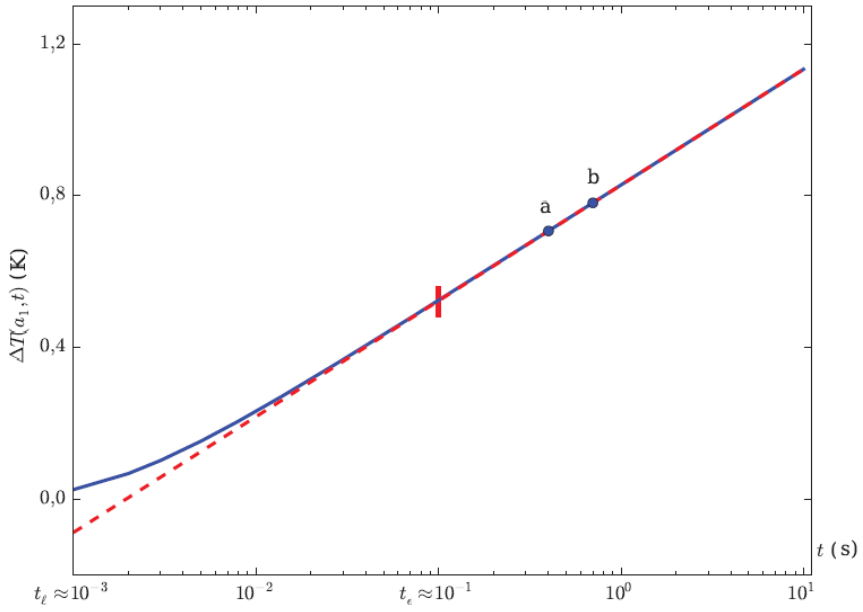

Figure 2.3: Semi-logarithmic scale representation of the variation ΔT (a_1, t) in the temperature of the heating filament immersed in pure water

Thermal constants analyzer technique

The Transient Plate Source method (TPS) is another variant of the transient method which this time uses a heating wire wound in a double spiral (Figure 2.4) which serves as both a temperature sensor and a source of thermal excitation of the fluid. The sensor is protected by a flexible kapton sheath which allows versatile use (liquids, solids, gels. . .); however, it must be fully immersed in the medium to be characterized.

The thermal constants analyzer utilizes the transient plane source (TPS) theory to calculate the thermal conductivity of nanofluid. The TPS method uses the Fourier law of heat conduction as its fundamental principle for measuring the thermal conductivity, just like the THW method.

Advantages of using this method are:

- The measurements are fast;
- Samples having wide range of thermal conductivities (from 0.02 to 200 W/m K) can be measured;
- No sample preparation is required;
- Sample size can be flexible [37]

The experimental setup (shown in figure 2.4) comprises of thermal constants analyzer, a constant temperature bath, a vessel, and a thermometer. The probe of the thermal constants analyzer is immersed vertically in the vessel containing the nanofluid. The vessel is placed in the constant temperature bath and the thermometer is immersed in the vessel to measure the temperature of the nanofluid. The thermal conductivity of the nanofluid is determined by measuring the resistance of the probe that's consists of an electrically conducting thin foil of a typical pattern which is sandwiched inside an insulating layer, as shown in figure2.5 [38].

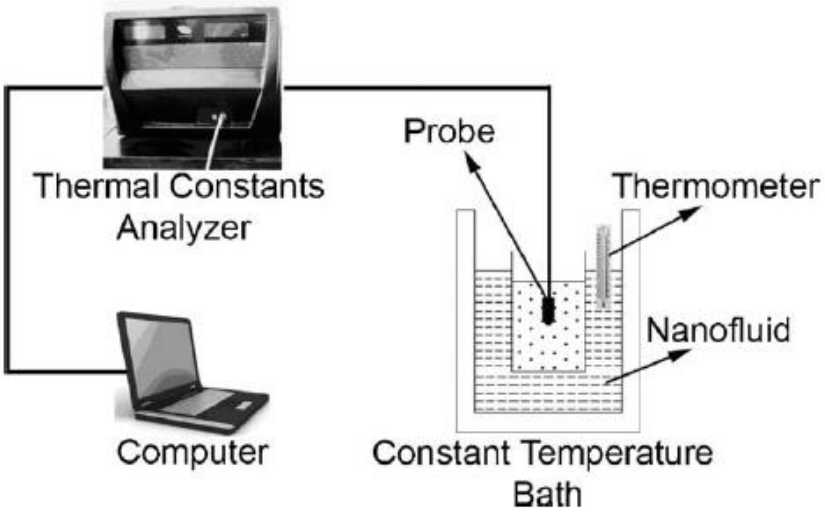

Figure 2.4: Schematic diagram of the experimental setup for transient plate source method

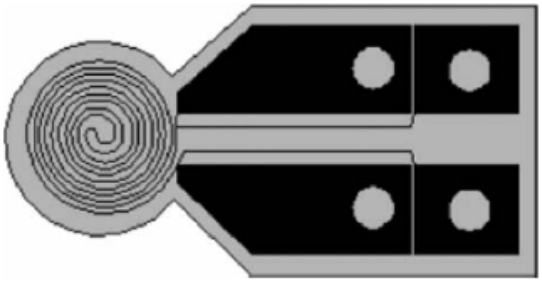

Figure 2. 5: Schematic diagram of TPS sensor.

When a constant electric power is supplied to the probe, the temperature rise ΔT (τ) of the probe, can be measured by the probe resistance with time Rp (τ) and is given according to [35] by this relation:

$$\Delta T(\tau) = \frac{1}{\alpha_R}\left[\frac{R(\tau)}{R_0} - 1\right] \quad (2.3)$$

With α_R is the temperature coefficient of the electric resistance **R** of the probe, R_0 is the electric resistance of the probe when $\tau = 0$, and τ is the variable on the time electrification and be defined as:

$$\tau = \sqrt{\frac{t\alpha}{a_1^2}} \quad (2.4)$$

With **t** time, **α** thermal diffusivity of the fluid and $\mathbf{a_1}$ the radius of the double spiral (probe).

According to Fourier Law of heat conduction, if no natural convection of a fluid occurs, **ΔT(τ)** can also be calculated as [39]:

$$\Delta T(\tau) = \frac{W}{K a_1 \pi^{1.5}} D(\tau) \quad (2.5)$$

With **k** is the thermal conductivity, **W** is the electric power supplied to the probe and **D(τ)** is a geometric function:

$$D(\tau) = \int_0^\tau d\sigma(\sigma^{-2}) \int_0^1 v dv \int_0^1 u du \times exp\left(\frac{-u^2-v^2}{4\sigma^2}\right) I_0\left(\frac{uv}{2\sigma^2}\right) \quad (2.6)$$

I_0 is a modified Bessel function.

The main disadvantages of this sensor are the price of its commercialization (in 2008 more than 10000 Euros with the instrumentation) and its dimensions which make it difficult to use with low quantities.

3ω method

The 3ω method is another variant of the transient method which uses a harmonic electric current $i(t) = \hat{I}\cos\omega_0 t$ rather than a constant current as in THW method with modern means of detection (synchronous detection amplifier, instrumentation amplifier, harmonic analysis, etc.) this method makes it possible to use excitation current of low amplitudes, thus limiting the losses by thermal radiation, as well as the influence of

convection in the liquid and the appearance of non-linear phenomena of self-heating of the liquid and the heating wire.

The harmonic current i(t) generates by Joule effect within the wire a thermal power of pulsation $\omega = 2\omega_0$ which itself generates a variation of the temperature of the wire, and therefore of its electrical resistance, each comprising a component of pulsation $2\omega_0$. Finally the electrical voltage across the wire will present a very low harmonic component (a few μV) of pulsation $\omega = 3\omega_0$ which contains all the information on the process heating and therefore on the thermal properties of the fluid. It is from the detection of this tension that the method takes its name.

It is Cahill [40] who proposed for the first time the equations which govern in method 3ω, the harmonic variation of temperature **ΔT (t)** of a thin heating tape (figure 2.6) of width 2b, deposited by spraying on a solid insulating substrate.

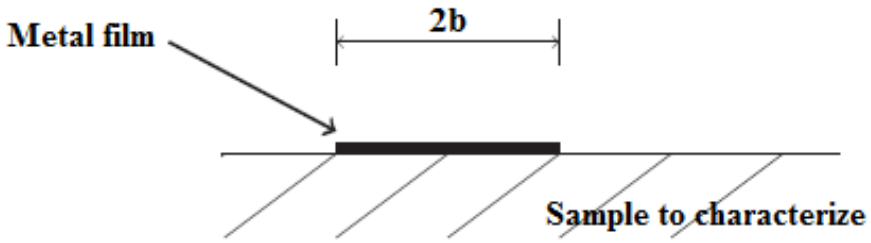

Figure 2.6: Metal film of width 2b that is evaporated on the surface of the sample to be characterized [40].

Assuming the semi-infinite substrate, Cahill has demonstrated that the amplitude of the averaged temperature **ΔT (t)** over the entire width of the ribbon is given by:

$$\Delta T = \frac{P}{l\pi K}\int_0^{\infty} \frac{sin^2 Kb}{(Kb)^2\sqrt{(K^2+q^2)}}\,dk \qquad (2.7)$$

With $\frac{P}{l}$ the amplitude of the power per unit length generated at a frequency 2ω in the line source of heat.

The magnitude of the complex quantity:

$$\frac{1}{q} = \sqrt{\left(\frac{\alpha}{i2\omega}\right)} \quad \text{and} \quad i^2 = -1 \qquad (2.8)$$

$\boldsymbol{\alpha}$ is the thermal diffusivity of the material.

The application of transient methods to the thermal characterization of liquids poses the delicate problem of the appearance of natural convection within the fluid. The 3ω method is no exception to this problem. In the case of glycerol, the influence of convection on thermal measurements is negligible at temperatures close to ambient.

Presentation of the model - Heat equation (Ideal physical model).

The ideal physical model used in the heating line method is as follows. An infinitely long and infinitely thin heating line, conductive of the electric current, plunges into an immobile fluid whose thermal conductivity must be measured. The fluid is assumed to have infinite spatial expanses. Thermal energy is suddenly supplied to the fluid due to the Joule effect reigning within the heating line. The equation that governs heat transfers in this device is the equation of heat for an unsteady radial (one-dimensional) heat transfer, the heating line being the axis of cylindrical symmetry of the device. The differential heat conduction equation satisfied by the temperature field T (x, y, z, t) in the surrounding environment the heating wire is written, in the usual Cartesian coordinate system:

$$\frac{\partial^2 T}{\partial x^2} + \frac{\partial^2 T}{\partial y^2} + \frac{\partial^2 T}{\partial z^2} = \frac{1}{\alpha}\frac{\partial T}{\partial t} \qquad (2.9)$$

With $\boldsymbol{\alpha} = \frac{K}{\rho C}$ the thermal diffusivity of the medium (in $m^2.s^{-1}$), **K** being the thermal conductivity of the medium surrounding the heating wire (in $W.m^{-1}.K^{-1}$), **ρ** being the density of the fluid (in $kg.m^{-3}$) and **C** being it's the specific heat (in $J.kg^{-1}.K^{-1}$). The physical characteristics of the fluid and the wire are assumed to be constant, it is the linear approximation.

We focused in this work on highlighting the influence of nanoparticles on the thermal properties of the host fluid, by comparison with the results obtained in the absence of particles. After a calibration and evaluation phase of the device on common fluids (deionizer water, pure Glycerol), we carried out relative measurements according to the temperature of the system and the volume fraction in nanoparticles.

This equation is used to deduce the thermal conductivity of the nanofluids from the measurement of X (the amplitude of the phase component) by varying the excitation frequency $\boldsymbol{\upsilon_o} = \frac{\omega_0}{2\pi}$

$$\boldsymbol{X} = \frac{\alpha_{pt} R_{ref} R(T_i) G\hat{I}^3}{8\pi K L}\left(\frac{1}{2} ln \frac{2\alpha}{a_1^2} - \gamma - \frac{1}{2} ln\omega_0\right) \qquad (2.10)$$

We then trace $\boldsymbol{X}$ as a function of $\boldsymbol{\upsilon_o}$ in logarithmic representation. The slope **PX** of the linear

part of this graph allows determining **K** with precision:

$$\boldsymbol{PX = -\frac{\alpha_{pt} R_{ref} R(T_i) G \hat{I}^3}{16\pi K L}} \qquad (2.11)$$

Note that it is not necessary to re-balance the bridge for each point in the interval] 0,$\upsilon_o max$] provided that the temperature $\mathbf{T_i}$ of the liquid is kept constant during the entire measurement. We validated the operation of our experimental device by measuring the thermal conductivity of pure glycerol. The measurements were performed at room temperature in order to minimize the effects of convection. The quantities of material used being small, we used a relatively short platinum wire.

The main characteristics of the materials used are recalled here:

Platinum wire: Teflon Insulated Platinum Wire of high purity (99.99%) of radius = 25 µm protected by a Teflon sheath of thickness e = 25 µm. The length L of the wire is 2 cm. The platinum temperature coefficient is α_{pt} = 3.92 × $10^{-3}K^{-1}$. The wire's reference resistance is R_{ref} = 1.2 Ω. For this graph the amplification is G = 995, the resistance of the platinum wire is R (Ti) = 1.13 Ω the intensity of the excitation current is equal to the equilibrium of the bridge Î= 148mA.

Glycerol: we used pure glycerol purchased from Sigma-Aldrich.

We reproduce here a typical series of measurements which lead, by the use of (2.10), to a thermal conductivity K_{mes} = 0.284 W/m.K. The accepted value at 25°C is K = 0.285 W/m.K. The relative error is 0.35%.

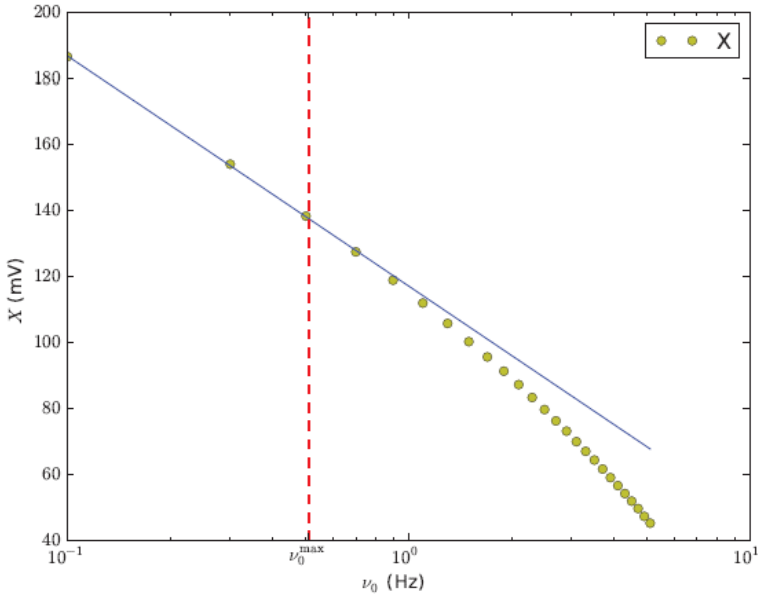

Figure 2.7: Typical experimental series of measurements of X obtained with Glycerol at 25 °C.

II. 1. 2 COMSOL Multiphysics Simulation of THW method

II. 1. 2. 1principle

COMSOL Multiphysics is a general-purpose simulation software for modeling designs, devices, and processes in all fields of engineering, manufacturing, and scientific research. In addition to using multiphysics modeling for our own projects, we can also turn our models into simulation applications. We can simulate electromagnetics, structural mechanics, acoustics, fluid flow, heat transfer, and chemical engineering.

The COMSOL Multiphysics software allows us to model the problem that interests us, namely the heating of a platinum micro-wire immersed in Glycerol. It is a tool for solving partial differential equations of finite elements. The modeling of a system such as the one studied here takes place in several stages. The first step is to define the physics “modules” that will be used. In this case, it will be the thermal module "heat transfer in solids and liquids" and the electrical module "Joule heating". The following modeling phases are common to other physical modeling software. In chronological order, there are:

- Representation of the geometry of the system.
- Choice of different materials in the library.
- Setting up of the boundary and initial conditions in each module.
- Mesh of the elements of the structure.
- Choice of the solvent and the parameters of convergence, then resolution of the problem.
- Processing of calculated temperature and electric current data.

In the last phase of results processing, several tools are available to represent any computable physical quantity in the complete model, along a plane, along a line or a point. The quantities represented in 2D can also depend on time if the study is carried out in an unstable state. We can then process the results directly in the software via the “report” tab or under another software such as Exel or OriginePro as in our case. The particular interest of COMSOL lies in the possibility of coupling different physical models. It is also possible to work in steady state and in transient regime. The convergence of calculations in stationary mode is obviously faster. The work presented below therefore consists of following the different stages of creating a model under COMSOL. One of the most delicate parts of this work consists in introducing the physics and the parameters used during the modeling (equation, initial conditions, boundary conditions, electrical model).

For this study, we approach the problem from two approaches. In the first case, we are

interested in the two-dimensional (2D) modeling of a section of the experimental setup. Secondly, given the limitations of the 2D model, the last part of this study is centered on the comparison between the results of numerical simulations and the experimental measurements obtained.

II. 1. 2. 2 Simulation using Comsol Multiphysics

This chapter presents our results of the numerical approach which are discussed and correlated with the experimental data. The numerical resolution of the equations is carried out with the commercial software Comsol Multiphysics dedicated to multiphysics simulation by the finite element method. This software has both a graphical interface allowing the implementation of models in an intuitive way and a script language whose syntaxes are similar to those of Matlab [Comsol 5.3].

In the finite element method, the digital resolution consists in finding discrete solutions of the function at the nodes of each mesh. If the mesh is infinitely refined, convergence can be assured. However, it is essential to limit the number of elements for reasons of calculation time and memory. In this section, we expose the methods that we have adopted for the discretization of the geometries allowing leading to the convergence of the thermal problem solution with a reasonable number of meshes. In this first section, the basic equations and the boundary condition equations used in COMSOL to make numerical simulations are recalled. We then present the main stages of a typical modeling.

II. 1. 2. 3Definition of geometries

We considered a two-dimensional (2D) modeling for the solution of the equations. This allows us, from a numerical point of view, to reduce the computation time and the complexity of the mesh.

The platinum wire is 25µm in radius, 2cm long. The sample of the rectangle shape of 1 cm width and 2.5 cm height. Figure 2.8 shows the material geometries.

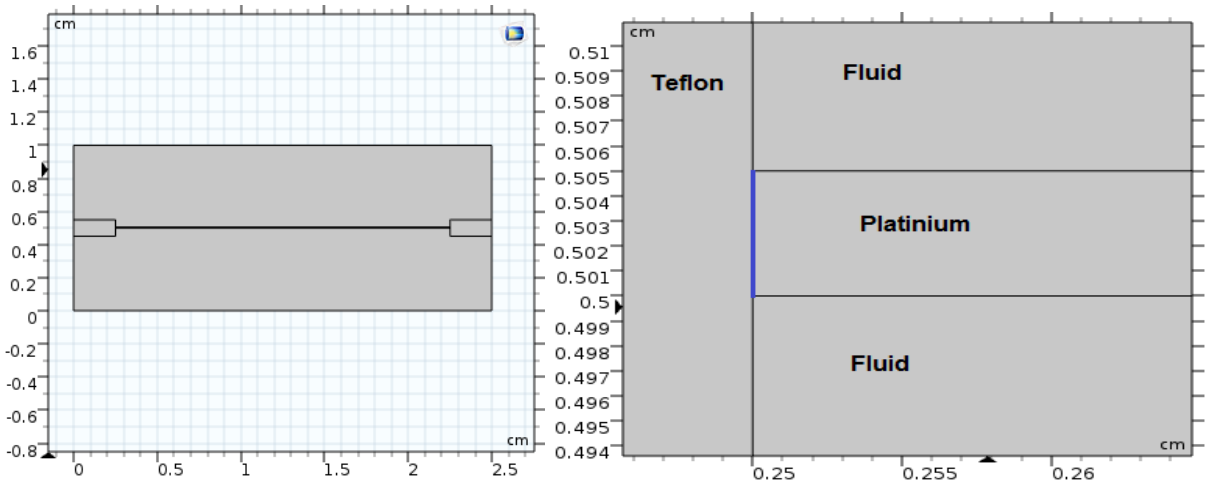

Figure 2. 8: Geometry of materials

II. 1. 2. 4Mesh of the structure

The principle of finite element simulation is based on the mesh. The choice of the latter is essential insofar as the precision of the solution depends on it. The mesh of the two subdomains modeling the platinum wire and the fluid (Glycerol). This means that the ratio between the dimensions of the elements is different from unity, which can lead to numerical instabilities.

The Comsol software offers the possibility of separating the subareas in different geometries. Figure 2.9 shows the mesh of the structure.

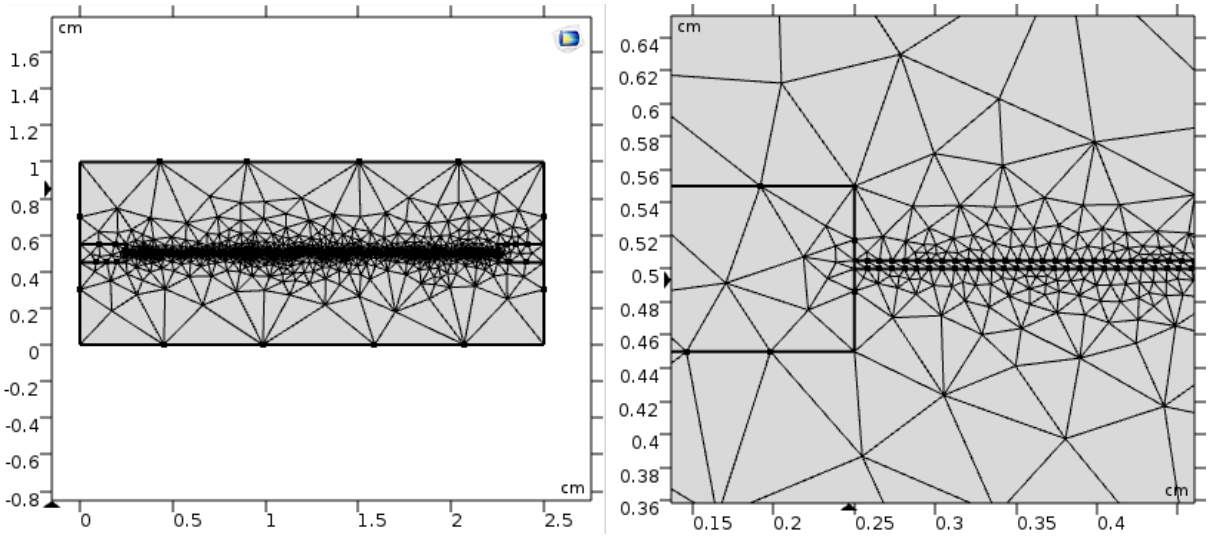

Figure 2. 9: Mesh of the structure (Normal)

II. 1. 2. 5 Heat transfer in solids and fluids

In a solid, the heat transfer equation is written:

$$\rho Cp \frac{\partial T}{\partial t} - K\,\Delta T = Q \qquad (2.12)$$

- ρ: the density, in $kg.m^{-3}$

- Cp: the thermal capacity, in J / kg.
- K: thermal conductivity, in W/m.K
- Q: the internal heat source, in W.
- T: the temperature field, in K

In the heat equation (equation 2.12), the temporal term, $\rho Cp \frac{\partial T}{\partial t}$ designates the variation of temperature as a function of time in the transient regime.

Conditions to the limits:

Thermal insulation: $(\Delta T) = 0$.

Imposed initial temperature, equal to the ambient temperature ($T_0 = 293.15$ K).

II. 1. 2. 6 Electric module

The equations solved by the electrical module are

$$\Delta . \boldsymbol{J} = \boldsymbol{Qc} \qquad (2.13)$$

$$\boldsymbol{J} = \boldsymbol{\sigma E} + \boldsymbol{Je} \qquad \text{Localized ohm's law}$$

$$\boldsymbol{E} = -\boldsymbol{\nabla V} \qquad (2.14)$$

$$\boldsymbol{\sigma} = \frac{\mathbf{1}}{\boldsymbol{\rho_0}(\mathbf{1}+\boldsymbol{\alpha}(\boldsymbol{T}-\boldsymbol{T_i}))} \qquad (2.15)$$

With:

- J is the density of the electric current, in $A.m^{-2}$
- σ: electrical conductivity, in $S.m^{-1}$
- E: electric field, in $V.m^{-1}$
- V: the electric potential, in Volt V.
- Qc: the source term, in W.
- $\rho_0 = 1{,}1.10^{-7} \Omega.m$: resistivity of Platinum
- $T - T_i = \Delta T(a_1,t)$: difference temperature in the wire of Platinum
- $\alpha = 3{,}92.10^{-3} K^{-1}$: resistivity temperature coefficient of Platinum

The experimental heating system is modeled by the term internal heat volume source Q and which represents the energy dissipated by the Joule effect in the control volume considered. This energy results from an electric power dissipated by the Joule effectper unit length:

$$\dot{\boldsymbol{q}}_{\boldsymbol{DC}} = \frac{\boldsymbol{U^2}}{\boldsymbol{R.L}} \qquad (2.16)$$

With: $\mathbf{R} = \frac{\boldsymbol{\rho_0 . L}}{\boldsymbol{S}}$: platinum resistance, **L** length of the platinum and **S** its section.

Like the THW method, the 3ω method derives from the theory of the ideal heating line developed by Carslaw and Jaeger [1]. We present the essential elements of this theory and we

apply it to the determination of the expression of the temperature variation of a platinum wire immersed in a fluid.

The thermal energy released by the heating line so continuous in time between times $t_0 = 0$ and t, is linked to the temperature variation **ΔT (r, t)** due to this heating which can be written [67]:

$$\Delta T(r,t) = \frac{1}{4\pi K}\int_0^t \dot{q}(t')\, e^{-\frac{r^2}{4\alpha(t-t')}} \frac{dt'}{t-t'} \qquad (2.17)$$

With $\dot{q}(t')$ the thermal power released per unit length of the heating wire (in W/m). Equation (2.17) is the starting point for the application of the heating line method in thermal characterization. The case of thermal power per unit of length $\dot{q}(t) = \dot{q}_{DC}$ constant is particularly interesting and can correspond, for example, to the excitation of a metal wire by an electric voltage or an electric current of constant intensities Û or Î. This situation allows us to determine the thermal conductivity of a fluid, this is the THW method. We can write:

$$\Delta T(r,t) = \frac{\dot{q}_{DC}}{4\pi K}\int_0^t e^{-\frac{r^2}{4\alpha(t-t')}} \frac{dt'}{t-t'} \qquad (2.18)$$

By setting the change of variable $u = \frac{r^2}{4\alpha(t-t')}$ we get:

$$\Delta T(r,t) = \frac{\dot{q}_{DC}}{4\pi K}\int_{\frac{r^2}{4\alpha t}}^{\infty} \frac{e^{-u}}{u} du \qquad (2.19)$$

We recognize the special "Exponential Integral" function Ei (Appendix A):

$$\Delta T(r,t) = \frac{\dot{q}_{DC}}{4\pi K} Ei\left(-\frac{r^2}{4\alpha t}\right) \qquad (2.20)$$

This relation makes it possible to determine the temperature variation ΔT (a_1, t) of a line of length L and radius a_1 verifying $a_1 \ll L$. Indeed by continuity of the temperature at the interface between the heating wire and the fluid, we have at $r = a_1$:

$$\Delta T(a_1,t) = \frac{\dot{q}_{DC}}{4\pi K} Ei\left(-\frac{a_1^2}{4\alpha t}\right) \qquad (2.21)$$

On the other hand, for t sufficiently large, we obtain from (A) in $r = a_1$:

$$\Delta T(a_1,t) \simeq \frac{\dot{q}_{DC}}{4\pi K} ln\frac{4\alpha t}{a_1^2} - \frac{\dot{q}_{DC}\,\gamma}{4\pi K} \qquad (2.22)$$

With $\gamma \approx 0,577216$ the constant of Euler. We thus find the relation (2.22) widely used in the THW method.

II. 1. 3 Simulation results and discussions

II. 1. 3. 1 Presentation of the simulation

We will present in this paragraph the simulation results of the temperature difference

as a function of time in order to determine the thermal conductivity of Glycerol by the hot wire method that we will compare them with the experimental results obtained by the 3ω method, the objective being to validate our digital model.

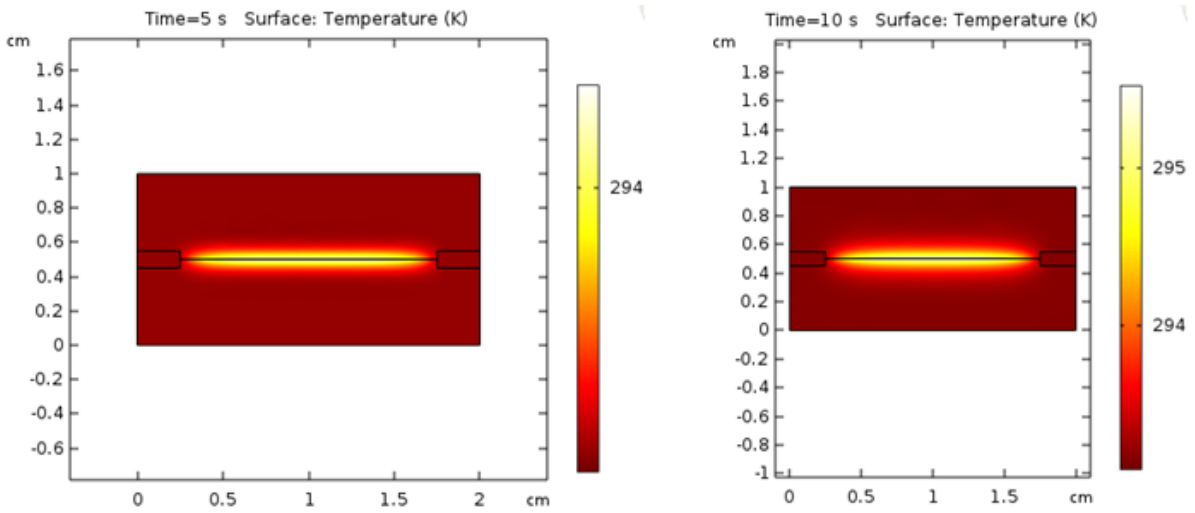

Figure 2. 10: Temperature mapping around the platinum at different times (t = 5s and t = 10s).

Figure 2.10 shows the temperature map resulting from simulations carried out in transient conditions takes into account the conduction time. The solutions are the same considering the time-dependent heat equation. For our digital study, we have considered the equation where the temperature changes over time.

It is therefore necessary to take great care in interpreting thermal conductivity measurements with our device for temperatures much higher than ambient. So we have voluntarily characterized our fluid at temperatures close to ambient in order to make the convection perfectly negligible.

The influence of natural convection is a delicate but essential question for the characterization of liquids. We have shown by numerical simulation that:

- The effect of natural convection is not detectable in the case of Glycerol at room temperature, due to its very high viscosity. The effective thermal conductivity measurements made on our fluids at room temperature are therefore clearly attributable to conduction and not to convection.
- We estimate that the maximum relative error at room temperature is an excess error of 4.36% in the case of Glycerol, using a platinum wire in a vertical position, with a length of about 2 cm and a radius of 25 μm and a variation ΔT in wire temperature of the order of 1K.

- For measurement temperatures above ambient, the influence of convection can be attenuated by lowering the variation ΔT in the temperature of the wire to values less than 1K. Only the use of synchronous detection allows the measurement of so small variations, this is the major advantage of the 3ω method over the THW method.

II. 1. 3. 2 Simulation results.

The thermal conductivity estimate by hot wire method (THW) is done from the temperature **T(*t*)** at the center of the side face of the platinum wire. We first compared the results measured experimentally by the 3ω method and the results estimated, said curves (Figure 2.11 and 2.12) being presented in the form of a relative temperature $\boldsymbol{T - T_i}$ **=ΔT(a_1,t)** where Ti denotes the initial temperature, i.e. around 293.15K.

It is observed that the two curves exhibit deviations, in particular at the start of the transient regime, which decreases over time until they become almost zero in steady state.

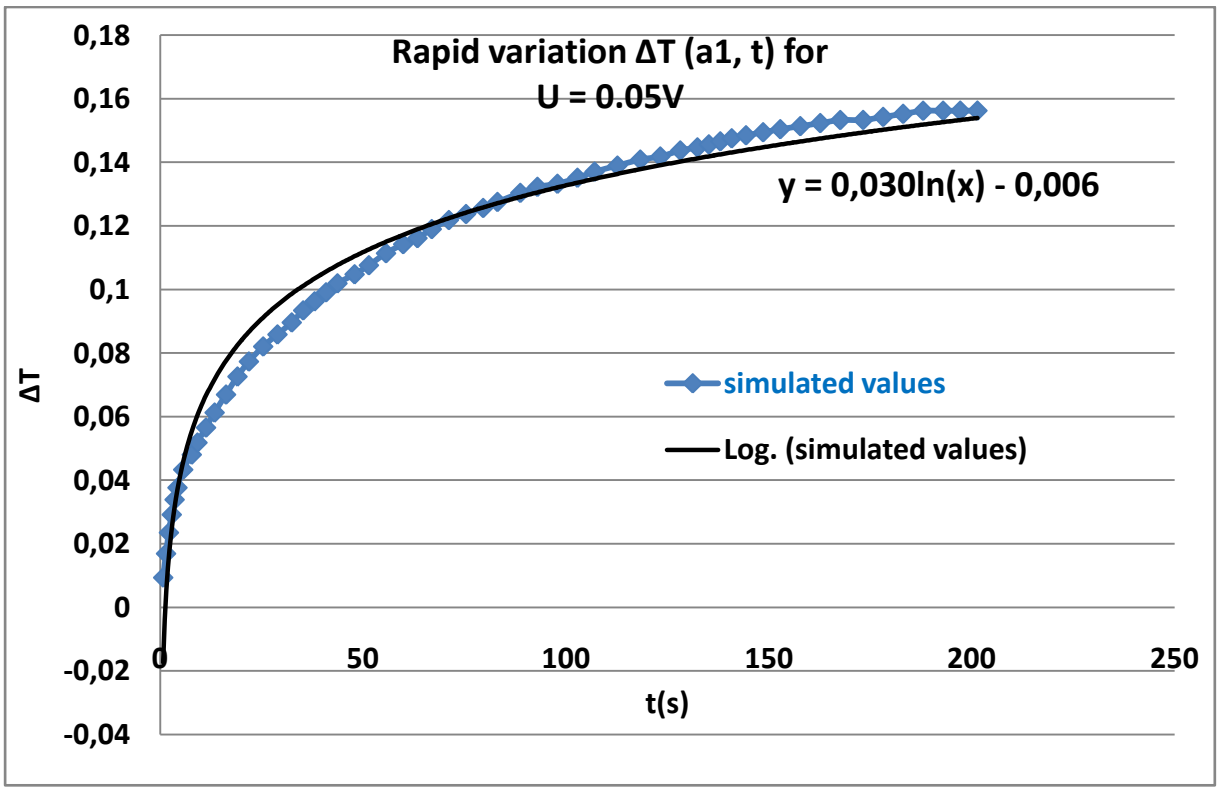

Figure 2. 11: Temperature difference at the surface along the platinum wire as a function of time in the transient case for U = 0.05V

From equation (2.22) and Figure (2.11) we can write:

$$\Delta T(a_1, t) \simeq \frac{\dot{q}_{DC}}{4\pi K} ln \frac{4\alpha t}{a_1^2} - \frac{\dot{q}_{DC}\gamma}{4\pi K} = 0.03\ln(t)-0.006$$

With: $\frac{\dot{q}_{DC}}{4\pi K} = 0.03$ and $\dot{q}_{DC} = \frac{U^2}{R.L} = \frac{0.05^2}{1.13*2*10^{-2}} = 0.1106$ W/m

And $R = \frac{\rho_0 . L}{S} = \frac{1.11*10^{-7}*2*10^{-2}}{\pi*(25*10^{-6})^2} = 1.13\Omega$ the platinum resistance.

Therefore we deduce the value of the thermal conductivity K of Glycerol:

$$K = \frac{\dot{q}_{DC}}{4\pi * 0.03} = 0.293\ W/m.K$$

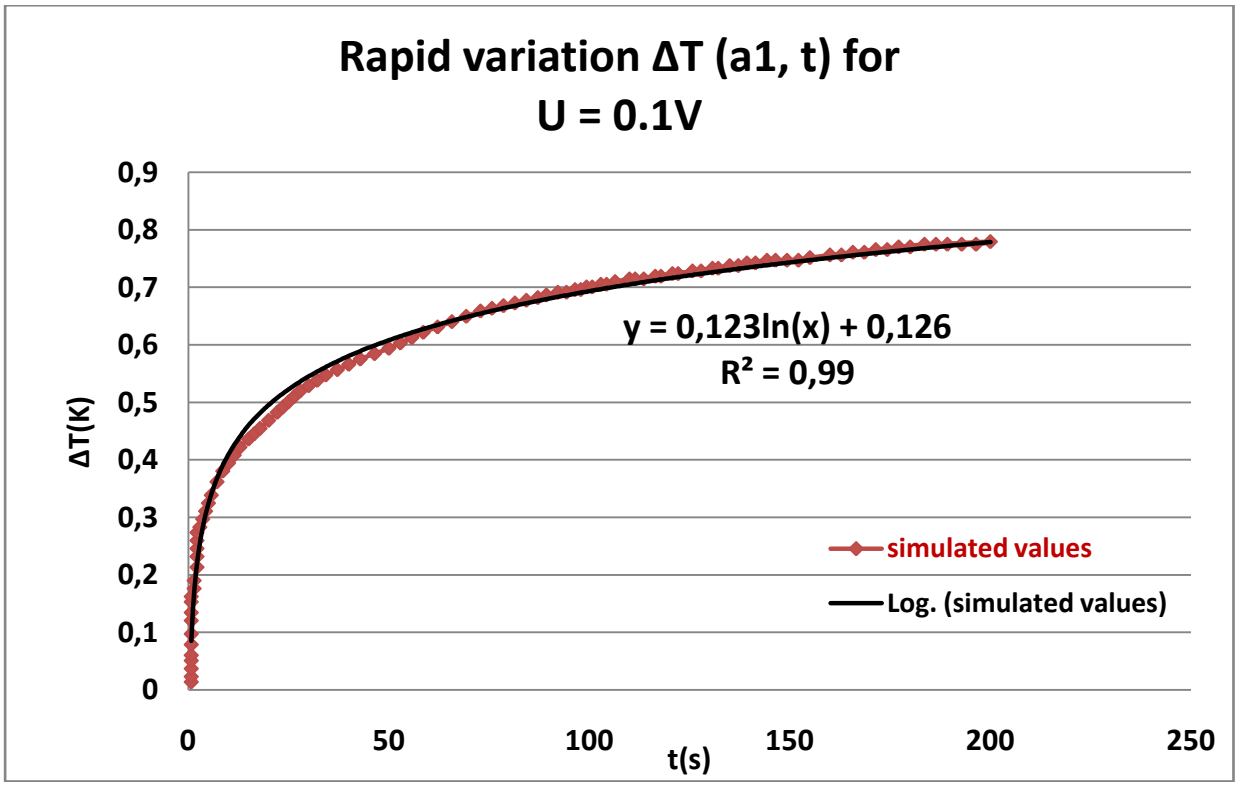

Figure 2. 12: Temperature difference at the surface along the platinum wire as a function of time in the transient case for U = 0.1V.

From Figure (2.12):

$$\Delta T(a_1, t) \simeq \frac{\dot{q}_{DC}}{4\pi K} ln \frac{4\alpha t}{a_1^2} - \frac{\dot{q}_{DC}\,\gamma}{4\pi K} = 0.123\ln(t) + 0.126$$

$$\dot{q}_{DC} = \frac{U^2}{R.L} = \frac{0.1^2}{1.13*2*10^{-2}} = 0.44248 \text{ W/m}$$

$$K = \frac{\dot{q}_{DC}}{4\pi * 0.123} = 0.286\ W/m.K$$

II. 2Experimental study on the effect of multiwall carbon nanotube (MWCNT) concentration on thermal and electrical properties of Glycerol nanofluid

II. 2. 1 State of the art on nanofluids based on carbon nanotubes

Nanofluids are composed of nanoparticles or nanofibers suspended in a liquid whose typical size is between 1 and 100 nm. This type of dispersion has aroused great interest in recent years since the discovery of their thermal properties particular. Indeed the addition in a liquid of certain types of nanoparticles, even in very small proportion (<1% by volume), is capable of increasing the thermal conductivity of the latter by 150% in the case of carbon nanotubes [9], and 40% for copper oxide nanoparticles [10]. Much research has been carried out since 2001 on this new class of fluids in order to provide a better understanding of the mechanisms involved, and thus to develop more efficient heat transfer liquids. The high thermal conductivity of nanofluids indeed designates them as potential candidates for the replacement of heat transfer fluids used in heat exchangers to improve their performance. [11] Some limitations that could reduce the impact of nanofluids as a replacement for heat transfer fluids have been studied.

Apart from the possible industrial applications of nanofluids the study of scientific interest in understanding the phenomena involved nanoscale. The thermal properties of nanofluids do not follow forecasts given by classical theories describing suspensions of solid particles in a liquid. Despite the high number of studies published on the subject in recent years, no theory succeeds in correctly describing the experimental results obtained on nanofluids [12]. It should be noted that the results obtained vary enormously from one publication to another which does not facilitate the comparison between these and the theories proposed. Additional research is needed to validate or refute the various theories proposed to describe the thermal properties of nanofluids.

In this work, we present an efficient method for measuring thermal conductivity $\boldsymbol{K_{nf}}$ for thermal applications, based on the hot wire method in periodic regime associated with a synchronous detection on the 3rd harmonic; this method has the advantage of allowing sufficiently weak thermal excitations to make the influence of convection almost negligible. G. Cahill proposed this method in 1987 [13] and then put it in place in 1990 [14] to measure the thermal conductivity of solids. This method is based on the exploitation of the frequency response of the temperature difference. These nanofluids possess enhanced electrical conductivity at very low concentrations of MWCNTs [16–19]. Also, significant enhancement

of electrical conductivity in glycerol doped by MWCNTs was reported [20]. MWCNTs +Glycerol are promising as nanofluids with intriguing heat transfer enhancement performance [21–24]. Large electrical conductivity of carbon nanotubes can result in significant increase in the electrical conductivity of nanofluid even at very small MWCNT fillings [15]. Finally, glycerol is biologically safe material, which finds widespread application in food-processing industry, medicine, and biology, and it is promising to use glycerol as a matrix in biological applications of carbon nanotubes [25].

II. 2. 2 Thermal conductivity

Thermal conductivity, noted K (W/m.K), is the ability of a material to conduct or transmit heat. This is a very important property for improving the thermal performance of a heat transfer fluid. Nanofluid synthesis meets the need to improve and amplify the thermal conductivity of liquids. Also, a lot of works has been done to measure this conductivity also to predict and explain this enhancement.

II. 2. 3 Materials and experimental methods

II. 2. 3. 1 Materials used

As a liquid system, we used glycerol (purity 99% to 101% purchased from Sigma-Aldrich) , $C_3H_8O_3$ which was characterized by a molecular weight of 92.09 g/mol, a melting point of 291.3 K, and a density of 1.261 g/cm^3 at a temperature of 293 K. The typical diameters of MWNTs used in this study, ranged from 50 to 120nm while the lengths were mostly from 2µm to 50µm and the density is about 1.65 g/cm^3. The nanofluid of Glycerol based MWCNT was prepared as follows:

In this paper, a stable solution was obtained by dissolving 1.3 mg of MWNTs measured by METLLER TOLEDO XPE 26 balance (a display accuracy of 1 µg) in 1.5 ml of Ethanol then it introduced in 30 ml of Glycerol , next the nanofluids were exposed in the Ultrasound (VWR Ultrasonic Cleaner USC-T) for 30 minutes to prevent agglomeration of nanoparticles. In this study: the MWCNT content in volume fraction Φ is given by the following equation:

$$\Phi = \frac{\left(\frac{m}{d}\right)}{\left(\frac{m}{d}\right)+V_s} \qquad (2.23)$$

Where **m** and **d** are the weight and density of MWCNT, respectively; **Vs** is the volume of the Solvent (Glycerol Ethanol) and Φ=0.0025% is the particle volume fraction in the suspension. Two other nanofluids were prepared by dispersing MWCNT in the Ethanol and it introduced in Glycerol with low volume fraction of 0.005% and 0.01% as shown in figure

(2.13)

Figure 2. 13: Three nanofluids with volume fraction 0.0025%, 0.005% and 0.01% exposed in Ultrasound for 30 minutes.

II.2. 3. 2 Objectives of this study

We sought to illustrate the influence of multi walled carbon nanotubes (MWCNT) on the thermal conductivity of a pure host liquid when we go to the nanoscopic scale without using a chemical additive capable of modifying considerably this affecting. We chose Glycerol (Aldrich: Glycerol for molecular biology, 99 to 101%) rather than water as the host fluid for nanoparticles for several reasons:

- There is no particular chemical reactivity of Glycerol towards MWCNTs. This allows us to put these particles in suspension without particular functionalization and without chemical additive promoting dispersion. This property of neutralityis important because it allows us to characterize, on a macroscopic scale, the real influence of the additive on the thermal properties of the host liquid.
- A mechanical ultrasonic dispersion for several minutes is sufficient to homogenize the solution. The high viscosity of Glycerol allows then a stability of the solution for durations much greater than the duration of the experiment; The FTIR spectra were recorded to confirm this stability.
- The high viscosity of Glycerol also allows us to minimize the effects of convection on the transport of thermal energy within the fluid. The measurements makethus it possible to

characterizeonlythe thermal conduction.

- Glycerol is a bio-compatible liquid widely used in various fields of application. To our knowledge, no study has so far focused on the modifications of the physicochemical properties of Glycerol by the inclusion of nanoparticles.
- Glycerol shows excellent anti-corrosive propertiesandcan be evaluated as a corrosion inhibitor for steel specimen.
- Finally, Glycerol is a model liquid for the study of glass transitions. It seems interesting to us, in a future work, to characterize the influence of nanoparticles on the glass transition of Glycerol.

The thermal conductivity of different fluids was measured in a temperature range from ambient to 40°C.

The measurement of the thermal conductivity of nanofluids as a function of temperature is a difficult operation, which is why we used an efficient method (3ω) to measure the thermo physical properties of nanofluid. The temperature of the medium containing the nanofluid equipped with a temperature sensor was varied and the thermal conductivity of the glycerol (Φ = 0.0025%, Φ = 0.005% and 0.01% of MWCNT) was measured as a function of the temperature ranging from 20 ° C to 40 ° C. The method used is based on the synchronous detection of the 3rd harmonic of the excitation current of the platinum wire whose electrical resistivity is 1.11*E-7 (Ω.m) as shown in the figures (2.14; 2.15; 2.16).

Figure 2. 14: Measurement bench instrumented with Labview software

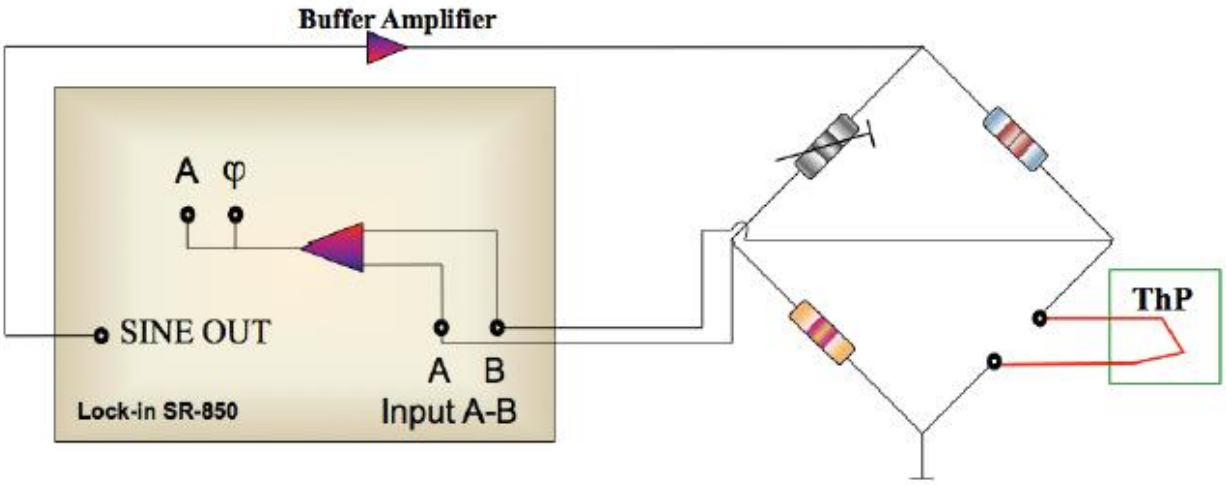

Figure 2.15: Experimental device for the 3ω method consisting of a thermal probe (ThP), a bridge Wheatstone, an amplifier (Lock-in) and a buffer amplifier

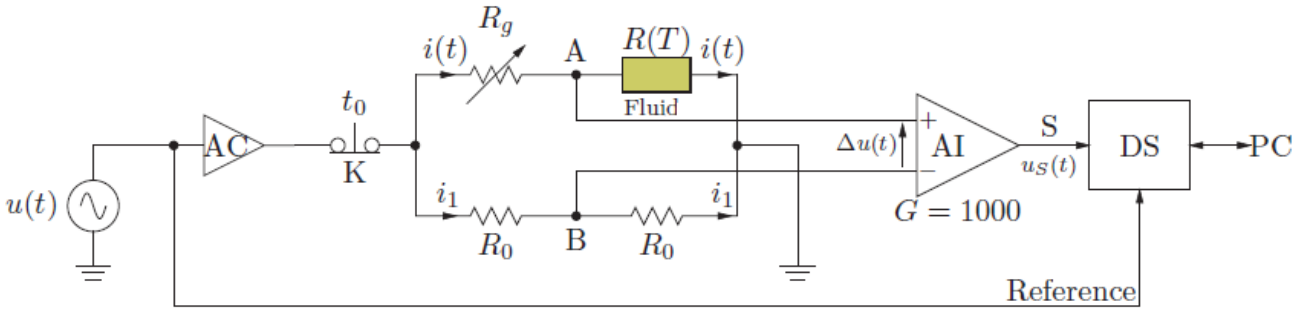

Figure 2.16: Assembly with bridge Wheatstone used in the 3ω method.

The electrical conductivities of the nanofluids were measured by Seven Compact S230 Conductivity (conductivity accuracy 0.5%; temperature accuracy 0.1°C; conductivity measuring range 0.001µS/cm to 1000mS/cm). The FTIR spectra were recorded on PerkinElmer Spectrum Version 10.4.2 FT-IR Spectrometer. FTIR studies were carried out in the range 400–4000 cm-1 in the transmittance mode.

II. 2. 4 Result and discussion

II. 2. 4. 1 Thermal conductivity analysis

Nanofluids (nanoparticle suspensions) proposed firstly by Choi [41] have attracted great interest of researchers for its intriguing properties including stabilities, good dispersibility, and high thermal conductivity. All these properties make it possible to apply nanofluids in heat transfer enhancements. According to theoretical predictions, additions of nanoparticles with high thermal conductivity into a base fluid result in enhancements of thermal conductivity of nanofluids. Carbon nanotubes (CNTs) are relatively novel materials

and many different applications have been explored because of the unique properties since their discovery by Iijima in 1991 [42]. Researchers managed to disperse small amount of CNTs with very high thermal conductivity into traditional fluids to make CNT contained nanofluids [43]. The effective thermal conductivity of the resulted nanofluids shows considerable enhancement compared with that of traditional heat transfer fluid.

The effect of temperature on the effective thermal conductivity of nanofluids is shown in Figure (2.17(a)), We observed that the thermal conductivity of nanofluid based MWCNT/Glycerol at 0.0025% volume fraction increases with temperature by up 50% over a small temperature range 20 to 40℃.Therefore, we want to investigate the temperature effect on the thermal conductivity and thermal conductivity enhancement ratio of nanofluids. It is clear that the thermal conductivities of Glycerol nanofluids are higher than those of the pure Glycerol at all the tested temperatures. It can be deduced that the temperature has a more significant effect on the thermal conductivity. The enhancement percentage of the thermal conductivity is calculated using the following equation:

$$\%\boldsymbol{K} = \left(\left(\boldsymbol{K_{nf}} - \boldsymbol{K_{bf}}\right)/\boldsymbol{K_{bf}}\right) \times \mathbf{100} \qquad (2.24)$$

Where $\boldsymbol{K_{bf}}$ is the thermal conductivity of the base fluid (Glycerol) and $\boldsymbol{K_{nf}}$ is that of the nanofluid From Figure (2.17(b)), it can be inferred that thermal conductivity enhancement ratio is affected by both temperature and volume fraction of MWCNT. Whereas, $\boldsymbol{K_{nf}}/\boldsymbol{K_{bf}}$ is the thermal conductivity enhancement ratio. By increasing the temperature at 0.0025% volume fraction from 20 to 40°C, the thermal conductivity of Glycerol nanofluid was increased between 4.3% and 50%. The maximum enhancement of thermal conductivity of MWCNT/Glycerol nanofluids occurs at 40°C. The enhancement is due to the synergistic effect of high thermally conducting Multi wall CNT sheets nanoparticles [44] Chen et al. reported that 1 vol.% of MWCNTs without surfactant, placed in ethylene glycol based nanofluid, yielded an enhancement of 17.5% [10].

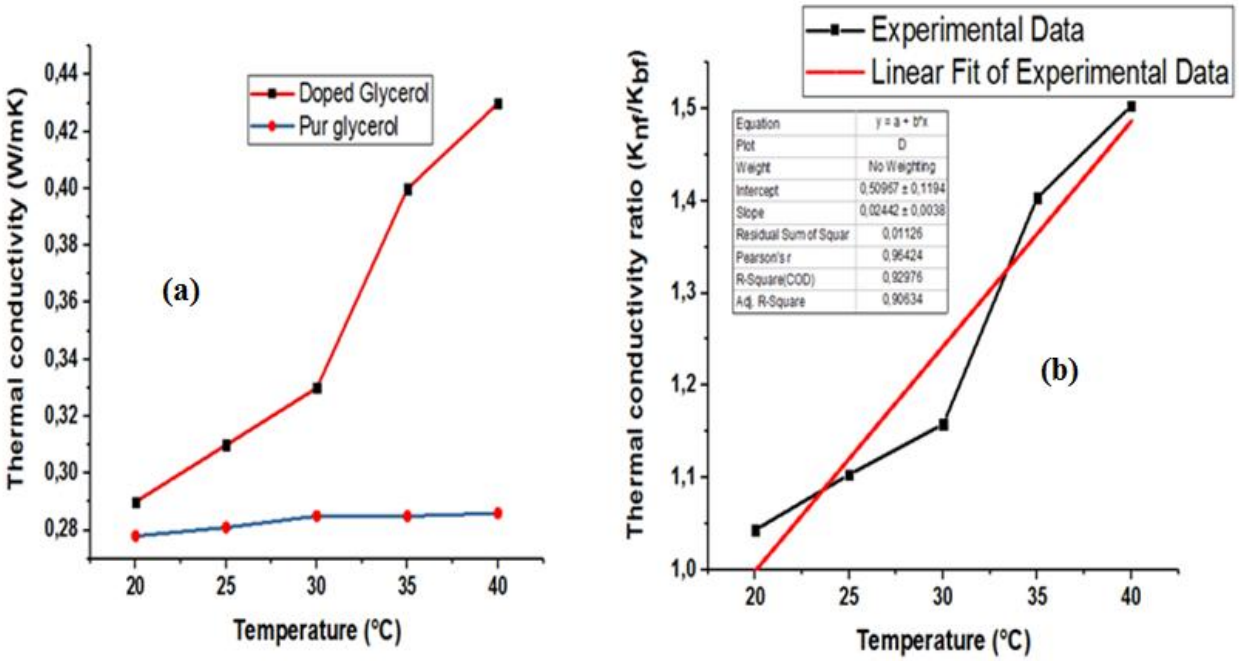

Figure 2. 17: Dependence of the thermal conductivity of MWCNT/Glycerol nanofluid and pure Glycerol on temperature (a); variation of thermal conductivity enhancement ratio of MWCNT/Glycerol nanofluids with temperature (b)

II. 2. 4. 2 Validation of the 3ω method (validation of the measuring device)

In order to verify the proper functioning of our experimental device, we measured the thermal conductivity of our pure glycerol as a function of temperature and we compared them with that of Abdellah Hadaoui [46] and CINDAS (Center for Information and Numerical Data Analysis and Synthesis). The results are shown in table 2.1.

Table 2.1: Measurements of the thermal conductivity of pure Glycerol as a function of the temperature according to CINDAS, our measurements and Hadaoui

$\theta(°C)$	**20**	**25**	**30**	**35**	**40**
K (W/m.K) (Hadaoui)	0,281	0,286	0,287	0,285	0,286
K (W/m.K) (CINDAS)	0.284	0.284	0.285	0.286	0.287
K(W/m.K) (our measurements)	0,278	0,284	0,285	0,285	0,287

We have represented in Figure (2.19) the evolution of the thermal conductivity of Glycerol as a function of temperature θ (°C) according to CINDAS, Hadaoui and our measurement

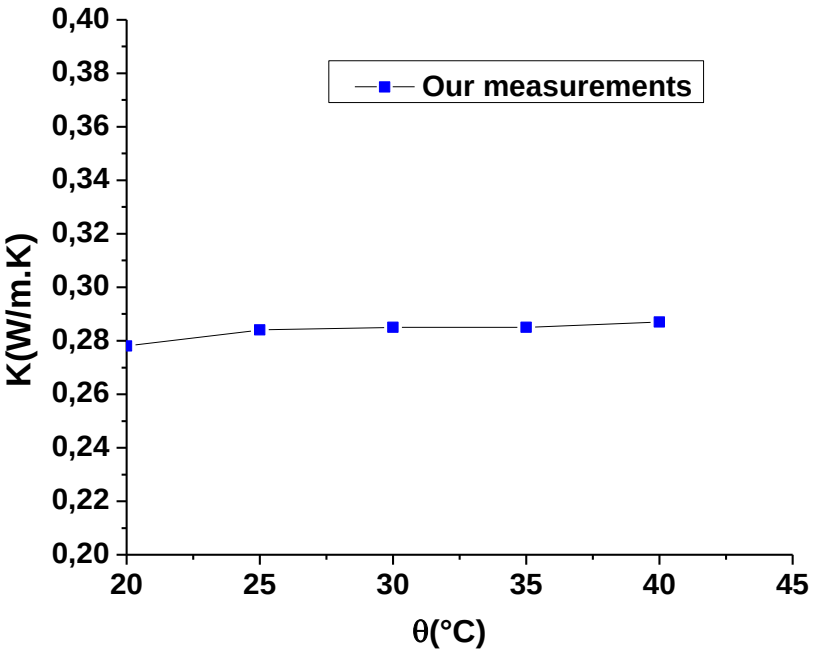

Figure 2. 18: Evolution of the thermal conductivity of pure Glycerol according to our measurements with temperature

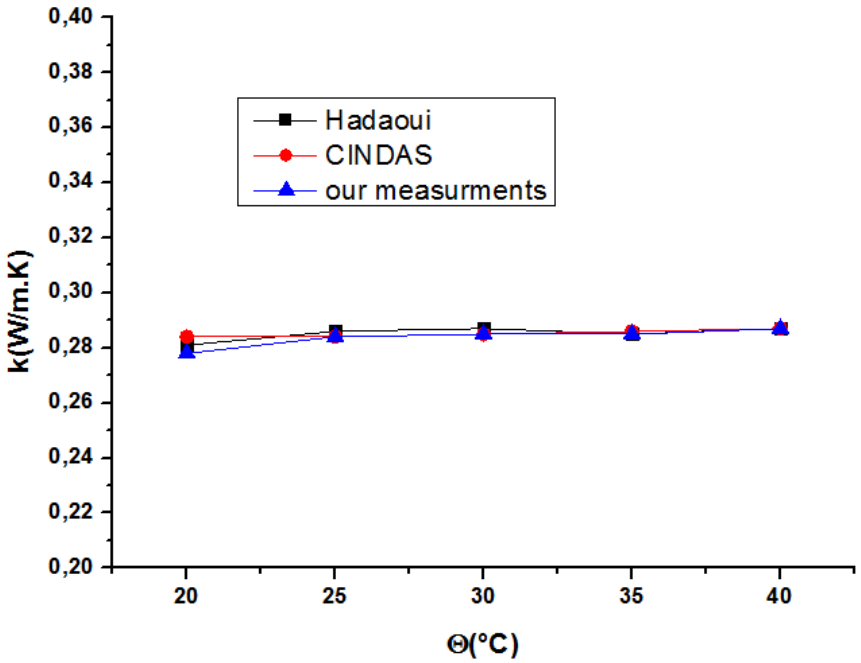

Figure 2. 19: Evolution of the thermal conductivity of pure Glycerol according to Hadaoui [46], CINDAS and our measurement with temperature

In order to validate the experimental protocol used and to assess the measurement uncertainty of the device. For this, the experimental results were compared with the data from the literature on pure Glycerol [46].

The experimental results of the evolution of the thermal conductivity of Glycerol as a function of temperature are reported in table 2.1. They show that the thermal conductivity of Glycerol increases very little with temperature, and that the maximum relative uncertainty is 2% at 20°C; this uncertainty decreases as the temperature increases, this validates the experimental protocol and establishes the confidence domain of the thermal conductivity measurements. The results are almost similar and fit well into the area of uncertainty.

II. 2. 4. 3 Bibliographic reviews

The thermal conductivity of CNT-based nanofluids has been the subject of several studies since the experimental results of Choi et al. [41] which show an increase in thermal conductivity of up to 160% at low volume concentration (1%). A significant increase in the thermal conductivity of nanofluids compared to that predicted by the conventional models presented above has often been observed. Wang et al. [47] compiled experimental results from thethermal conductivity of CNT-based nanofluids from several research teams (Figure 2.21).

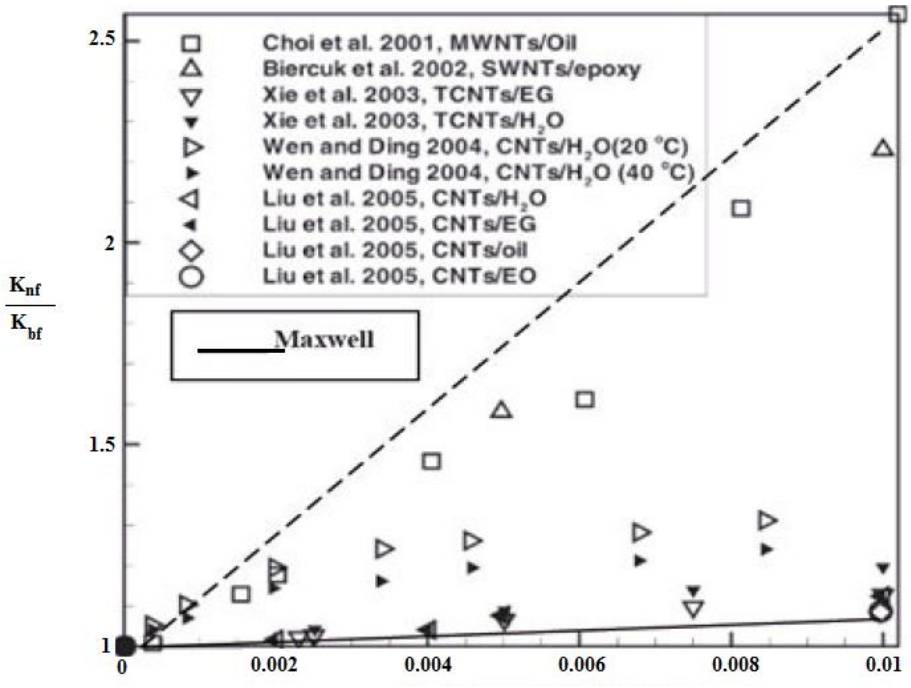

Figure 2. 20: Evolution of the relative thermal conductivity for suspensions based on carbon nanotubes according to Wang et al [47]

Figure 2.20 shows the evolution of the relative thermal conductivity of CNT-based nanofluids as a function of the volume fraction. The results of this figure show an improvement in the thermal conductivity of the nanofluids compared to the basic fluids as a function of the

volume fraction, but also a great dispersion of the experimental values of the thermal conductivity. The results also show that the model of Maxwell represented by a line in figure (2.20) does not allow the experimental points to be reproduced; the values predicted by this model are very low.

Beyond the hazards linked to the experimental characterization (type of test, uncertainty ...) Several factors can influence the thermal conductivity of nanofluids and be the cause of the disparities noted between the experimental results. Among these factors, the effects of which are discussed below, we can cite:

- The addition of CNTs or the volume fraction of CNTs;
- The temperature and nature of the base fluid;
- The presence of agglomerates

As shown in the previous figure, most of the experimental work published in the literature has revealed that the thermal conductivity of nanofluids increases in a way significant with the volume fraction of nanoparticles. Thus, Choi et al. [41] observed a non-linear increase in thermal conductivity with the volume concentration of a nanofluid based on MWCNT dispersed in oil.According to their results, the non-linear change in thermal conductivity may be due to the size, shape or interface between the CNTs and the base fluid. Unlike the results of Choi et al. [41], the results of Liu et al [48] show a moderate increase in thermal conductivity as a function of the volume concentration (12.4% for MWCNT / EG at 1% by volume and 30% for MWCNT / oil to 2% by volume), for nanofluids based on MWCNT dispersed in oil and in ethylene glycol (EG).

Xie et al. [49] experimentally measured the conductivity of a MWCNT-based nanofluid dispersed in ethylene glycol for volume fractions of 0.2%, 0.6% and 1%. Their results show an improvement in maximum thermal conductivity of around 12% at the volume fraction of 1%. These results are in agreement with those of Liu et al. [48]. Ding et al. [50] presented a maximum improvement in thermal conductivity for an MWCNT / water nanofluid at 1% by volume of around 79%. Ruan and Jacobi [51] have shown that even at very low volume fractions, between 0.05% and 0.24%, the addition of MWCNT leads to an increase in thermal conductivity from 7.5% (0.05% by volume) to 8.4% (0.24% by volume) for the nanofluid MWCNT / water studied. In the vast majority of existing work, it is established that the thermal conductivity of nanofluids increases with temperature [52], whether for nanofluids at CNT base or containing other types of nanoparticles. Ding et al. have thus found for an aqueous solution of MWCNT, that the improvement in thermal conductivity varies significantly with the temperature. According to their results, the increase in thermal

conductivity is around 15% at 20°C, 30% at 25°C and can reach up to 79% at 40°C at a mass fraction of 1 %. For the same type of nanofluid, Indhuja et al. [53] have shown that the relative thermal conductivity increases with temperature.

II. 2. 4. 4 Experimental results

We present in figure 2.21, the thermal conductivity $\mathbf{k_{nf}}$ measured experimentally by 3ω method as a function of temperatures for the nanofluids (MWCNT/Glycerol) obtained from different volume fractions ϕ = 0.0025%, 0.005% and 0.01%. The results are shown in table 2.2.

Table 2.2: Results of the thermal conductivity at different volume fractions

Temperature	Thermal conductivity at Φ=0.0025	Thermal conductivity at Φ=0.005	Thermal conductivity at Φ=0.01
20	0.29	0.32	0.35
25	0.31	0.35	0.38
30	0.33	0.39	0.43
35	0.40	0.44	0.48
40	0.44	0.47	0.52

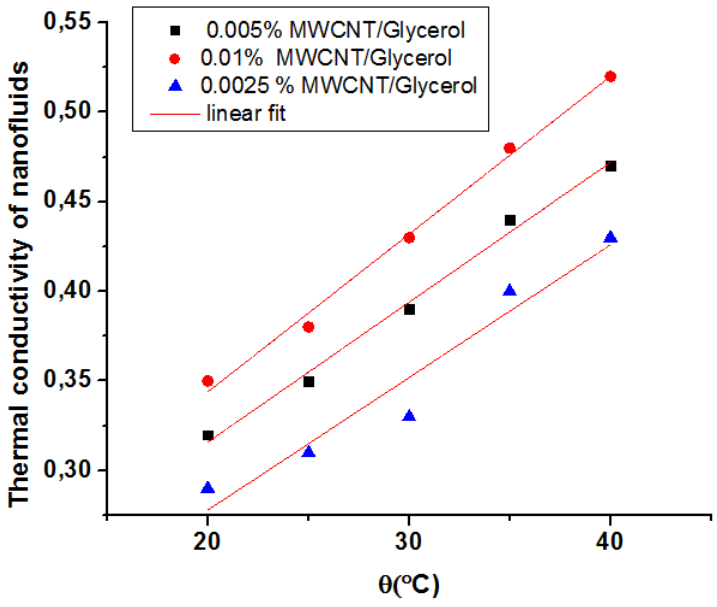

Figure 2.21: Dependence of the thermal conductivity of MWCNT/Glycerol nanofluid on temperature for different volume fractions (0.0025%, 0.005% and 0.01% of MWCNT) according to our measurements.

We observed that for a dispersion of a very small amount of nanotubes produces a remarkable change in the effective thermal conductivity of the base fluid. The thermal conductivity of

nanofluids increases in a way significant with the volume fraction of carbon nanotubes dispersed in Glycerol; these results are in agreement with those of literature and those predicted by theories using conventional models but our measured data are greater than predictions although we used small volume fractions ($\Phi \leq 0.01\%$). These are the studies of nanofluids based on carbon nanotubes that have shown up the thermal conductivity increases higher today; The shape and nature of the MWCNT nanotubes, the preparation methods, the various functionalizations and the nature of the host medium differ from a publication to another, causing great variability in the results relating to the increase in thermal conductivity. Thus it can be noted that the thermal conductivity increases for example by 10% for a concentration of 1% of nanotubes in water [54] against 38% for a concentration 0.6% nanotubes still in water [55].

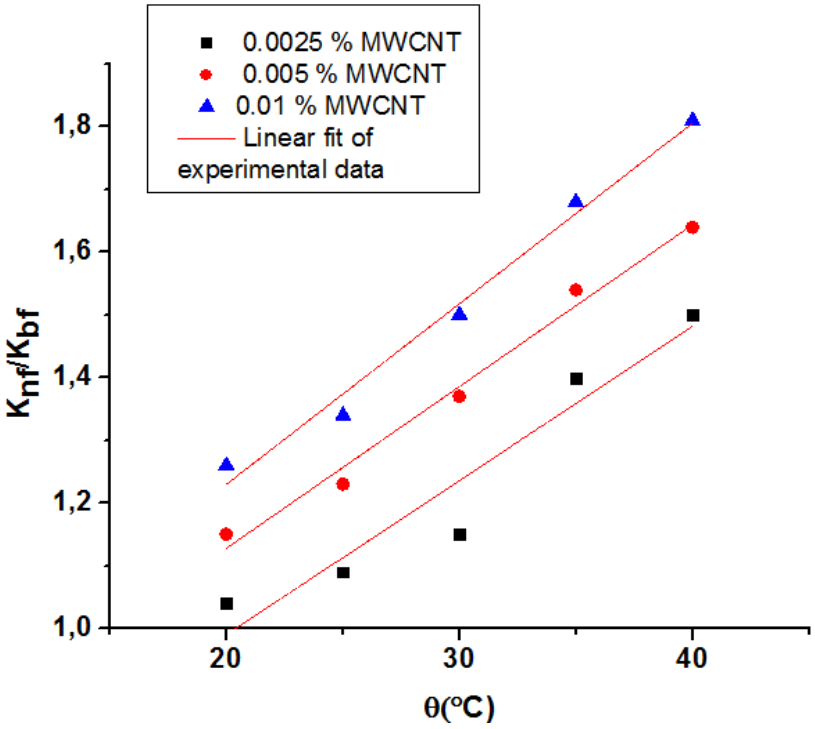

Figure 2.22: Variation of thermal conductivity enhancement ratio of MWCNT/Glycerol nanofluids with temperature for different volume fraction according to our measurement

We have noticed according to figure 2.22 that for temperatures between 20°C and 40°C, an almost linear increase in the thermal conductivity of MWCNT based nanofluidsdispersed in Glycerol, our result is comparable with that of Nassiri et al. [57], they have shown that for temperatures between 15°C and 40°C, the evolution of the rate of improvement of the thermal conductivity of nanofluids based on SWCNT, MWCNT or even DWCNT dispersed in water increases linearly with temperature while Choi et al [56] found that the thermal conductivity

of nanotube suspensions is nonlinear with nanotube volume fraction, while all theoretical predictions clearly show a linear relationship [58].

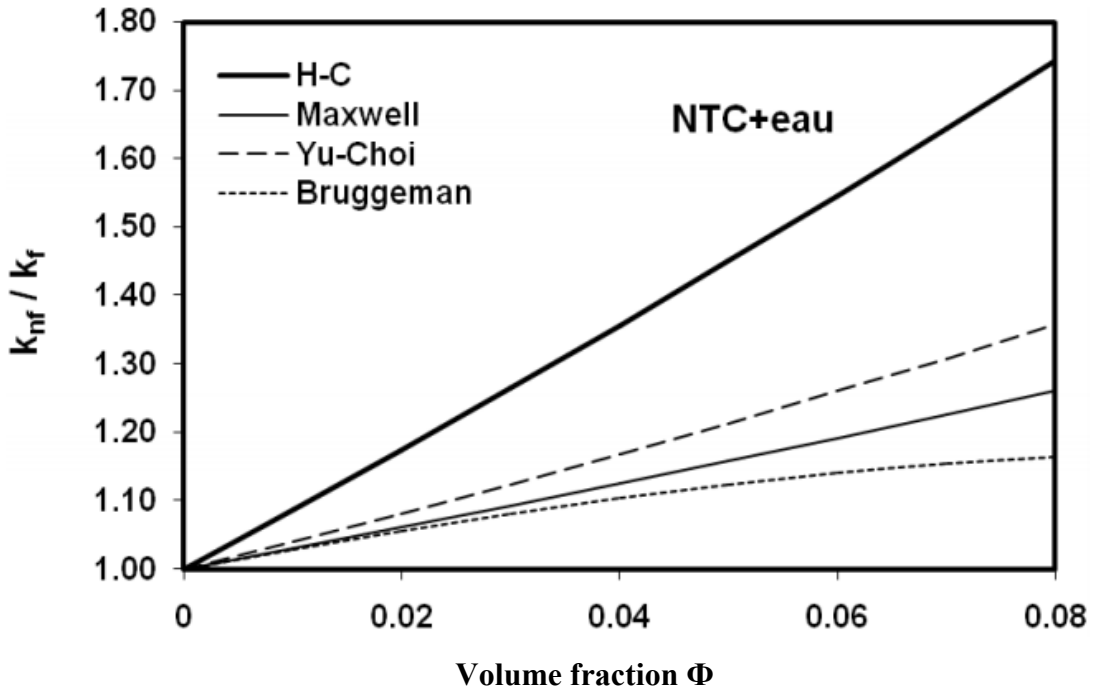

Figure 2.23: Comparison between the prediction models for the nanofluid (NTC / Water). [58]

The improvement in the thermal conductivity of nanofluids (water, carbon nanotubes) increases with volume fractions for ϕ varying from 0% to 8%.

Using carbon nanotubes as thermal conductivity k_{np} = 2500 $W.m^{-1}.K^{-1}$they obtain a 74% improvement for a volume fraction of 8% as shown in Figure 2.18.Assael et al. [58] found an improvement in thermal conductivity of the nanofluid (water + CNT) of 28% while Choi et al. [56] found an improvement of 160% for a volume fraction of 1% for the nanofluid (NTC + oil).

Remarkably, dispersion of a very small amount of nanotubes produces a dramatic increase in the effective thermal conductivity of the base fluid, with the thermal conductivity ratio exceeding **1.81** at approximately 0.01 vol % of MWCNT as shown in Figure 2.24. To show the significance of this work, we compared our measurements with theoretical predictions, it is remarkable to see that the measured conductivity enhancements, for nanotubes in Glycerol suspensions are greater than those predicted by existing theories. For example, the measured enhancement in thermal conductivity for 0.01 % of MWCNT/Glycerol is **85%** at 40°C and up to **50%** for 0.0025% at the same temperature, while the enhancements predicted by the theoretical models are not more than 15%.The interpretation of this enhancement is due to the

synergistic effect of high thermally conducting Multi wall CNT sheets nanoparticlesand an organized structure at the solid/liquid interface.

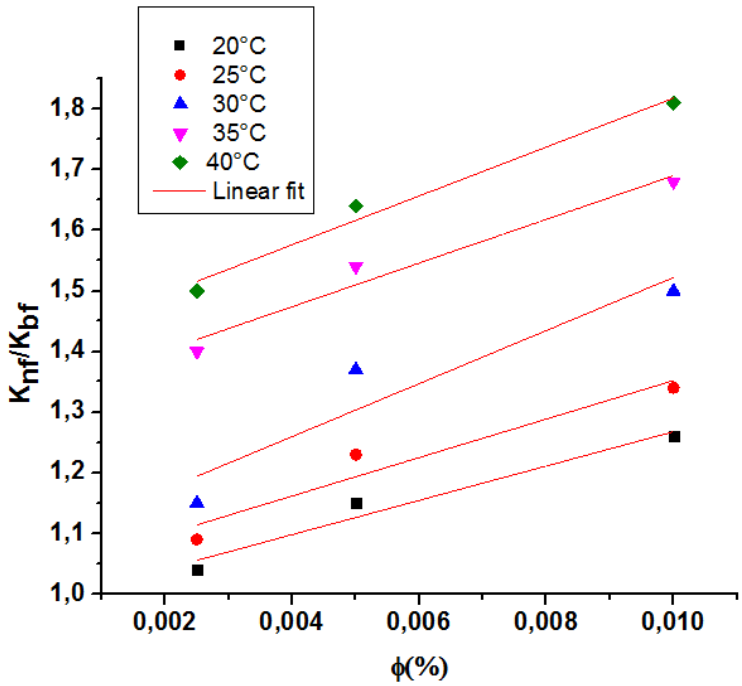

Figure 2.24: Variation of thermal conductivity enhancement ratio of MWCNT/Glycerol nanofluids with volume fraction Φ.

The use of carbon nanotube suspended in liquid for the improvement of thermal conductivity is made by Choi et al. [56] which have dispersed multi layers of carbon nanotubes 25nm in size and 50µm in length in Polyolefin Oil (PAO)at room temperature. The improvement in thermal conductivity ratio was more than 160% with ϕ = 1%, this indicates that the interaction between the fibers leads to a more high value of thermal conductivity.

Other studies have led to different results for carbon nanotubes dispersed in water. Xie et al. [49] dispersed (MWCNT) in water, the improvement in thermal conductivity of the nanofluid is 20% at a concentration of 1% by volume.

Wen and Ding [60] measured the improvement of (MWCNTs) suspended in water as a function of temperature and concentration. They found that below 30°C the thermal conductivity of the nanofluid increases linearly with increasing temperature. The maximum improvement obtained is 31% for ϕ = 0.84% at 60 ° C. The same experiment was carried out by Ding et al. [50] who found an 80% improvement for ϕ = 1% and at a temperature of 30 °C. Assael et al. [59] obtained 38% for a volume fraction of 0.6% of nanotubes in water or 150% for a concentration of 1% of nanotubes in ethylene glycol.

II. 2. 5 Comparison with Theoretical models in the literature

There are several theoretical models for estimating, under certain conditions, the thermal conductivity of suspensions. We will present in this part the most used models in the case of nanofluids.

Maxwell model

Maxwell was the first to derive a model to estimate the thermal conductivity of a suspension containing particles [26]

$$\frac{K_{nf}}{K_{bf}} = 1 + \frac{3(\alpha-1)\Phi}{(\alpha+2)-(\alpha-1)\Phi} \qquad (2.25)$$

With $\alpha = \frac{K_{np}}{K_{bf}}$

Where K_{nf}, K_{bf} and K_{np} represent respectively the thermal conductivity (W/m.K) of the nanofluid the basic fluid and the nanoparticles. Φ represents the volume fraction of nanoparticles. Maxwell's model is satisfactory for suspensions containing spherical particles of relatively low volume concentrations but does not take into account the effect of the size or shape of the particles. It should also be noted that the effect of inter-particle interactions is neglected in this model.

Bruggeman model

The Bruggeman model (Eq. 2.26) [27] complements that of Maxwell (Eq.2.25) for relatively high volume concentrations.

$$\Phi\left(\frac{K_{np}-K_{nf}}{K_{np}+2K_{nf}}\right) + (1-\Phi)\left(\frac{K_{bf}-K_{nf}}{K_{bf}+2K_{nf}}\right) = 0 \qquad (2.26)$$

This model does not take into account either the particle size or their shape.

Hamilton & Crosser model

The Hamilton-Crosser model [28] is an extension of the Maxwell model, which takes into account the shape of the particles. Indeed, to take into account the non-sphericity of the particles (case of CNTs), this model integrates a geometric factor called sphericity, and noted Ψ, referring to spherical geometry. This coefficient is defined as the ratio of the area of a sphere of the same volume as the particle to the area of this same particle.

$$\frac{K_{nf}}{K_{bf}} = \frac{K_{np}+(n-1)K_{bf}-(n-1)(K_{bf}-K_{np})\Phi}{K_{np}+(n-1)K_{bf}+(n-1)(K_{bf}-K_{np})\Phi} \qquad (2.27)$$

Where **n** is the empirical shape factor, which is defined individually by $\mathbf{n} = \frac{3}{\Psi}$ and Ψ is the sphericity. There are also some research suggested that n is generally set as 1 and 0.5 for the regularly spherical and cylindrical shapes, respectively. This model can be used when the thermal conductivity of the particles is at least 100 once higher than that of the basic fluid [28].

Xue model

Xue [29] suggested a model for calculating the thermal conductivity of CNT nanofluid, which is expressed as follows:

$$\frac{K_{nf}}{K_{bf}} = \frac{1-\Phi+2\Phi\frac{K_{np}}{K_{np}-K_{bf}}ln\frac{K_{np}+K_{bf}}{2K_{bf}}}{1-\Phi+2\Phi\frac{K_{bf}}{K_{np}-K_{bf}}ln\frac{K_{np}+K_{bf}}{2K_{bf}}} \qquad (2.28)$$

Models taking into account Brownian motion

Brownian motion is a mathematical description of the random displacements of nanoparticles within the base liquid. This movement is caused by collisions with the molecules of the base liquid which move in all directions under the effect of thermal excitation. The nanoparticles are small enough to be pushed by the shocks received and they can then travel a certain distance (very small), before leave in another direction due to new shocks and so on. This results in a chaotic overall movement which is called the Brownian motion.

Several models based on this concept have been developed in order to predict the evolution of thermal conductivity of nanofluids. Thus, Koo and Kleinstreuer [30] proposed a model in which they assumed that the thermal conductivity is made up of two terms (Eq. 2.5). The first, called static, relates to Maxwell's model, and the second is linked to the Brownian motion.

$$K_{nf} = K_{static} + K_{Brownian} \qquad (2.29)$$

$$K_{static} = K_{bf}\frac{K_{np}+2K_{bf}-2\Phi(K_{bf}-K_{np})}{K_{np}+2K_{bf}+2\Phi(K_{bf}-K_{np})} \quad \text{and} \quad K_{Brownian} = \frac{K_B T}{3\pi\mu_{bf}d_{np}}$$

With K_B the Boltzmann constant, T the nanofluid temperature, $d_{np}$the diameter of nanoparticle and μ_{bf} (Pa.s) the dynamic viscosity of the base fluid.

It should be note that for nanofluids based MWCNT, there are very few theoretical models to estimate the evolution of the thermal conductivity of the nanofluids. The Hamilton-Crosser

model (Eq 2.27) remains however the most used model in an attempt to model the experimental results. However, it appears that this model fails to reproduce the evolution of the thermal conductivity of NTC-based nanofluids [31-32], generally underestimating the measured values.

Recently, Walvekar et al. [33] proposed a thermal conductivity model for nanofluids containing CNTs which takes into account the effect of diameter, the aspect ratio of CNTs as well as the effect of Brownian motion due to temperature. This model, represented by equation 2.30, is the result of an extension of a model initially introduced by [34].

$$K_{nf} = K_{bf}\left[1 + \frac{K_{np}\left(\frac{2\Phi(r_{np}+l_{np})}{r_{np}l_{np}}\right)}{K_{bf}\left(\frac{3(1-\Phi)}{r_{bf}}\right)}\right] + \frac{C\Phi(T-T_0)}{r_{np}^2 l_{np}^2 \mu_{bf}} \ln\left(\frac{l_{np}}{d_{np}}\right) \qquad (2.30)$$

In this equation, r_{np} and l_{np} are the radius (m) and the length (m) of the CNTs, respectively. r_{bf} the mean radius of the basic fluid molecule (m).

The first part of the model is mainly related to the shape, the aspect ratio of the CNTs and the thermal conductivity of the CNTs and that of the base fluid. The second part of the equation represents the contribution of the Brownian motion of the nanoparticles related to the temperature and the viscosity of the basic fluid. T_0 is taken equal to 273 K, which corresponds to the reference temperature below which the Brownian movement becomes negligible. C is a constant which depends on the Boltzmann constant [33].

Most authors have proposed models of thermal conductivity of nanofluids that incorporate the effects of nanoparticle size, concentration, thermal conduction and Brownian motion. We have shown that it is possible to considerably increase the thermal conductivity of nanofluids without noticeable contribution of Brownian micro-convection.

As we mentioned in the literature review, the classical models of Einstein and Hamilton Crosser may be valid for suspensions of spherical particles and do not take into account the effect of size / shape of MWCNTs or interactions between the nanotubes. This is partly why these two models cannot reproduce the evolution of the thermal conductivity of the MWCNT/Glycerol nanofluid.

Xue's model (Eq. 2.28) integrates the effect of the shape of nanoparticles and it can optionally be applied for our experimental data for suspensions based on MWCNT whose volume

fraction can go up to 0.01%. The comparison of Hamilton Crosser and Xue model predictions with experimental data for Glycerol nanofluids as shown in the figure 2.25.

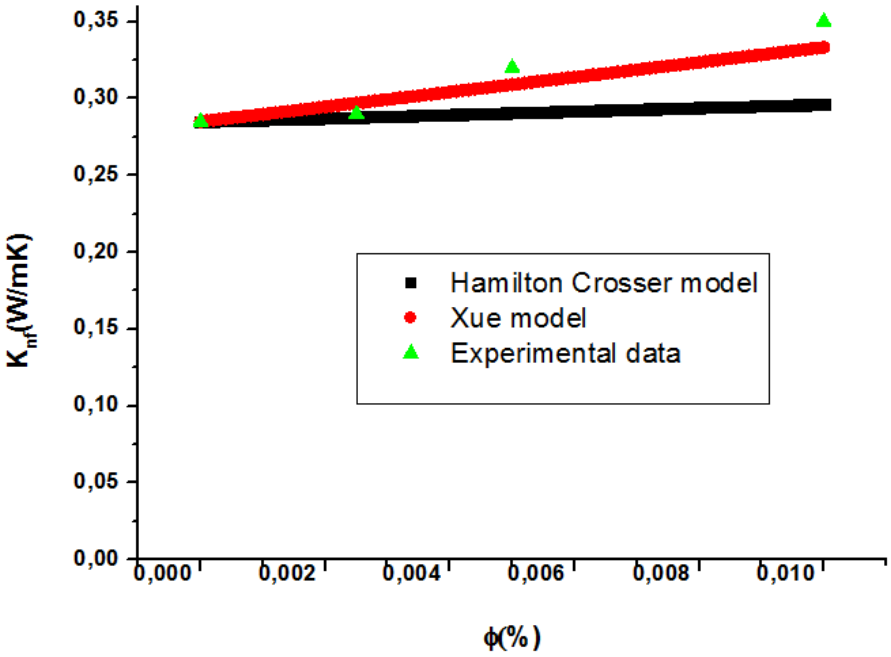

Figure 2.25: Comparison of Hamilton Crosser and Xue model predictions with experimental data for Glycerol nanofluids at room temperature

II. 2. 6 Comparison of the experimental data and the values estimated by COMSOL

The aim of this section is to study the validity of the 2D numerical model developed in order to judge its reliability in the estimation of thermal conductivity. For this, the estimation of thermal conductivity is not made here only from data from the COMSOL model but also from the experimental values measured by the 3ω method.

Table 2.3: Thermal conductivity estimated by the 2D model of COMSOL and the experimental values obtained by 3ω

	Thermal conductivity (W/m.K)	
COMSOL	**0.293**	**0.286**
Experimental (3ω method)	**0.285**	**0.284**

The table (2.3) shows the comparison between the values estimated by COMSOL and the experimental data measured by the 3ω method. It follows that the 2D model under COMSOL is suitable for estimating the thermal conductivity of our base fluid; moreover this model approaches the experimental values with an error of at most 2.8%, which makes it possible to

validate this model.

We therefore consisted of modeling the thermal conductivity of Glycerol by the hot wire method (THW) through the resolution of the heat equation under the Comsol Multiphysics software while comparing it with the experimental results obtained by 3ω method. This simulation made it possible to evaluate thermophysical quantities such as the temperature reached in the platinum wire and electrical quantities such as the potential between the terminals of the wire. The initial temperature conditions were examined. Different hypotheses were considered to carry out the modeling and avoid the numerical problems caused by the resolution of strongly nonlinear equations. These assumptions have allowed us to approach convergence as well as possible, to reduce computation times and capacity memory.

II. 2. 7 Electrical conductivity analysis

The contribution of electrical properties in nanofluids is revealed in this work. There is a significant dependence on the dispersed particles and its concentration. A detailed study on electrical conductivity of nanofluids with various parameters is thoroughly analysed. The solvent used in this study must satisfy two requirements: the electrical conductivity of Glycerol should be as low as possible; MWCNT must be dissolved by the solvent well to form homogenous solution. The electrical conductivity of MWCNT/Glycerol was also investigated to review the influence of MWCNT in this study. The effect of temperature on the electrical conductivity of Glycerol/MWCNT nanofluids has been studied and the results are shown in Figure 2.26 (a), the electrical conductivity and its temperature dependence were measured for multi-walled carbon nanotube solution. The conductivity was remarkably dependent on the content of MWCNT, which was in accordance. The electrical conductivity changed with the temperature range 28 to 60°C, we observed that the electrical conductivity of nanofluid at 0.0025% volume fraction increases with temperature and we notice that the electrical conductivities are higher than those of the pure Glycerol at all the tested temperature, the highest electrical conductivity of 1.43 µScm-1 at 65 ˚C, was observed for the nanofluide due to high electrical conductivity of MWCNT. The measurements made on MWCNTs showed electrical conductivity values around 104 Sm^{-1} at room temperature [61]. Other studies have shown that carbon nanotubes become superconductors at low temperatures. The enhancement percentage of the electrical conductivity is calculated using the following equation:

$$\%\boldsymbol{\sigma} = \left(\frac{(\boldsymbol{\sigma_{nf}} - \boldsymbol{\sigma_{bf}})}{\boldsymbol{\sigma_{bf}}}\right) \times \mathbf{100} \qquad (2.20)$$

Where σ_{bf} is the electrical conductivity of the base fluid (Glycerol) and σ_{nf} is that of the nanofluid. The electrical conductivity Glycerol nanofluid was decreased between 64% and 26.8 at high temperature. There is no appreciable enhancement of electrical conductivity with temperature for low volume fraction (0.0025%) presented in the Figure 2.26 (b).

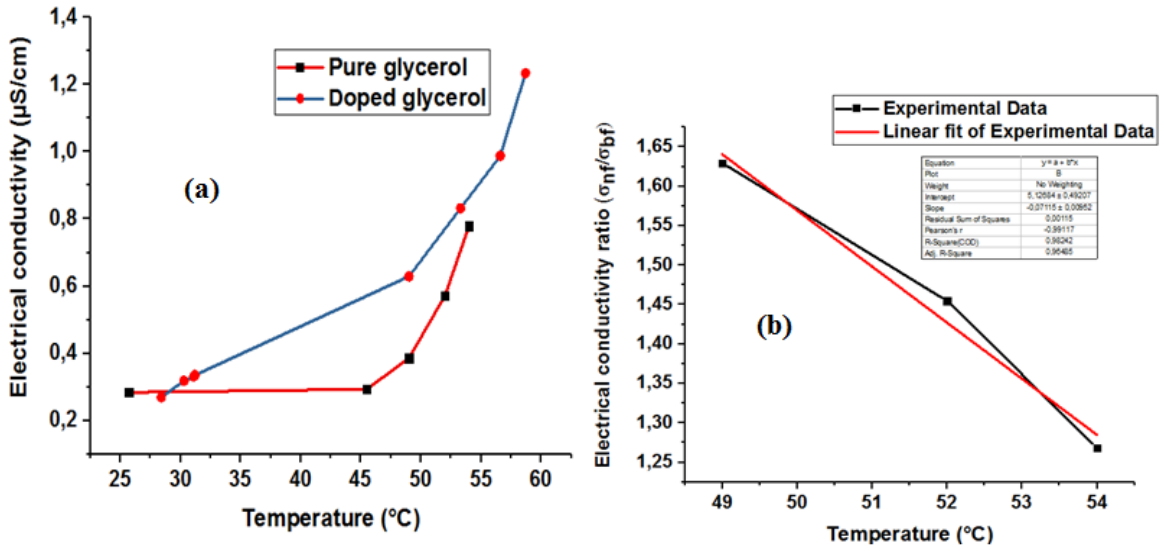

Figure 2.26: Dependence of electrical conductivity σ of MWCNT/Glycerol nanofluid and pure Glycerol on temperature (a); variation of electrical conductivity enhancement ratio of MWCNT/Glycerol nanofluids with temperature (b)

II. 2. 8 Infrared analysis

Our aim is to study the possible interactions between the surface of MWCNT nanoparticles and Glycerol molecules, FTIR spectra of pure Glycerol and doped Glycerol were recorded (Fig. 2.27). The x-axis represents the wave number in cm^{-1}; the axis is oriented from right to left by [400-4000cm^{-1}]. The ordinate axis is oriented upwards and represents the transmittance in%. Comparing both the FTIR spectra of doped Glycerol by nanoparticles of MWCNT and the pure Glycerol as shown in Figure (2.27), it has been found that many peaks obtained in the case of pure Glycerol spectrum were repeated in the FTIR spectrum in the presence of MWCNT nanoparticles with low changes in position as well as in intensity of transmission bands. The relatively broad transmission band, positioned at 3293 cm^{-1} in the pure Glycerol spectrum, which is attributed to the stretching vibrations of hydroxyl groups (-OH), became narrower with a decrease in band intensity in the spectrum of nanofluid. Many researchers use these peak areas as a measure of the oxidation extend, due to the fact that oxidation generates such group [62-63]. The peak observed at 1030 cm^{-1} which is attributed to the C-O stretching vibrations of the alcohol (Glycerol solvent), is displaced to 1031 cm^{-1} in

the spectrum of the nanofluid accompanied by a decrease in intensity [64]. These results indicate that hydroxyl groups of Glycerol and Ethanol molecules are involved in the synthesis and stabilization of the nanofluid. We observed the bands that could be assigned to transmittance of C–H (1210–1412 cm^{-1}) [65]. The weak bands in the region of 1000–1150 cm^{-1} assigned to C–O, C–C is the characteristic feature of many carbon materials and of the materials of our interest. The strong bands at 2933 and 2879 $cm^{-1}$are due to asymmetrical and symmetrical stretching of –CH2–, respectively [66]. The peak at 482 cm^{-1} is associated with –CH3 bending vibrations. The intensity of the asymmetrical stretching of –CH3 decreases significantly, especially in the nanofluid and the intensity of the bands associated with the bending vibration of –CH3 also decrease seriously but not be eliminated the existence of similarity between the two curves confirmed that nanofluid (MWCNT/Glycerol) were successfully prepared.

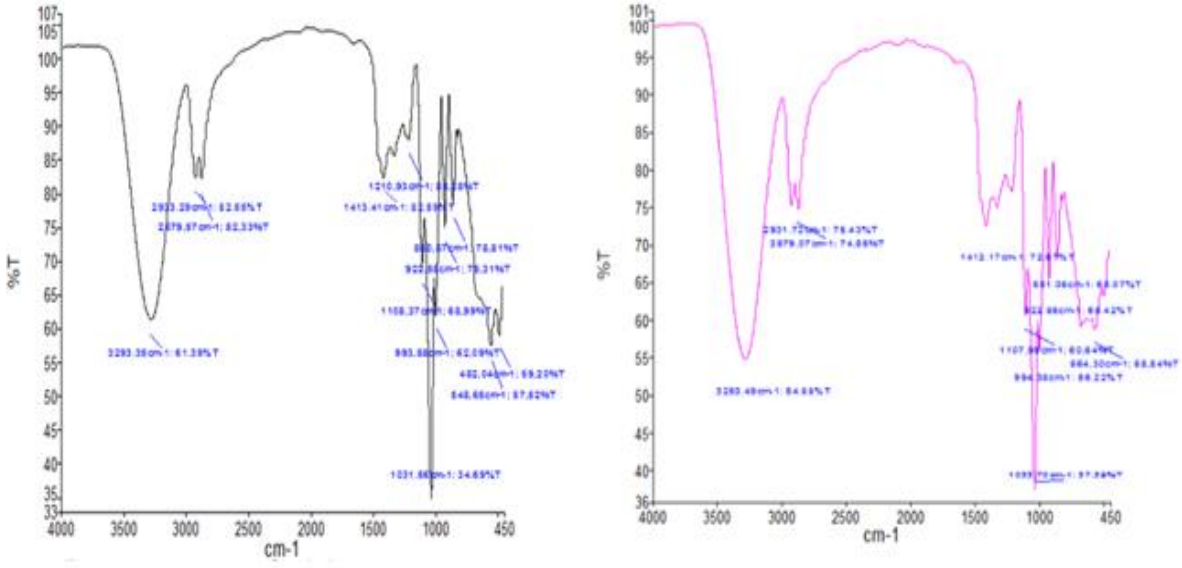

Figure 2.27: FTIR spectrum of Glycerol based MWCNT (left);
FTIR spectrum of pure Glycerol (right)

CONCLUSION 2

The results obtained with this new system are interesting because the increase in thermal conductivity reaches significant values: 85% and 50% respectively for volume fractions as low as 0.01% and 0.0025% of MWCNT / Glycerol. These results are quite comparable to those obtained with certain nanofluids based on carbon nanotubes for which the increase is 160% for a volume fraction of 1%. The results obtained are compared and

discussed towards to existing classical models and we have found that Xue's model is the appropriate model to describe the thermal conductivity of the MWCNT / Glycerol nanofluid for low volume fractions. In particular, we observed that the effective thermal conductivity of this nanofluid increases with the concentration of nanoparticles and with the temperature. It is difficult to compare the different experimental studies on nanofluids because each one was conducted for nanoparticles of different sizes and different sample preparations. However, the size of the particles and the preparation of the samples are determining factors which strongly influence the results obtained. Other theoretical approaches have emerged to try to understand the origin and importance of this increase in the thermal conductivity of nanofluids. However, none of them managed to adequately describe all the behaviors obtained experimentally**.**

Results obtained on nanofluids based on carbon nanotubes show increases in thermal conductivity as a function of the volume concentration much greater than those obtained with metallic nanoparticles.

Nanofluids MWCNT/Glycerol show good stability due to the functional groups attached on surfaces of MWCNT. For the same fraction there is no appreciable enhancement of electrical conductivity with temperature. It will be possible to design and engineer nanotechnology-based coolants with widespread industrial and biomedical applications in high-heat-flux cooling. Finally, it should be noted that nanofluids are still an emerging field and present a wealth of opportunities and challenges for thermal scientists.

Our simulation is able to provide thermal conductivity measurements with a relative uncertainty of less than 2.8%. This accuracy is certainly sufficient to follow the evolution of the thermal conductivity of Glycerol with temperature by transient methods.

Our numerical modeling can also be improved to take into account the 3ω method. This would make it possible to predict, depending on the temperature or the potential, the thermal conductivity of MWCNT / Glycerol nanofluids for different fractions.

References

[1] Arani, A. A. A. and Amani, J., .Experimental study on the effect of TiO2. Waternanofluid on heat transfer and pressure drop.,Exper. Therm. Fluid Sci., 42, 107 (2012)
[2] Wang, X. Q. and Mujumdar, A. S., .A review on nanofluids-part l: theoretical and numerical investigations., Braz. J. Chem. Eng., 25, 613 (2008).
[3] Choi, S. U. S., .Enhancing thermal conductivity of fluids with nanoparticle., ASME FED, 231, 99 (1995).
[4] Xie, H. and Chen, L., .Adjustable thermal conductivity in carbon nanotube nanofluids., Phys. Lett. A, 373, 181 (2009).
[5] Lisetski L.N., Minenko S.S., Ponevchinsky V.V. et al. Microstructure and incubation processes in composite liquid crystalline material (5CB) filled with multiwalled carbon nanotubes, Materials Science and Engineering Technology Materialwissenschaft Und Werkstofftechnik, 42 (2011) 5.
[6] Chen, L., Xie, H., Li, Y. and Yu, W., .Applications of cationic gemini surfactant in preparing multi-walled carbon nanotube contained nanofluids., Colloids Surf., A,330, 176, (2008).
[7] Huxtable, S. T., Cahill, D. G., Shenogin, S., Xue, L., Ozisik, R., Barone, P., Usrey, M.,Strano, M. S., Siddons, G., Shim, M. and Keblinski, P., .Interfacial heat flow in carbon nanotube suspension., Nat.Mater., 2,731 (2003).
[8] Raykar, V. S. and Singh, A. K., .Dispersibility dependence of thermal conductivity of carbon nanotube Based nanofluids., Phys. Lett. A, 374, 4618 (2010).
[9] S.U.S. Choi, Z.G. Zhang, W. Yu, F.E. Lockwood, and E.A Grulke. Anomalous thermal conductivity enhancement in nanotube suspension. Applied Physics Letters, 79(14): 2252-2254, 2001
[10] J.A. Eastman, S.U.S. Choi, S. Li, W. Yu, L.J. Thompson, Anomalously increased effective thermal conductivities of ethylene glycol-based nanofluids containing copper nanoparticles, Appl. Phys. Lett. , 78,718, (2001)
[11] P. Keblinski, J. A. Eastman, and D. G. Cahill, Nanofluids for thermal transport, materials today,8, 36, (2005)
[12] P. Vadasz, heat conduction in nanofluide suspension, Journal of heat transfer, 128, 465, (2006),
[13] D.G. Cahill, R.O. Pohl, Thermal conductivity of amorphous solids above the plateau, Phys. Rev. B 35 (8) 4067–4073. (1987)
[14] D.G. Cahill, Thermal conductivity measurement from 30 to 750 K: the 3omega method, Rev. Sci. Instrum. 61 (2) 802–808, (1990)
[15] Pegel S., Pötschke P., Petzold G. et al. Dispersion, agglomeration, and network formation of multiwalled carbon nanotubes in polycarbonate melts, Polymer, 49 974. (2008)
[16] Ma X., Yu J., Wang N. Glycerol plasticized-starch/multiwall carbon nanotube composites For electroactive polymers, Composites Science and Technology, 68 268. (2008)
[17] Liu Z., Zhao L., Chen M., Yu J. Effect of carboxylate multi-walled carbon nanotubes on the performance of thermoplastic starch nanocomposites, Carbohydrate Polymers, 83 447. (2011)
[18] Dadfar S.M.M., Kavoosi G. Mechanical and water binding properties of carboxymethyl cellulose/multiwalledcarbon nanotube nanocomposites, Polymer Composites, 36, 7. (2014)
[19] Yurdakul H., Durukan O., Seyhan T. et al. Microstructural characterization of corn starch-based porous thermoplastic composites filled with multiwalled carbon nanotubes, Journal of Applied Polymer Science, 127 812. (2013)
[20] Bulavin L.A., Lebovka N.I., Kyslyi Y.A. et al. Microstructural, rheological, and conducto-metric studies of multiwalled carbon nanotube suspensions in glycerol, Ukr. J. Phys., 55 (2010).
[21] Xie H., Yu W., Li Y., Chen L. Discussion on the thermal conductivity enhancement of nanofluids, Nanoscale Research Letters, 6 X1–12. (2011)
[22] Wang B., Lou W., Wang X., Hao J. A gel-sol transition phenomenon of oxidation multi-walled carbon nanotubes-glycerol nanofluids induced by polyvinyl alcohol, New Journal of Chemistry, 36 1273. (2012)
[23] Song P.C., Liu C.H., Fan S.S. Improving the thermal conductivity of nanocomposites by increasing The length efficiency of loading carbon nanotubes, Applied Physics Letters, 88 153111.
[24] Chen L., Xie H., Yu W., Li Y. Rheological behaviors of nanofluids containing multi-walled carbon nanotube, Journal of Dispersion Science and Technology, 32 (2011) 550. (2006)

[25] Liu Q., Wu J., Tan T. et al. Preparation, properties and cytotoxicity evaluation of a biodegradable polyester elastomer composite, Polymer Degradation and Stability, 94, 1427. (2009)
[26] C. Maxwell, A Treatise on Electricity and Magnetism. Oxford University Press, Cambridge,UK, (1904).
[27] Bruggeman G., Calculation of Various Physics Constants in Heterogeneous Substances I Dielectricity Constants and Conductivity of Mixed Bodies from Isotropic Substances, Annalen der Physik, Vol. 416, No. 7, pp.636-664. doi:10.1002/andp.19354160705, 1935.
[28] Hamilton R. L., CrosserO.K., Thermal conductivity of heterogeneous twocomponentsystems, Industrial & Engineering Chemistry Fundamentals, 1/3, 187-191. (1962)
[29] Q.Z. Xue, Model for thermal conductivity of carbon nanotube-based composites, Phys. B Condens. Matter 368 (1–4), 302–307. (2005)
[30] Koo J., KleinstreuerC., A New Thermal Conductivity Model for Nanofluids, Journal of Nanoparticle Research, 6/, 577-588. (2004)
[31] Xie H., Lee H., Youn W., ChoiM., Nanofluids containing multiwalled carbon nanotubes and their enhanced thermal conductivities, J. Appl. Phys., 94, 4967–4971. (2003)
[32] Yang, Y., GrulkeE. A., ZhangZ. G., Wu G., Thermal and rheological properties of carbon nanotube-in-oil dispersions J. Appl Phys., 99, 114307. (2006)
[33] Walvekar R., Faris I.A., Khalid M., Thermal conductivity of carbon nanotube nanofluid-Experimental and theoretical study, Heat Transfer-Asian Research 41(2), 145-163. (2012)
[34] Kumar D.H., Patel H.E., Rajeev Kumar V.R., Sundararajan T., Pradeep T., DasS.K., model for heat conduction in nanofluids, Phys. Rev. Lett. 93, 144301-144304. (2004)
[35] Paul G., Chopkar M., Manna I., Das P.K., Technique for measuring the thermal conductivity of nanofluids: review, Renewable and substainable energy review, 14, 1913-1924**.** (2010)
[36] H.S. Carslaw, J.C. Jaeger, Conduction of heat in solids, 2nd ed, London: Oxford (1959).
[37] Zhu DS, Li XF, Wang N, Wang XJ, Gao JW, Li H. Dispersion behavior and thermal conductivity characteristics of Al2O3–H2O nanofluids. CurrAppl, 9:131–9. 2009.
[38] Xuan Y, Li Q. Heat transfer enhancement of nanofluids. Int J Heat Mass Transfer 2000;21:58–64
[39] Bleazard JG, Teja AS. Thermal conductivity of electrically conducting liquids by the transient hot-wire method. J ChemEng Data, 40(4):732–7. 1995.
[40] D. Cahill, Thermal conductivity measurement from 30 to 750 K: the 3ω method, Rev. Sci. Instrum.61, 802 (1990).
[41] S.U.S. Choi, Developments and Applications of Non-Newtonian Flows, FED-vol. 231, ASME, New York, pp. 99–102. 1995.
[42] S. Iijima, Helical microtubules of graphitic carbon, Nature 354, 56–58. (1991)
[43] S. Berber, Y.-K. Kwon, D. Tomanek, Unusually high thermal conductivity of carbon nanotubes, Phys. Rev. Lett. 84, 4613–4615. (2000)
[44] A. A. Balandin, Nat. Mater., 10, 569–581 CrossRef CAS PubMed. 2011.
[45] Chen L, Xie H, Li Y, Yu W. Nanofluids containing carbon nanotubes treated by mechanochemical reaction. ThermochimicaActa. 477(1–2):21–24. 2008.
[46] Hadaoui A. effect of size and concentration on the thermal and rheological properties of nanofluids. Doctoral thesis, University of Orléans and Cadi Ayyad de Marrakech, 2010.
[47] Wang X.Q., Mujumdar A.S., Heat transfer characteristics of nanofluids: a review, International Journal of Thermal Sciences 46, 1-19. (2007)
[48] Liu M. S., Lin M. C. C., Huang I. T., Wang C. C., Enhancement of thermal conductivity with carbon nanotube for nanofluids. International Communication of Heat Mass Transfer, 32, 1202-1210. (2005)
[49] Xie H., Lee H., Youn W., Choi M., Nanofluids containing multiwalled carbon nanotubes and their enhanced thermal conductivities, J. Appl. Phys., 94, 4967–4971. (2003)
[50] Ding Y., Alias H., Wen D., Williams R.A., Heat transfer of aqueous suspensions of carbon nanoubes (CNT nanofluids), International Journal of Heat and Mass Transfer, 49/1-2, 240-250. (2006)
[51] Ruan B., Jacobi A. M., heat transfer characteristics of Multi-walled carbon nanotubes suspensions (MWCNT nanofluids) in intertube falling film flow, International Journal of Heat and mass transfer, 55, 3186-3195. (2012)

[52] Halelfadl S., Adham A. M., Mohd-Ghazali N., Maré T., Estellé P., Robiah A., Optimization of thermal performances and pressure drop of rectangular microchannel heat sink using aqueous carbon nanotubes based nanofluid, Applied Thermal Engineering, Under Review, 2013.
[53] Indhuja A., Suganthi K. S., Manikandan S., Rajan K. S., Viscosity and thermal conductivity of dispersions of gum arabic capped MWCNT in water: Influence of MWCNT concentration and temperature, article in press, 2013
[54] X. Wang, A. S. Mujumdar. Heat transfer characteristics of nanofluids: a review. International Journal of Thermal Sciences 46, 1-19. (2007)
[55] M. J. Assael, C. F. Chen, I. Metaxa, and W. A. Wakeham.Thermal Conductivity of Suspensions of Carbon Nanotubes in Water.International Journal of Thermophysics, 25 (2004).
[56] S.U.S. Choi, Z.G. Zhang, W. Yu, F.E. Lockwood, and E.A Grulke. Anomalous thermal conductivity enhancement in nanotube suspension. Applied Physics Letters, 79(14): 2252-2254, 2001
[57] Nassiri A., Shariati-Niasar M., Rashidi A. M., Khodafari R., Effect of CNT structures on thermal conductivity and stability of nanofluid, International Journal of heat and Mass transfer, 55, 1529-1535. (2012)
[58] GladésBachir., Contribution to the study of natural convection in nanofluidsin Rayleigh-Benard configuration. Doctoral thesis, University of Toulouse, 2010.
[59] M.J. Assael, C.F. Chen, I. Metaxa, and W.A. Wakeham.Thermal conductivity of suspensions of carbon nanotubes in water. International Journal of Thermophysics, 25(4): 971-985, 2004.
[60] D.S. Wen and Y.L. Ding. Effective thermal conductivity of aqueous suspensions of carbon nanotubes (carbon nanotubes nanofluids). Journal of Thermophysics and Heat Transfer, 18(4):481-485, 2004.
[61] Electrical transport properties of individual disordered multiwalled carbon nanotubes, Applied Physics Letters, 2006.
[62] Dovbeshko G.I., Gnatyuk O.P., Nazarova A.N. et al. Vibrational Spectra of Carbonaceous Materials: A SEIRA Spectroscopy versus FTIR and Raman, Fullerenes, Nanotubes, and Carbon Nanostructures, 13, 393. (2005)
[63] Bikiaris D., Vassiliou A., Chrissafis K., Paraskevopoulos K.M. Effect of acid treated multi-walled carbon nanotubes on the mechanical, permeability , thermal properties and thermo-oxidative stability of isotactic polypropylene, Polymer Degradation and Stability, 93, 952. (2008)
[64] Brichka S.Y., Prikhod'ko G.P., Sementsov Y.I. et al. Synthesis of carbon nanotubes froma chlorine-containing precursor and their properties, Carbon, 42, 2581. (2004)
[65] H. Kong, C. Gao and D. Yan, Macromolecules, 37, 4022– 4030. 2004.
[66] L.Q. Jiang, L. Gao, J. Sun, Production of aqueous colloidal dispersions of carbon nanotubes, J Colloids Interface Sci. 260 (2003).
[67] H.S. Carslaw, J.C. Jaeger, Conduction of heat in solids, 2nd ed, London: Oxford (1959).

CHAPTER III:

EXPERIMENTAL STUDY ON THE RHEOLOGY OF THEMWCNT / GLYCEROL NANOFLUID

INTRODUCTION

From the end of the 90s, significant progress in physics and chemistry allowed the synthesis of particles of nanometric dimensions, which, dispersed in a carrier liquid, constitute nanofluids; their synthesis met the need to improve the thermal diffusivity of coolants by adding a solid phase (nanoparticles) with better thermal conductivity and which remains in stable suspension.

The announced increase in the thermal conductivity of these suspensions reached unexplained levels and very different from those predicted by conventional models. This subject has therefore aroused great interest in recent years because it combines fundamental aspects (thermal exchanges at small-scale interfaces) and applied aspects. Regarding this last point, it is necessary to precisely quantify the overall energy balance of the flow of a nanofluid, that is to say to know, among other things, its viscosity because a viscous flow dissipates energy by internal friction in the fluid.The rheology of nanofluids has given rise to much less research than thermal behavior, and until today, the analysis of the rheological properties of nanofluids remains superficial. The predominance of surface effects and the influence of Brownian motion are the two elements distinguishing a conventional suspension of a nanofluid. Both from a thermal and rheological point of view, the presence of aggregates and their size will influence the transport properties of nanofluids. Indeed,the insertion of MWCNT in the base solution makes it possible to improve the thermal conductivity of the nanofluid but can also lead to an unfavorable increase in dynamic viscosity and relatively modify the density and specific heat of thissolution.Although Newtonian behavior is observed for fluids containing low concentrations of nanoparticles, suspensions based on carbon nanotubes (MWCNT)
obey a different constitutive law. In the absence of reliable relationships and models making it possible to theoretically predict the evolution of these properties, it is therefore necessary to consider an experimental characterization of nanofluids in order to better control the solution used.

In this chapter we are interested in studying the viscosity and the density of the nanofluids that we have prepared, for different volume fractions and different temperatures.

III. 1 Rheology reminders

III. 1. 1 Rheological parameters

Rheology studies the flow or deformation of a body under the effect of the stresses applied to it. If one considers the fluid in flow under continuous shear represented figure 3.1, three fundamental quantities make it possible to describe the deformations of the fluid:

• The shear stress noted in general τ expressed in N / m^2;

• The shear rate (or speed gradient) noted in general $\dot{\gamma} = \frac{v}{d}$ expressed in s^{-1};

• The dynamic shear viscosity μ expressed in Pa.s.

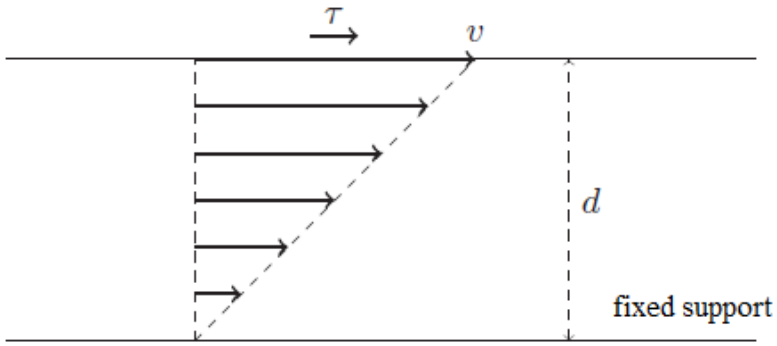

Figure 3.1: Fluid under continuous shear: v is the speed of the upper blade of fluid relative to the fixed support and d is the thickness of the fluid layer considered.

In the important case of Newtonian fluids, the dynamic viscosity does not depend on the shear rate $\dot{\gamma}$ it is therefore constant at constant thermodynamic parameters.

We can define the dynamic viscosity of a Newtonian fluid by the relation:

$$\tau = \mu . \dot{\gamma} \qquad (3.1)$$

Withμ = cste. Many simple liquids like water, certain oils, or glycerol are Newtonians. This model is also suitable for cases of dilute suspensions with a very small volume concentration of particles. We also define the kinematic viscosity υ by:

$$\upsilon = \text{?}/\rho \qquad (3.2)$$

Where ρ is the density of the fluid expressed in kg / m^3. Kinematic viscosity is expressed in m^2/s or in Stokes (1 St = 10^{-4} m^2/s).

III. 1. 2 Power dissipated in the fluid by the stress

A viscous flow dissipates mechanical energy by friction internal to the fluid. The mechanical power dP_f dissipated by the elementary force dF = τ.dS is expressed by:

$$dP_f = d\vec{F}.\vec{v} \qquad (3.3)$$

We deduce the power density dissipated for a Newtonian fluid:

$$P_f^v = \frac{dP_f}{dxdydz} = \tau\dot{\gamma} = \mu\dot{\gamma}^2$$

More dynamic viscosity is important more the mechanical power is dissipated by the viscous forces within the flowing fluid.

In terms of the energy balance of a machine (engine, compressor...), this loss is harmful and must be limited. It is therefore important to quantify the influence of nanoparticles in suspension on the dynamic nanofluid viscosity.

III. 2 Some rheological laws of suspensions

III. 2. 1 Presentation

In the field of nanofluids, we can distinguish two types of suspensions. A dilute suspension is characterized by a very low volume fraction of solid species. As the particles are very far from each other, no short or long distance interaction disturbs their trajectory. For this type of suspension, the viscosity increases linearly independing on the concentration of solid elements. Concentrated suspensions, which we have not studied, are characterized by volume concentrations that exceed 50%.

The literature contains numerous equations governing the dynamic viscosity of a suspension μ from the dynamic viscosity of the host fluid and the volume fraction insolid species Φ.

Several theoretical models have been developed to predict the evolution of the dynamic viscosity of suspensions under certain conditions. In this part, we will focus on the most used models in the case of nanofluids.

III. 2. 2 Theoretical models

In general, the existing formulas are derived from the fundamental work of Einstein (1906). Based on the assumption that energy has a linear dependence on viscosity,

Einstein determined the energy dissipated around a single particle in a fluid by combining its energy with the work done to make it move forward relative to the fluid.

From this result, he determined the expression describing a linear dependence of the viscosity of suspensions in a fluid with the concentration [1]

$$\mu_{nf} = \mu_{bf}(1 + 2.5\Phi) \qquad (3.4)$$

Einstein's formula has since been verified experimentally and is considered satisfactory for very dilute suspensions of spherical particles (Brownian or non-Brownian), typically for volume concentrations less than 1%.

Note that this model does not take into account the effects of particle size and interparticle interactions. Brinkman's formula [2] complements Einstein's model up to a volume concentration of less than 4% (Eq.3.5).

$$\boldsymbol{\mu_{nf} = \mu_{bf} \frac{1}{(1-\Phi)^{2.5}}} \qquad (3.5)$$

This relation describes a nonlinear evolution of the dynamic viscosity with the volume concentration but does not take into account the collision between the particles. Indeed, the flow around each particle is influenced by the possible presence of other nearby particles and by particle collisions. Thus, this results in taking into account a term Φ^2 in the Batchelor model [3].

$$\boldsymbol{\mu_{nf} = \mu_{bf}(1 + \eta\Phi + K_H\Phi^2)} \qquad (3.6)$$

Where η is the intrinsic viscosity and k_H is the Huggins coefficient. The value of η and k_H is 2.5 and 6.5 respectively for spherical particles.

Graham (1981) proposed a generalized formula (Eq.3.7) which tends towards the Einstein model for very low volume concentrations:

$$\boldsymbol{\mu_{nf} = \mu_{bf}(1 + 2.5\Phi + 4.5\Phi^2)\left(\frac{1}{\left(\frac{h}{d_{np}}\right)\left(2+\frac{h}{d_{np}}\right)\left(1+\frac{h}{d_{np}}\right)^2}\right)} \qquad (3.7)$$

Where $\mathbf{d_{np}}$ and **h** are the radius of the particle (m) and the distance between the particles (m), respectively.

For higher volume fractions, Krieger and Dougherty [4] (Eq.3.8) developed a model based on the maximum rate of compaction (or the maximum concentration particles in a suspension) which consists in calculating the dynamic viscosity of a suspension by assuming that the particles are successively added to a base fluid considered to be homogeneous. Each particle sees around it a homogeneous fluid whose viscosity depends only on the volume fraction of the particles and the viscosity of the interstitial fluid. This model is effective for estimating the dynamic viscosity of nanofluids without presence of agglomerates. In the first and second order, it corresponds respectively to the models of Einstein and Batchelor.

$$\boldsymbol{\mu_{nf} = \mu_{bf}\left(1 - \frac{\Phi}{\Phi_M}\right)^{-\eta\Phi_M}} \qquad (3.8)$$

η is the Einstein coefficient, i.e. η = 2.5 and $\Phi_M \approx 0.64$ in the case of spherical particles.

In general, the Krieger-Dougherty model derives from a generalized formula for the evolution of the relative viscosity which depends on the volume fraction $\frac{\Phi}{\Phi_M}$ and an exhibitornegative n (Eq.3.9).

$$\boldsymbol{\mu_{nf} = \mu_{bf}\left(1 - \frac{\Phi}{\Phi_M}\right)^{n}} \qquad (3.9)$$

Different values of n have been proposed in the literature, from −1 to −4, according to the authors [5]. The exponent n = −2 (Eq.3.10), initially proposed by Maron & Pierce (1956) and based on the theoretical Ree-Eyring flow model [6-7] is the most commonly reported.

$$\boldsymbol{\mu_{nf} = \mu_{bf}\left(1 - \frac{\Phi}{\Phi_M}\right)^{-2}} \qquad (3.10)$$

The model of Brenner and Condiff (Eq. 3.11) integrates the effect of the shape of nanoparticles and it can possibly be applied for suspensions based on CNTs.

Its field of application is limited to the volume fraction equal to $\frac{1}{r_a^2}$ (r_a is the aspect ratio of CNTs) and to high shear rate flow regimes.

$$\boldsymbol{\mu_{nf} = \mu_{bf}(1 + \eta\Phi)} \qquad (3.11)$$

With: $$\boldsymbol{\eta = \frac{0.312 r_a}{ln2r_a - 1.5} + 2 - \frac{0.5}{ln2r_a - 1.5} - \frac{1.872}{r_a}}$$

Similarly, Boobo [8] also considered the effect of Brownian motion and mutual forces in suspension and presented two following equations to determine the viscosity of suspension.

$$\boldsymbol{\mu_{nf} = \mu_{bf}(1 + a\Phi + b\Phi^2)} \qquad (3.12)$$

The results published to date, concerning the suspensions of nanoparticles of spherical or non-spherical geometry, demonstrate, like the work of Ngyuen et al.[9] for example, that the previous models are often insufficient to explain the strong increases in the viscosity of nanofluids with the concentration of nanoparticles, and this for dilute or more concentrated solutions. In addition, the difference between experimental and theoretical results increases with the concentration of suspensions. This disparity can be explained by the presence of aggregates, this causes a variation in the size and the effective concentration of the nanoparticles.

III. 2. 3 Previous experimental results

III. 2. 3. 1 Measurement techniques

Using rheometers or viscometers, it is possible to generate flows which make it possible, from geometric considerations and hypotheses on the flow, to link the macroscopic parameters (torque, speed of rotation, flow rate, pressure difference ... .) with the parameters governing the constitutive laws previously described in appendix A-1 (shear stress, and shear rate).

Commonly used techniques to evaluate these parameters are:

- Capillary rheometer: whose the principle is based on the flow in a cylindrical pipe.
- Rotary rheometer: the fluid is sheared in this case between two coaxial cylinders, between two circular planes or between a circular plane and a cone. Note that it is this type of geometry that will be used in this work.

III. 2. 3. 2 State of the art

The experimental studies carried out on the rheological behavior and the dynamic viscosity of nanofluids, based on CNTs, are more limited compared to those relating to the thermal conductivity of these same suspensions. In addition, most of the work carried out on dynamic viscosity concerns nanofluids based on spherical nanoparticles. As the thermal conductivity, several factors can influence the rheological behavior and dynamic viscosity of nanofluids. These factors include:

- The volume fraction
- The temperature
- Stabilization methods (chemical and mechanical)
- Speed / shear stress
- The base fluid

Several experimental works have been carried out to study the impact of these factors on the rheological behavior and dynamic viscosity of CNT-based nanofluids. The main results are described below.

III. 2. 3. 2. 1 Effect of volume fraction

Research on the effect of volume concentration on the dynamic viscosity of CNT-based nanofluids shows that dynamic viscosity increases with volume concentration. Phuoc et al. [10] observed that the viscosity dynamic increases with the concentration of the MWCNT /

water nanofluid for mass fractions between 0.5% and 3%. According to their results, the rheological behavior MWCNT / water is Newtonian at low concentrations (0.5%) and becomes shear thinner at higher concentrations. Similar results were observed by Kinloch et al. [11]. Ding et al. [12] have shown experimentally that for mass concentrations of 0.1% and 0.5% of MWCNT / water, the rheological behavior of the nanofluid is shear thinner at low shear rates and becomes Newtonian for rates high shear (Figure 3.2).

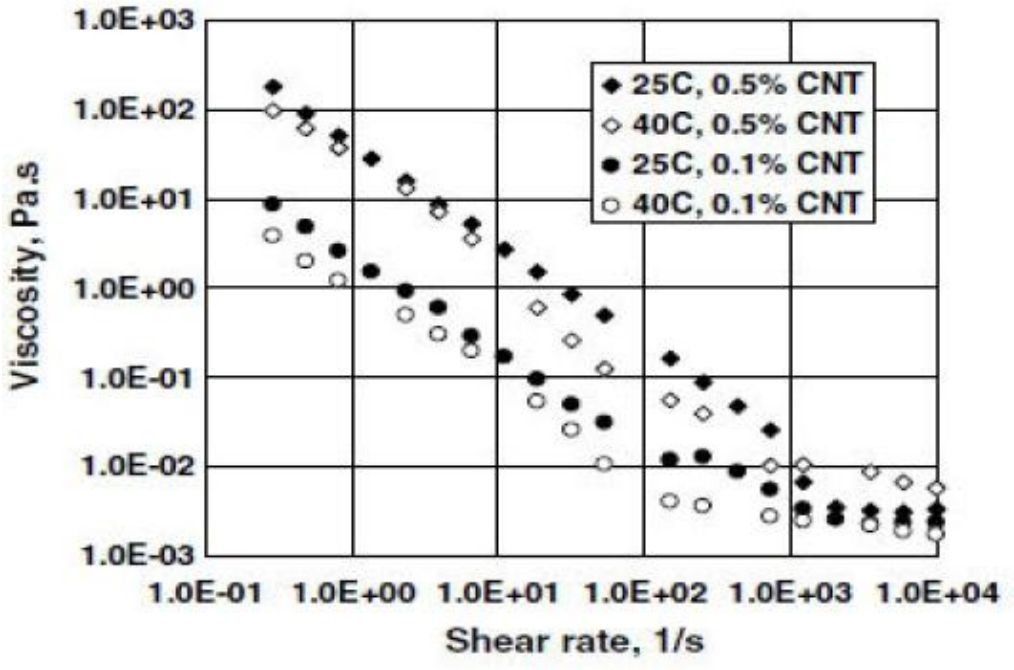

Figure 3.2: Evolution of the viscosity as a function of the shear rate [11]

Wang et al [13] have shown that the addition of a volume fraction of 1.27% MWCNT results in an increase in the dynamic viscosity of the nanofluid on the order of five times compared to the base fluid. Indhuja et al. [14] presented a linear evolution of the dynamic viscosity with the volume fraction of an aqueous solution of MWCNT for a range of volume concentration varying from 0.05 to 0.24%.

III. 2. 3. 2. 2 Effect of temperature

Numerous studies have shown that the dynamic viscosity of nanofluids decreases when the temperature increases. Aladag et al. [15] studied the rheological behavior of an MWCNT / water nanofluid at low temperatures (from 2 to 10 ° C) and they observed that the dynamic viscosity of the nanofluid decreases when the temperature increases and that the rheological behavior of the nanofluid at these temperaturesis shear thinner at low shear rates and becomes Newtonian for shear rates greater than $100s^{-1}$. Gholarmeza and Donany[16] studiedexperimentally the effect of temperature (25 ° C to 100 ° C) on a nanofluid based on

SWCNTs dispersed in oil without the presence of surfactant. Their results show that the dynamic viscosity of the nanofluid is highly temperature dependent. In other words, when as the temperature increases, the dynamic viscosity of the nanofluid decreases significantly. The results of Indhuja et al. [17] show that the effect of temperature on the dynamic viscosity of an aqueous solution of MWCNT is significant at low concentrations.

III. 2. 3. 2. 3 Effect of stabilization methods (chemical and mechanical)

The processes involved in preparing stable and well-dispersed suspensions of CNTs can also have an impact on the rheological behavior and the evolution of the dynamic viscosity of the suspensions. Several studies have shown that the addition of surfactant generally results in an increase in dynamic viscosity [18].Ko et al. [19] compared the dynamic viscosity of two MWCNT nanofluids dispersed in water. The first is stabilized by adding a small amount of SDS (Sodium dodecyl sulfate) and the second nanofluid is stabilized by the functionalization of the MWCNTs by acid treatment. The dynamic viscosity of the first nanofluid thus appears to be slightly greater than that of the second. Indeed, Chen and Xie[20] observed a sharp decrease in the dynamic viscosity of a nanofluid composed of MWCNTs dispersed in silicone oil due to the addition of hexamethyldisiloxane (HMDS) as a surfactant especially at low temperatures (Figure 3.3).

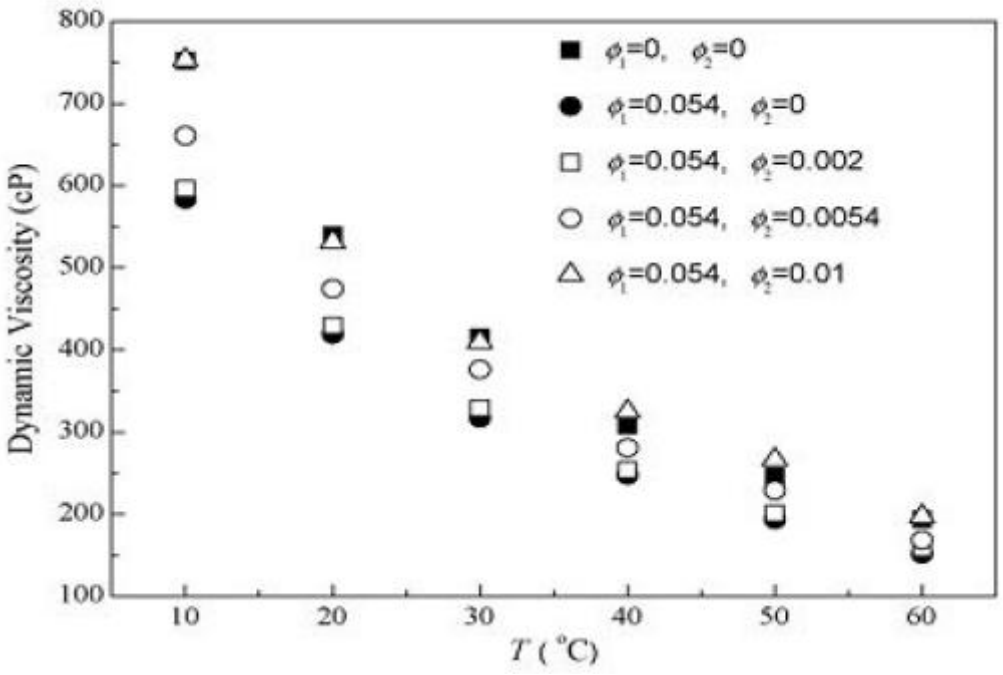

Figure 3.3: Evolution of dynamic viscosity with temperature, Φ1 volume fraction of HMDS and Φ2 volume fraction of MWCNT [20]

Garg et al. [21] have shown that increasing the ultrasonic mixing time breaks up agglomerates and even reduces the aspect ratios of CNTs. Yang et al. [22] have also studied the effect of ultrasonic mixing time on the size of agglomerates and the aspect ratio of CNTs dispersed in oil. They observed a decrease in the size of the agglomerates and a reduction in the aspect ratio of CNTs with dispersion energy and ultrasonic mixing time, resulting in a decrease in the dynamic viscosity of the nanofluid.

III. 2. 3. 2. 4 Effect of shear rate

The rheological behavior of nanofluids can also depend on the shear rate. Although Newtonian behavior is generally observed at strong shear speeds, Wang et al. [13] observed shear thinning behavior of a nanofluid based on MWCNT dispersed in water, for volume fractions of 0.05 to 1.27%, at very low speeds of shear (less than$10s^{-1}$) and Newtonian for shear rates greater than $10s^{-1}$. Similar results were observed for a suspension based on MWCNT dispersed in ethylene glycol at volume fractions of 0.03 to 0.18% [23]. These results show that the MWCNT / ethylene glycol nanofluid is shear thinner at shear rates of less than $100s^{-1}$. The observed shear-thinning behavior is explained by the alignment of the structure in the direction of the shear, which results in a decrease in dynamic viscosity as a function of the applied shear force [24]. Other experimental studies have shown a Newtonian behavior even at very low shear speeds. Chen and Xie, [20] observed Newtonian behavior of MWCNTs dispersed in silicone oil at low shear rates(less than $10s^{-1}$) for temperatures of 10 to 60°C. According to their results, Newtonian behavior is due to the high dynamic viscosity of the base fluid.

Other effects can also influence the dynamic viscosity and the rheological behavior of CNT-based nanofluids, such as the presence of agglomerates [24], CNT synthesis methods.

From a general point of view, there is a significant disparity between experimental results, but also theoretical. It is therefore difficult to compare the different studies and to establish a reference physical model for evaluating the dynamic viscosity of CNT-based suspensions making it possible to maintain account of all the effects described above.

III. 3 Protocols and experimental results;

III. 3. 1 Aim of the study

The objective of our experimental study is the analysis of the influence of carbon nanotubes (MWCNT) on the viscosity of Glycerol (Aldrich: Glycerol for molecular biology,

99 to 101%) in which the nanotubes can remain in stable suspension thanks to a high viscosity when going to the nanoscopic scale.

III. 3. 2 Dynamic viscosity of Glycerol

We measured the viscosity of the host liquid as a function of temperature, using the Kinexus Malvern rotary rheometer equipped with cone-plane geometry (Figure 3.4). Glycerol is a Newtonian liquid in the temperature range that we have studied (10-60) ° C). The results are shown in figure 3.5.

Figure 3.4: Kinexus Malvern rotary rheometer

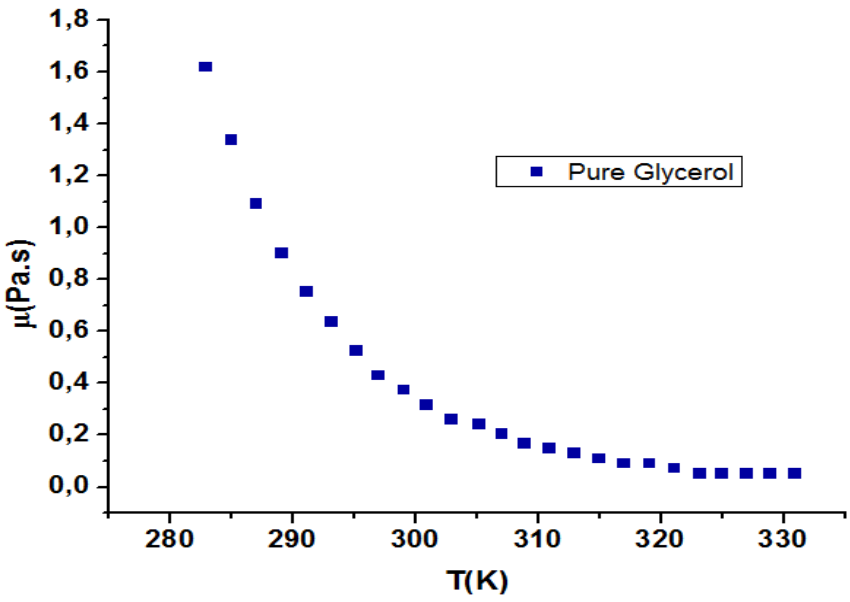

Figure 3.5: Dynamic viscosity of Glycerol as a function of the absolute temperature T.

The usual Arrhenius law does not allow a very good description of the data, on the other hand a law (equation 3.13) of the same type but slightly modified and which allows a good agreement with our measurements (Figure 3.6).

$$\mu = Ae^{-BT} \qquad (3.13)$$

With in the case of glycerol A =2.10^9, B = -0.07 and R^2> 0, 98.

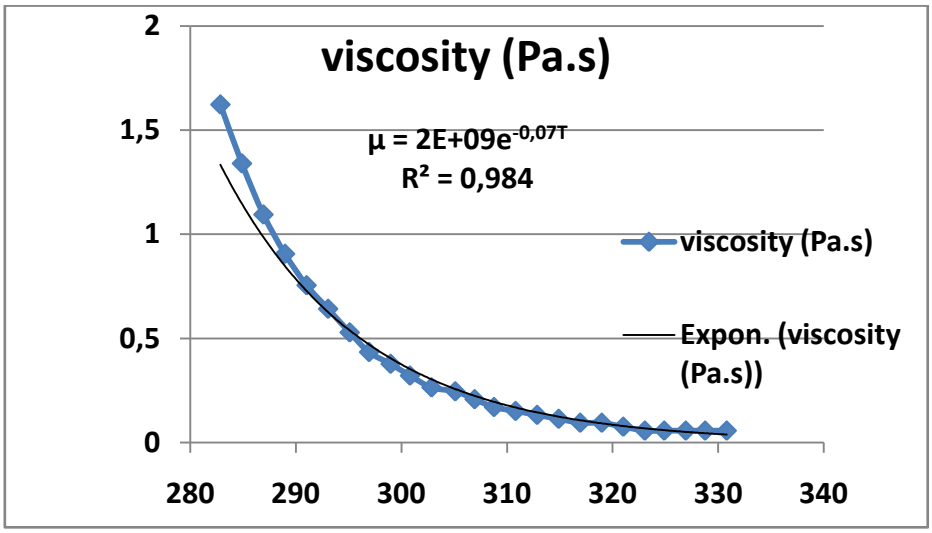

Figure 3.6: Comparison of model predictions with experimental data for pure Glycerol

III. 3. 3 Dynamic viscosity of the MWCNT / Glycerol nanofluid

We evaluated the influence on the viscosity of suspending various concentrations of carbon nanotubes (MWCNT). All the results are shown in Figure (3.7) for the various volume fractions that we prepared. The figure also shows the viscosity of the obtained nanofluids with various concentrations of MWCNTs as a function of temperature. The viscosity of the obtained nanofluids is higher than that of Glycerol, even though the MWCNT volume fraction gets to 0.01%.At the same time, the viscosity of the obtained nanofluids increases with increasing MWCNT volume fraction and diminishes with increasing temperature.

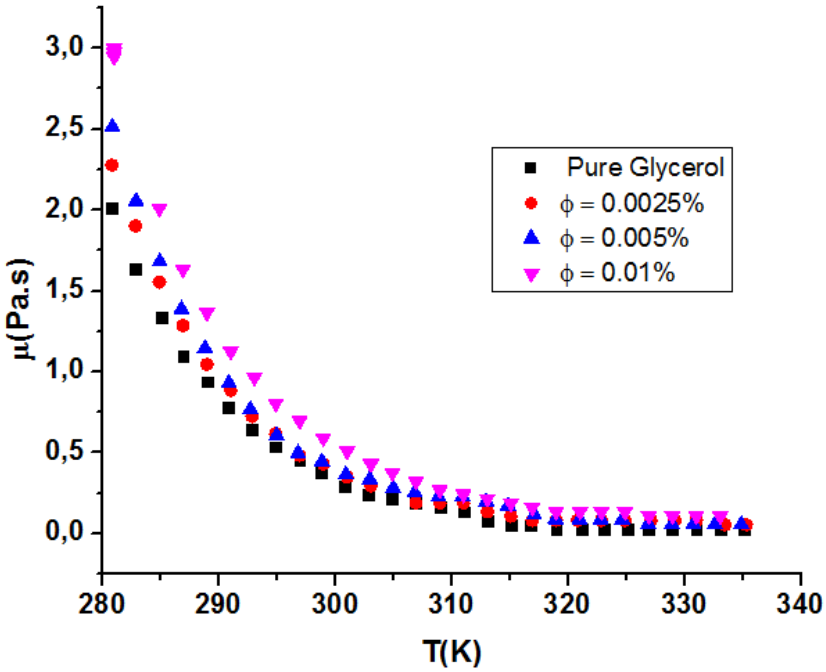

Figure 3.7: Influence of the volume fraction on the dynamic viscosity of the MWCNT / Glycerol nanofluid

There are several important results:

1- The inclusion of carbon nanotubes (MWCNT) greatly increases the dynamic viscosity of the fluid over the entire temperature range studied. An increase of approximately 50% in the viscosity of the fluid is observed for a maximum volume fraction of 0.01%. This is a significant increase which can generate significant internal mechanical losses in the fluid and constitute a handicap for technological applications.

2- The law of change of viscosity with temperature is not affected by the inclusion of MWCNT. This observation may reflect the fact that, given the small volume fractions studied, the carbon nanotubes do not considerably modify the interactions between the molecules of glycerol. It is therefore the solvent which imposes the law of variation of viscosity with temperature.

3- As mentioned in the literature review in this chapter, the classical models of Einstein and Brinkman may be valid for suspensions of spherical particles and do not take into account the effect of size / shape or interactions between nanoparticles. This is partly why these two models cannot reproduce the evolution of the relative viscosity of the nanofluid. The model of Brenner and Condiff (Eq.) Integrates the effect of the shape of the nanoparticles and it can optionally be applied for suspensions based on MWCNT whose volume fraction can go up to 0.005%). This explains at relatively high volume fractions (greater than 0.01%), this model fails to reproduce our experimental points. The increase in viscosity obtained with carbon

nanotubes (MWCNT) is greater than that predicted by theoretical laws, therefore, to our knowledge, there is no model to explain this difference.

III. 3. 4 Rheological behaviors of Glycerol based MWCNT nanofluids

The rheology of nanofluid includes Newtonian and non-Newtonian manners. In order to verify the rheological behaviors of Glycerol based MWCNT nanofluid, the relation between dynamic viscosity and shear rate at different temperatures was measured by using the Brookfield LV DV-II Pro viscometer (Figure 3.8). Figure (3.9) illustrates the nanofluid viscosity as a function of shear rate at different temperatures between 20 °C and 60 °C with Φ=0.0025%. Over the measured temperature range, the viscosity is independent of shear rate also, the dynamic viscosity decreases with increasing temperature. As temperature increases, the intermolecular interactions between the molecules weaken and therefore the viscosity decreases. Hence, glycerol based MWCNT nanofluids acts as a Newtonian fluid at very low volume fractions and its viscosity depends strongly on temperature.

Figure (3.10) presents the dynamic viscosity for both pure Glycerol and the nanofluids of MWCNT/Glycerol with different volumes fractions at 20°C. The Newtonian behavior of Glycerol as a base fluid is mostly changed to non-Newtonian for the nanofluid at $\Phi \geq 0.005\%$ for low values of shear rate which is less than $20 s^{-1}$because of the complex interactions between the Glycerol and MWCNT. With increasing MWCNT in the base fluid, Glycerol, the non-Newtonian behavior becomes important. This graph also show the viscosity of the nanofluid enhances with increasing the volume fraction of MWCNT. It can be seen that the viscosity is almost independent of the shear rate, indicating the Newtonian behavior of the Glycerol based MWCNT nanofluids at a small volume fractions.

Figure 3.8: Brookfield LV DV-II Pro viscometer and his spindles

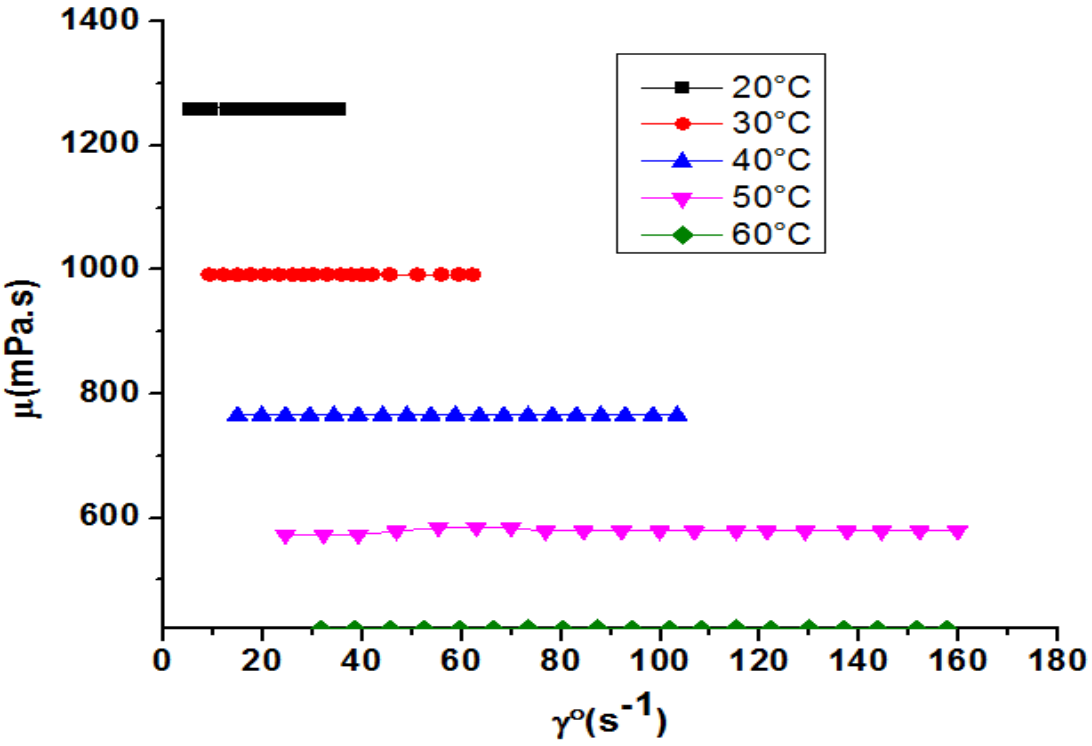

Figure 3.9: Dynamic viscosity versus shear rate for MWCNT /Glycerol with Φ=0.0025% at different temperatures.

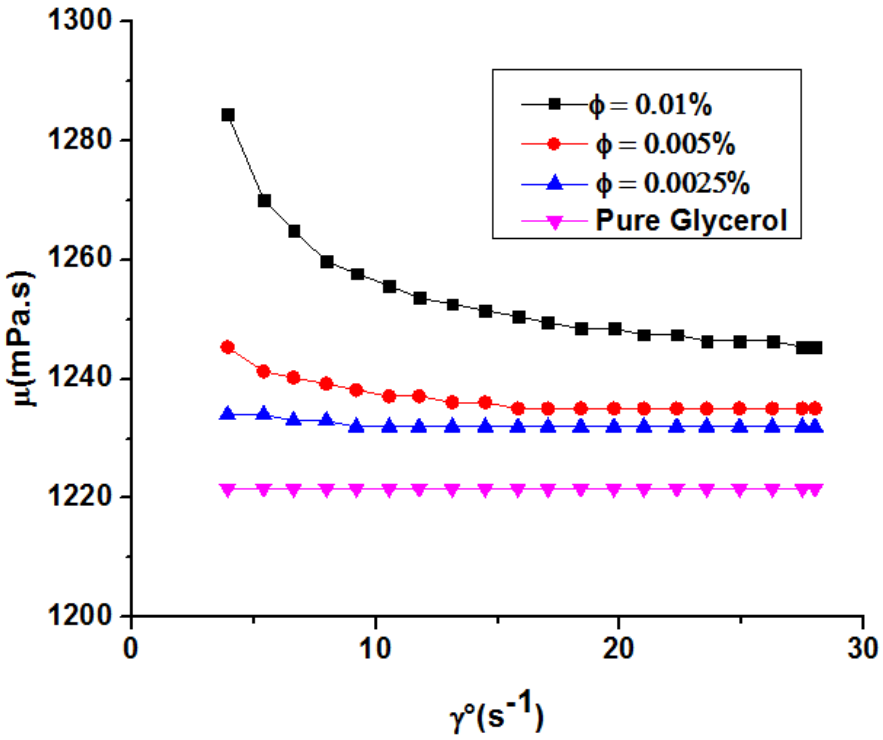

Figure 3.10: Viscosity of MWCNT/Glycerol nanofluids as a function of shear rate at different volume fractions at 20 °C.

III. 3. 5 A new model of dynamic viscosity

The applicability of theoretical models to nanofluids is a still unsolved problem. We therefore propose a new model of dynamic viscosity of MWCNT/Glycerol nanofluids, inspired by previous work of Bobooto correlate these experimental data.

None of the usual mixing laws has made it possible to adequately describe the variation in the dynamic viscosity of MWCNT /Glycerol nanofluids with the volume fraction Φ. On the other hand, Boboo's model, which takes into account relevant parameters of the nanofluid, allows a very satisfactory description of our measurements. Boboo established the correlation (3.12) from data published on the dynamic viscosity of the SWCNT / Water nanofluid. To facilitate the discussion, we recall here the model of Boboo is written in the form:

$$\boldsymbol{\mu_{nf} = \mu_{bf}(1 + a\Phi + b\Phi^2)}$$

For the same base fluid and nanoparticle, this equation was regressed on the viscosity data at different temperatures (taken into account by means of the base fluid viscosity at that temperature)and nanofluid concentrations.

We have gathered in table 3.1 the values of the various parameters **a** and **b** found by Boboo for the SWCNT / Water nanofluid and by us for the MWCNT / Glycerol nanofluids.

Table 3.1: Comparative study of the parameters of the Boboo model for the nanofluids SWCNT / Water and MWCNT / Glycerol.

	a	b
Boboo model SWCNT/Water	-0.504	1.744
Our model MWCNT/Glycerol	155	-7040

This equation well represents the experimental data that shown in figure 3.11.

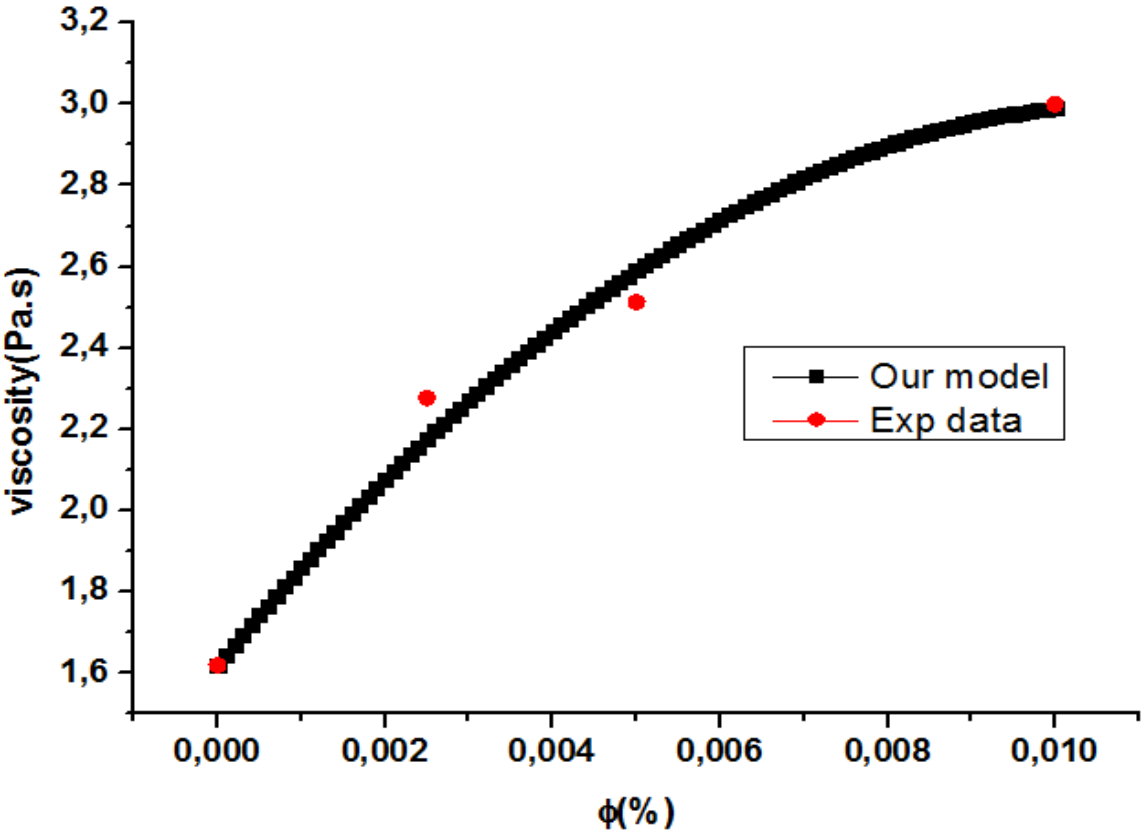

Figure 3.11: Comparison of our model predictions with experimental data for Glycerol nanofluids at room temperature.

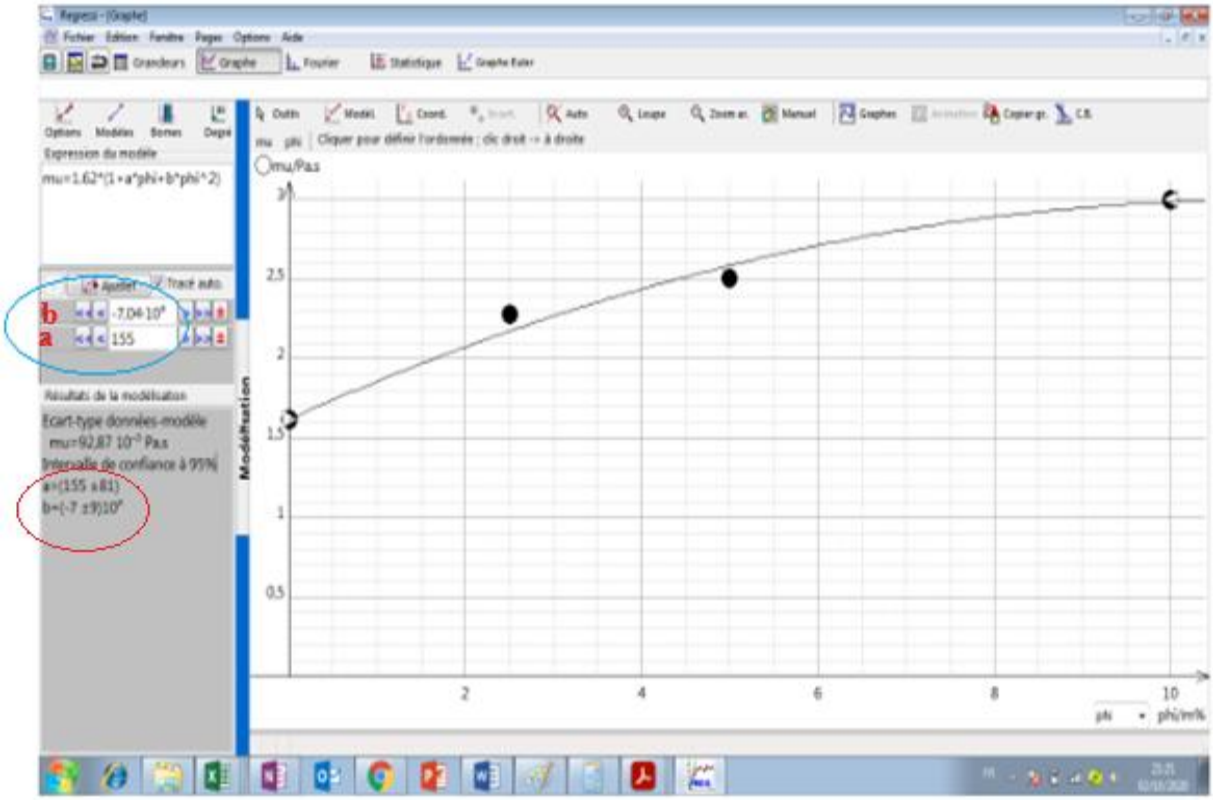

Figure 3.12: Photography of the Regressi software interface showing the correlation

From the measurement of the rheological properties of MWCNT/Glycerol nanofluids, the following conclusions can be drawn:

- Although Glycerol behaves as a Newtonian fluid, the nanofluids exhibit shear thinning behavior.
- The viscosity increases with the volume fraction of MWCNT.
- For volume fractions less than 0.005%, the nanofluids exhibit Newtonian behavior over the entire range of the shear rate studied. Beyond this concentration, the behavior of nanofluids becomes shear thinner at low shear rates,
- Temperature has a strong effect on the rheological properties of the MWCNT/Glycerol nanofluids. The viscosity of nanofluids decreases significantly with increasing temperature.
- A 50 % enhancement in viscosity of glycerol was achieved by loading of 0.01% MWCNT.
- No theoretical model is applicable to describe the viscosity of the MWCNT/Glycerol nanofluid that we have studied.
- We have ameliorate the Boboo model to create our own model

III. 4 Experimental characterization of density of MWCNT/Glycerol nanofluid

The objective of this part is to characterize experimentally the density of nanofluids in order to study the validity of the mixing law used in the literature to estimate the density of nanofluids in general and of suspensions based on MWCNT in particular, in the absence of experimental data.The density of nanofluids is proportional to the volume fraction of particles and increases with the addition of nanoparticles. In the literature, and in the absence of experimental results, the density of nanofluids is often calculated from the mixing law in which the nanofluid is assumed to be homogeneous (good dispersion of nanoparticles in the fluid).

III. 4. 1 Measurement of density: results and discussion

The density of nanofluids is often calculated from the law of mixture (equation 3.15)

$$\boldsymbol{\rho_{nf}} = \left(\frac{\boldsymbol{m}}{\boldsymbol{V}}\right)_{\boldsymbol{nf}} = \frac{\boldsymbol{m_f}+\boldsymbol{m_s}}{\boldsymbol{V_f}+\boldsymbol{V_s}} = \frac{\boldsymbol{\rho_f V_f}+\boldsymbol{\rho_s V_s}}{\boldsymbol{V_f}+\boldsymbol{V_s}} \qquad (3.14)$$

We then deduce the density of the nanofluid:

$$\boldsymbol{\rho_{nf}} = (\mathbf{1}-\Phi)\boldsymbol{\rho_f} + \Phi\boldsymbol{\rho_s} \qquad (3.15)$$

Where $\boldsymbol{\rho_{nf}}$: The density of the nanofluid,

$\boldsymbol{\rho_f}$: The density of the base fluid

$\boldsymbol{\rho_s}$: The density of solid nanoparticles (MWCNT)

Kumaresan and Velraj [25] carried out an experimental study on the density of a solution composed of MWCNTs dispersed in a mixture of water and ethylene glycol (30/70) and stabilized with SDBS (figure 3.13). According to their results, the density of the nanofluid increases with the volume fraction of the particles, and the deviation between the mixing law and the experimental measurements is of the order of 0.4% at the volume fraction0.15%, of 0.9% at 0.3% and of 1% at 0.45%.

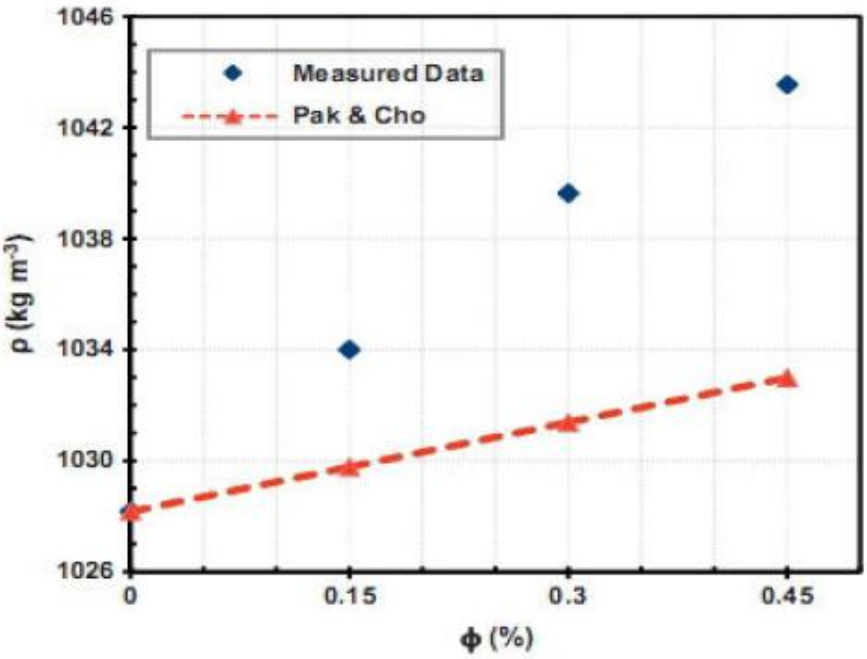

Figure 3.13: Evolution of density with the volume fraction [25]

Pakdamana et al. [26] observed a maximum deviation between the mixing law and their experimental measurements for an aqueous solution of MWCNT of the order of 1% at the mass fraction of 0.4%. Which confirms, according to them, that the law of mixture allows to predict the evolution of density.

In our work we used a density meter coupled with a DMA 602 cell, used to perform high precision density measurements of liquids (Figure 3.14).The DMA 602 cell is thermostatically controlled using a cry thermostat capable of ensuring the stability of the temperature of the oscillator of the order of 0.01K. For this, we measured experimentally the density of nanofluids for a temperature range between 20 and 40 ° C, the volume fraction of tested suspensions is between 0.0025% and 0.01%.

Figure 3.14: Densitymeter DMA 602

III. 4. 2 Effect of volume fraction and temperature

Experimental measurements of the density of our samples as a function of temperature and at different volume fractions were compared with the classical mixing law model in which the density of the particles is considered constant in the temperature range used.

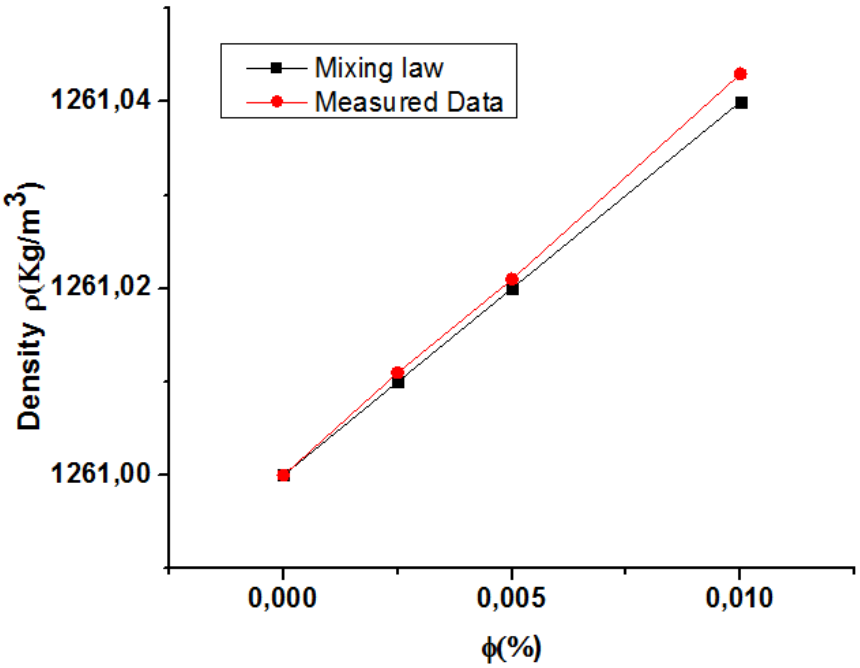

Figure 3.15: Evolution of density with the volume fraction at 20°C

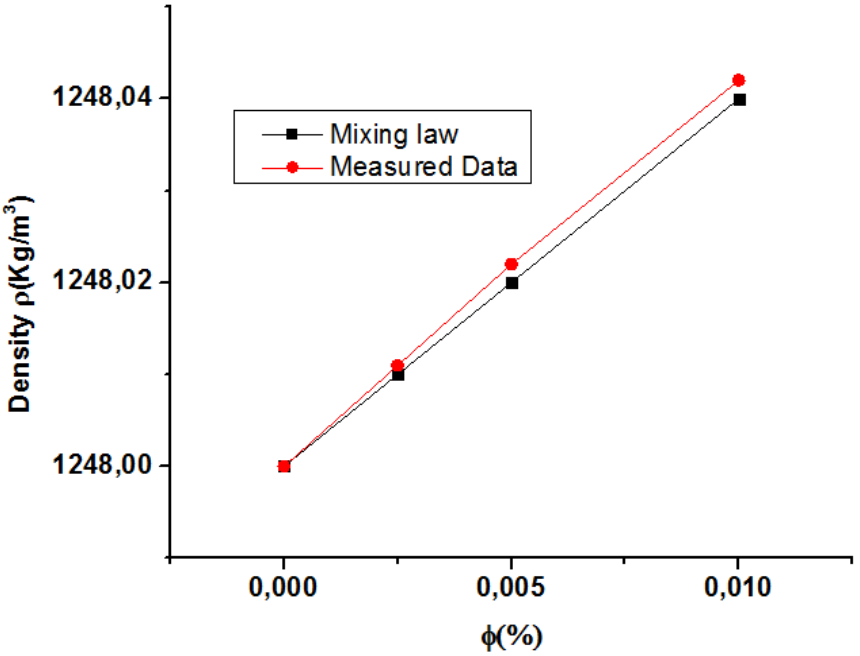

Figure 3.16: Evolution of density of nanofluids with the volume fraction at 40°C

Figures 3.15and 3.16 respectively represent the variation in the density of the nanofluid studied as a function of the volume fraction at 20 and 40°C. The experimental results show us,

for each test temperature, an increase in the density of the nanofluid with the increase in the volume fraction of the MWCNT. We observe a similar trend in the change in density predicted by the model of Equation 3.15.

The classical mixing law makes it possible to estimate and correctly predict the evolution of the density of suspensions at volume fractions less than 0.01% with a relative error of the order of 2.4 10^{-4} %. This can be explained by the homogeneity and the stability of the nanofluids. Thus, we can deduce that the classic mixing law remains valid at low volume fractions.

It can be seen from figure 3.17 that the density of nanofluids decreases linearly with temperature.

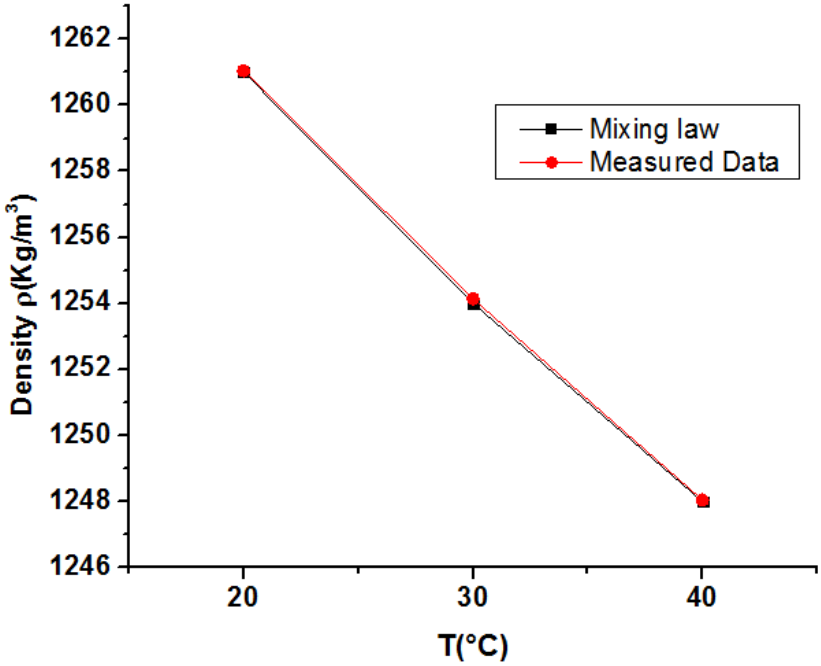

Figure 3.17: Variation of density of nanofluids as a function of temperature at volume fraction Φ = 0.01%

From Figure 3.16 above, we can draw the evolution of the relative density, defined as the ratio between the density of the nanofluid and that of the associated base fluid, depending on the volume fraction and temperature (Figure 3.18).

There is a linear evolution in the relative density as a function of the volume fraction of the MWCNTs. In other words, the temperature does not have a significant effect on the evolution of the relative density.

Based on these results and the previous conclusions, the density of nanofluids is calculated from equation 3.13.The density of the nanofluid depends on the density of the base fluid, that of the MWCNTs and the volume fraction of the MWCNTs.

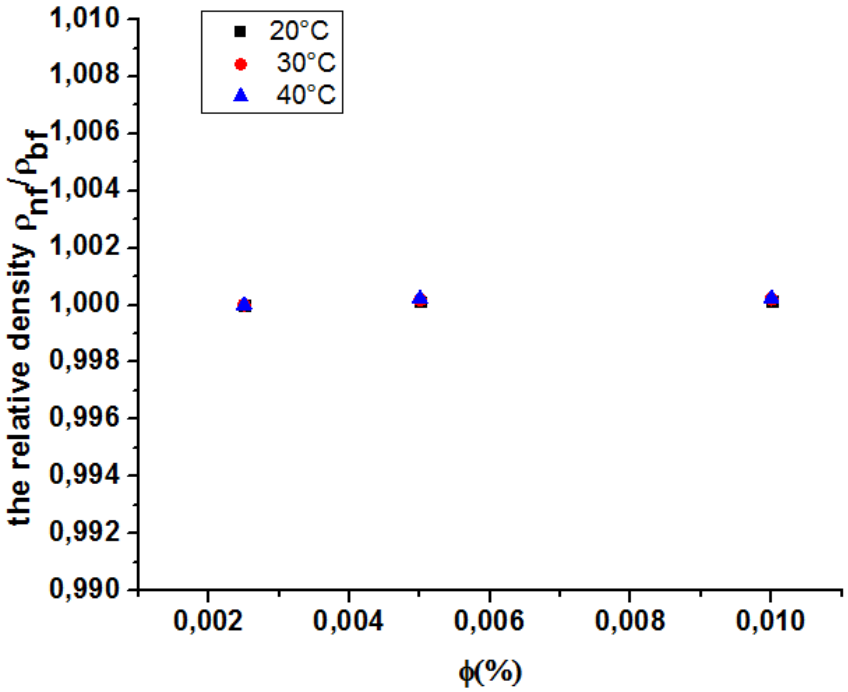

Figure 3.18: Evolution of the relative density as a function of the temperature and the volume fraction

CONCLUSION 3

Our experimental study of the influence of MWCNTs on the dynamic viscosity of Glycerol yielded several important and original results.

The inclusion in glycerol of carbon nanotubes in low proportions considerably modifies the viscosity of the glycerol, increasing by almost 50% for a volume fraction Φ = 0.01%. The inclusion of nanoparticles does not change the law of behavior of the host fluid this observation can reflect the fact that nanotubes, in low concentration, do not significantly modify the interactions between glycerol particles. The latter therefore imposes his law of behavior depending on the temperature.

The results show that at low concentrations, less than 0.01% for MWCNT/Glycerol that the rheological behavior of nanofluids is Newtonian for a high shear rate. Then, a new correlation was proposed to represent the experimental data for the MWCNT/Glycerol nanofluids.

In order to elucidate the significant increase in viscosity, it seems interesting to us to study in the future the properties dynamics of Glycerol at the molecular scale, in the presence of

nanoparticles.These considerable increases in viscosity represent a significant obstacle to the use of nanofluids with machines such as motors, compressors . . .

The density of the nanofluid depends on the density of the base fluid, that of the MWCNTs and the volume fraction of the MWCNTs.The results show that at low concentrations, less than 0.01% for MWCNT/Glycerol that is a linear evolution in the relative density as a function of the volume fraction of the MWCNTs and also the classical mixing law makes it possible to estimate and correctly predict the evolution of the density of suspensions with a relative error of the order of $2.4\ 10^{-4}$ %. This can be explained by the homogeneity and the stability of the nanofluids, in other hand the temperature does not have a significant effect on the evolution of the relative density.

It is therefore important for the future of such fluids to be able to establish an energy balance that takes these mechanical aspects into account.

References

[1] Einstein A., Eine neue Bestimmung der Moleküldimensionen, Annalender Physik 19, 289–306, 1906.
[2] Brinkman H. C., The viscosity of concentrated suspensions and solutions. J Chem.Phys., 20, 571–581, 1952.
[3] Batchelor G., The effect of Brownian motion on the bulk stress in a suspension of spherical particles., J. of Fluid Mech., 97-117. 83,1977
[4] Krieger I. M., Dougherty T.J., A mechanism for non-Newtonian flow in suspension of rigid spheres, J. Trans. Soc. Rheol. 137e152 , 3, 1959
[5] Boyer F., Suspensions concentrées : Expériences originales de rhéologie, thèse de doctorat, Université d'Aix-Marseille (2011).
[6] Maron, S.H., Pierce, P.E., Application of Ree-Eyring generalized flow theory to suspensions of spherical particles. J. Colloid Sci.11, 80-95. 1956.
[7] Cross M. M., Viscosity-concentration-shear rate relations for suspensions Rheological Acta, 14,402-403. (1975).
[8] S. Bobbo, L. Fedele, A. Benetti, L. Colla,M. Fabrizio, C. Pagura, S. Barison, Viscosity of water based SWCNH and TiO2 nanofluids, Exp. Thermal Fluid Sci. 36 (1) 65–71. (2012)
[9] Nguyen C.T., Desgranges F., Roy G., Galanis N., Maré T., Boutcher S., AngueMintsa H., Viscosity data for Al2O3 water nanofluid hysteresis: is heat transfer enhancement using nanofluids reliable?, International Journal of Thermal Sciences, 47, 103-111. (2008)
[10] Phuoc T. X., Massoudi M., Chen R. H., Viscosity and thermal conductivity of nanofluids containing carbon nanotubes stabilized by chitosan, Int J. Thermal Sci., 50, 12-18. (2011)
[11] Kinloch I. A., Roberts S. A., Windle A. H., A rheological study of concentrated aqueous nanotube dispersions, Polymer 43,7483-7491. (2002)
[12] Ding Y., Alias H., Wen D., Williams R.A., Heat transfer of aqueous suspensions of carbonnanoubes (CNT nanofluids), International Journal of Heat and Mass Transfer, 49/1-2, 240-250. (2006)
[13] Wang J., Zhu J., Zhang X., Chen Y., Heat transfer and pressure drop of nanofluids containing carbon nanotubes in laminar flows, Experimental Thermal and Fluid Science, 44, 716-721. (2013)
[14] Indhuja A., Suganthi K. S., Manikandan S., Rajan K. S., Viscosity and thermal conductivity of dispersions of gum arabic capped MWCNT in water: Influence of MWCNT concentration and temperature, article in press, 2013
[15] Aladag B., Halelfadl S., Doner N., Maré T., Duret S., Estellé P., Experimental investigations of the viscosity of nanofluids at low temperatures, App. Energy, 97 ,876-880. (2012)
[16] Gholamnez V. N., Dorany A., Effect of single walled Carbon nanotubes on the viscosity of lubrifiants, ICAEE, Energy Procedia, 14, 512-517. (2012)
[17] Indhuja A., Suganthi K. S., Manikandan S., Rajan K. S., Viscosity and thermal conductivity of dispersions of gum arabic capped MWCNT in water: Influence of MWCNT concentration and temperature, article in press, 2013.
[18] Kim Y.J., Ma H., Yu Q., Plasma nanocoated carbon nanotubes for heat transfer nanofluids. Nanotechnology; 21:295703. 2010
[19] Ko G. H., Heo K., Lee K., Kim D. S., Kim C., Sohn Y., Choi M., An experimental study on the pressure drop of nanofluids containing carbon nanotubes in a horizontal tube, International Journal of Heat and Mass Transfer, 50, 4749-4753. (2007)
[20] Chen L, Xie H, Silicon oil based multiwalled carbon nanotubes nanofluid with optimized thermal conductivity enhancement, Colloids and Surfaces A: Physicochemical and Engineering Aspects, 352, 136-140, 2009.
[21] Garg P., Alvarado J. L., Marsh C., Carlson T. A., Kessler D. A., Annamali K., An experimental study on the effect of ultrasonification on viscosity and heat transfer performance of multi-wall carbon nanotube-based aqueous nanofluids, Int J Heat Mass Transfer, 52, 5090-5101, 2009.
[22] Yang, Y., Grulke E. A., Zhang Z. G., Wu G., Thermal and rheological properties of carbon nanotube-in-oil dispersions J. Appl Phys., 99, 114307. (2006)

[23] Ruan B., Jacobi A. M., heat transfer characteristics of Multi-walled carbon nanotubes suspensions (MWCNT nanofluids) in intertube falling film flow, International Journal of Heat and mass transfer, 55, 3186-3195. (2012)
[24] Chen F. L., Yang J. C., Zhou W., He Y., Huang Y., Jiang B., Experimental study on the characteristics of thermal conductivity and shear viscosity of viscoelastic-fluidbasednanofluids containing multiwalled carbon nanotubes, ThermochimicaActa, 556, 47-53. (2013)
[25] Kumaresan V., Velraj R., Das S. K., Convective heat transfer characteristics ofsecondary refrigerant based CNT nanofluids in a tubular heat exchanger, InternationalJournal of Refrigeration, 35, 2287-2296. (2012)
[26] Pakdamana M. F., Akhavan-Behabadi M. A., Razi P., An experimental investigation on thermo-physical properties and overall performance of MWCNT/heat transfer oil nanofluid flow inside vertical helically coiled tubes, Experimental Thermal and Fluid Science 40, 103-111. (2012)

CHAPTER IV:

PHOTOSTORAGE OF ENERGY IN NOVEL NANO-SYSTEM OF GLYCEROL/$ER_2P_4O_{13}$/MWCNT

INTRODUCTION

Most organic liquids like Glycerol are called insulators, as opposed to molten metals and electrolyte solutions. In fact, while the conductivity of the liquids in question is generally low (10^{-6} to 10^{-12} Ω^{-1}.cm^{-1}) in their usual state of purity, it is often much greater than that of common solid insulators (<10^{-13} Ω^{-1} cm^{-1}) and it does not it is hardly possible to use them in electrical engineering and electronics.The mechanisms of this conduction result of the interaction of chemical phenomena that create ions and physics that condition the displacement of these ions and consequently the transport of electric current.

Rare earths, also called strategic metals, have electronic, magnetic properties, Optical and catalytic technologies very sought after in the new technology industry. The interest for these metals appeared from the beginning of the nineteenth century, but the generalization of their use dates back to the 1970. Today, they are found in the production of permanent magnets, in certain metal alloys and as catalysts in the oil and automobile industry. They are also used in the aviation and energy sector renewable (electric or hybrid car engines, wind turbine batteries). Lanthanides can be inserted into oxide matrices giving them electronic, optical and magnetic properties which have given rise to many applications in various fields. In addition to their use as a phosphor or in the field of medical radiography [1], rare earths are also used to produce laser sources or optical amplifiers for optical fiber transmissions in e visible and infrared [2,3]. Erbium ions (Er^{3+}) have played an important role in the development of optical telecommunications in the last years. The emission of Er^{3+} ions is crucial for optical telecommunications because this emission corresponds to the minimum attenuation of the silica fibers used to carry information. Unfortunately, the absorption cross section of Er^{3+} ions is low, of the order of $10^{-21}cm^2$ [4]. For this reason, the sensitization of Er^{3+} ions by species whose cross section Absorption is high, as nanoparticles (MWCNT) dispersed in Glycerol for example, is of major interest. Glycerol will be one of the key platform chemicals of this new industry as it offers a key competitive advantage: Its unique chemical versatility due to uniquely high functionalization of the C3-backbone with three hydroxyl groups. It is this versatility, indeed, that made possible the synthesis of the first thermoset polymer, Plantics-GX, or that of squalane and vitamin D [5], or long chain C16-C18 fatty acids from glycerin and lignocellulosic hydrolysates [6], The biotechnology squalane derived from pure glycerol is of high purity (99% to 101%) and completely devoid of color and odor ever more, glycerol will be obtained by oleo chemicals manufacturing from vegetable oil and tallow, while biodiesel production will continue to grow to eventually reach a plateau, and cultivation of drought resistant crops such as Jatropha curcas in arid lands, not in competition with food or

feed, will provide another source of valued vegetable oil feedstock. A number of research efforts aimed at understanding the dynamics of nanofluids thermal properties have been published, such as on thermal conductivity [7–10], electrical resistivity and electrical conductivity [11–13]. Finally, significant enhancement of electrical conductivity in glycerol doped by nanomaterials was reported [14]. Much of the work done in this emerging field as portrayed above and widespread in the literature is on MWCNT with different base fluids. Nevertheless, there are no experimental data on electrical resistivity, electrical conductivity, and viscosity of MWCNT/$Er_2P_4O_{13}$/ Glycerol. Hence, this gave credence to the present research, which focuses on the viscosity, electrical conductivity, of glycerol-based MWCNT and Tetrapolyphosphate of Erbium $Er_2P_4O_{13}$ nanofluids. This work is carried out in the Einstein's concentration regime of $\Phi \leq 2\%$, temperature range of 20–70◦C.

IV. 1 Reminder on the theory of energy bands

According to the figure 4.1, we can see the difference between, from left to right, metal, semiconductor and an insulator.

The notion of energy band is, in general, associated with ordered crystal lattices. In this type of network, the interactions between molecular orbits of atoms form degenerate states leading to two distinct bands: the valence band and the conduction band called allowed bands. In the valence band, holes can move and in the conduction band, electrons can move freely. These two bands are separated by a bandgap. In the permitted bands, the number of places varies depending on energy. According to the model of the energy bands, the material becomes dielectric that is to say a poor conductor of electricity, when the width of the bandgap is greater than 5 eV but less than 10 eV. Then, only a very small number of electrons receive, at room temperature, the thermal energy necessary to effect a transition in the conduction band.

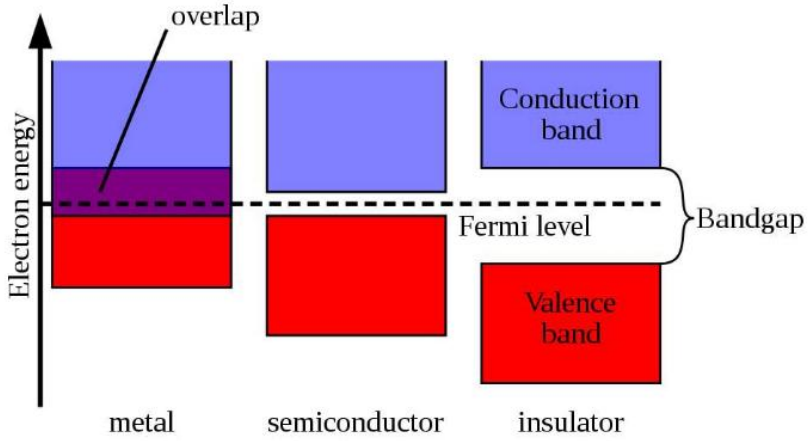

Figure 4.1: Representation of conduction and valence bands in a solid.
© Wikipedia, Pieter Kuiper

When the temperature rises, the probability of transition increases and the electrical conductivity σ is expressed by:

$$\sigma = \sigma_0 exp\left(-\frac{W}{K_B T}\right) \quad (4.1)$$

Where W is the activation energy of the conduction process, T is the absolute temperature and $\mathbf{K_B}$ is the Boltzmann constant =1.38064852 × 10^{-23} m^2 kg s^{-2} K^{-1}

IV. 2 Synthesis of TPE powder and his Electrical conductivity and resistivity

IV. 2. 1 Synthesis of TPE ($Er_2P_4O_{13}$) powder

For the synthesis of TPE by solid way, the Erbium oxide Nano powder Er_2O_3 of pink color and the Ammonium of hydrogen phosphates $NH_4H_2PO_4$ a white solid, were mixed. This mixture was then heat treated thermally at 250 ° C to eliminate water molecules then at 500 ° C to decompose the dihydrogen ammonium phosphorus $(NH4)_2HPO_4$ and finally at 850 °C necessary for the obtaining the $Er_2P_4O_{13}$ phase with a pink color as shown in figure (4.2) and a molar mass M = 666.403g / mol, the chemical reaction is:

$$\boldsymbol{Er_2O_3 + 4NH_4H_2PO_4 \rightarrow Er_2P_4O_{13} + 4NH_3 + 6H_20} \quad (4.2)$$

Figure 4.2: Photograph of TPE at 850°C

IV. 2. 2 Electrical conductivity and resistivity of TPE ($Er_2P_4O_{13}$) powder

Reminders on the conductivity of the solutions, is the ability of a material or a solution to the electrical conductivity, unlike the resistivity let the electric charges move freely, in other words to allow the passage of the electric current. Among the best conductors, there are metals (such as copper, aluminum, etc.) for which charge carriers are the "free electrons". In the case of electrolyte solutions, the flow of current is ensured by the ions. The conductivity of these solutions depends on the nature of the ions present and their concentrations. It can be measured using a conductivity meter. The knowledge of conductivity makes it possible to evaluate the ion concentration of a solution. Any charged species is likely

to carry electric current within a solution. The current is transported by displacement of the positive charges (cations) in the direction of the electric field, towards the negative pole. Recall that, according to Ohm's law, the electrical resistance R characterizes the difficulty of passing an electric current through a medium. Resistivity is the capacity of a medium to oppose the passage of an electric current. This is an intrinsic property of the material which does not depend on its geometry or its dimensions. It is defined as the ohmic resistance of a cylinder of unit section and length. The electrical resistivity **ρ** which is expressed in Ω.m, is the inverse of the electrical conductivity **σ** (capacity of the medium to pass an electric current) which is expressed in S / m. The resistivity **ρ** can be calculated using the relation:

$$\boldsymbol{\rho = \frac{R.S}{L}} \qquad (4.3)$$

Where ρ: electrical resistivity [Ω.m]

R: electrical resistance [Ω]

L: sample length [m]

S: plane section of the sample [m²]

The value of resistance R is obtained by taking the ratio of the potential difference between the two opposite surfaces to the intensity of the current flowing through the material (Ohm's law).

$$\boldsymbol{R = \frac{\Delta V}{I}} \qquad (4.4)$$

With: ΔV: difference in electric potential [V]

I: the intensity of the current [A]

IV. 3 Experimental and analytical methods

Ultrasound is used for the synthesis of nanoparticles of TPE material by the addition of Glycerol to evaluate the electrical properties; we analyzed the conductivity and resistivity during aqueous phase oxidation as a function of temperature so this method was used to insert TPE into a multi-walled carbon nanotube (MWCNT). The synthesized composites contained only TPE compound in the MWCNT. The table (4.1) below represents the masses of precursors used in the synthesis of nanoparticles of $Er_2P_4O_{13}$ (TPE) powder.

Table 4.1: Composition of compounds

	Glycerol	TPE/Glycerol	MWCNT/TPE /Glycerol	MWCNT/PTE /Glycerol
MWCNT(mg)	0,0	0,0	0,1	0,50
TPE (mg)	0,0	5,0	11,1	11,00
Ethanol (ml)	0,0	0,0	1,0	1,00
Glycerol (ml)	10,0	10,0	9,0	9,00

IV. 4 Result and discussion

IV. 4. 1 Conductivity and resistivity measurement

Electrical conductivity characterizes the ability of a body to pass electrical current. It is the reciprocal unit of electrical resistivity that expressed in MegaOhm.m (MΩ.m) and is expressed, most often, in siemens/cm (S/cm), in microsiemens/cm (µS/cm). We notice that before performing conductivity measurement of an electrolytic solution, the instrument is, firstly, calibrated to a standard solution with known conductivity value. The conductivity and resistivity were measured by the Mettler "Seven Compact" at different temperatures. Results the compositions of compound of nano-system are summarized in table (4.2).

Table 4.2: Composition of compound after analysis

Compound	Glycerol	
Temperature on °C	Conductivityσ	Resistivityρ
25,7	0,284	3,76
45,5	0,293	3,7
49	0,386	2,91
52	0,572	1,83
54	0,779	1,28
Compound	PTE/Glycerol	
Temperature on °C	Conductivity	resistivity*0,01
23	0,053	0,1495
49,5	0,061	0,1336
63,7	0,097	0,1115
compound	0,1MWCNT+PTE/Glycerol	
Temperature on °C	Conductivity	resistivity*0,01
23	0,027	0,2724
49,5	0,053	0,1942
63,7	0,14	0,0054
compound	0,5MWCNT+PTE/Glycerol	
Temperature on °C	Conductivity	resistivity*0,01
23	0,082	0,1116
49,5	0,122	0,0852
63,7	0,189	0,0536

Figure 4.3 shows examples of the temperature dependences of electrical conductivity and resistivity for pure Glycerol. The pronounced percolation behavior of electrical conductivity was observed for Glycerol. However, significant decrease of electrical resistivity ρ and small enhancement of its electrical conductivity σ.

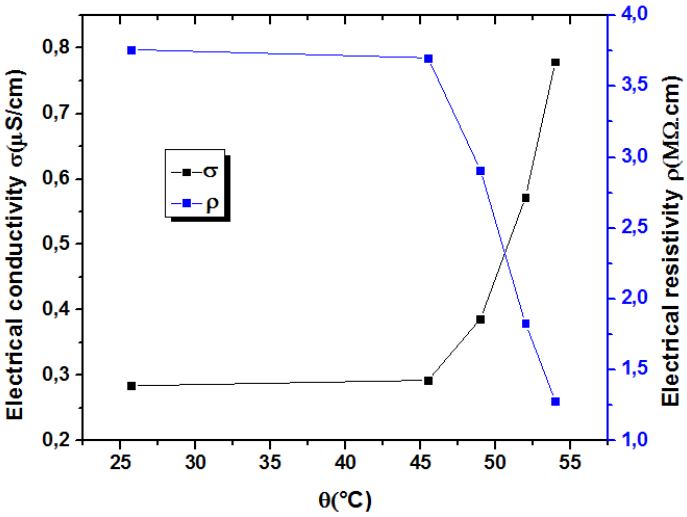

Figure 4.3: Electrical conductivity and resistivity of Glycerol as a function of temperature

This graph represents the evolution of the resistivity and the variation of the electrical conductivity of the TPE / Glycerol nanofluid as a function of temperature, the value of the electrical conductivity increases and the resistivity drops equivalent to the increase. From these results, we deduce that the electric current is transported by the ions of the solution such as that of Erbium Er^{3+} and of phosphate $P_4O_{13}^{6-}$ the effects due to the variations of temperature, because this factor has a primordial importance on the behavior of nanofluid resistivity as shown in the figure(4.4).

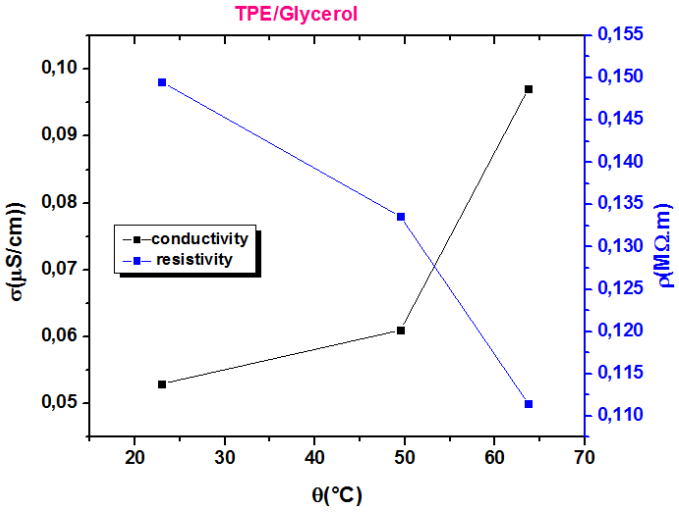

Figure 4.4: Electrical conductivity and resistivity of TPE/Glycerol as a function of temperature

While porous and well connected grains give higher electronic conductivity. It can be explained in term of angle P-O-P and O-P-O observed which basically lead to competitive variation in Grain boundary energy and surface energy then, This is very common phenomena known as pulverization which creates micro cracks in the medium result in increase in resistance and decrease in particle size as shown in the (Figures 4.3- 4.4).

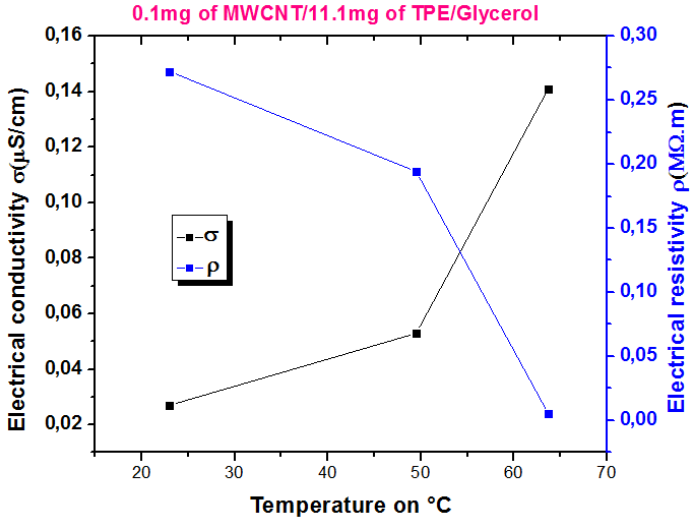

Figure 4.5: Electrical conductivity and resistivity of MWCNT/TPE/Glycerol as a function of temperature.

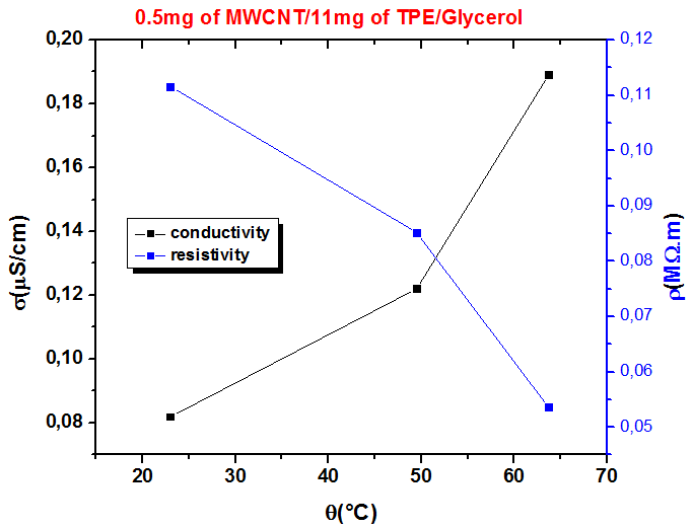

Figure 4.6: Electrical conductivity and resistivity of MWCNT/TPE/Glycerol as a function of temperature

This graph represents the evolution of the resistivity and the electrical conductivity of the MWCNT/TPE/Glycerol nanofluid as a function of temperature, it should be noted that the latter have a conductivity higher than that of glycerol [15], this remark illustrates the fact that the results obtained do not depend only on the high conductivity of the nanoparticles us shown in the figure 4.3 and 4.4, but also depend on the mass fraction of the latter. The effect

of temperature on the electrical conductivity of the MWCNT/TPE/Glycerol nanofluids has been studied and the results show that temperature greatly influenced the electrical conductivity, as presented in the figure 4.5 and 4.6. The data presented reveal the effect of MWCNT and TPE nanoparticle loading on the electrical conductivity of glycerol. In the figure, it is convenient to say that the increase in volume fraction have much significant effect on the electrical conductivity [16]. However, at 0.1 mg of MWCNT, the highest value of electrical conductivity was recorded is 0.141µS/cm and at 0.5 mg of MWCNT, the highest value of electrical conductivity was recorded is 0.189µS/cm also we notice that the electrical resistivity decreases with the volume fraction and temperatures. Increasing electrical conductivity is obvious with increasing temperature. This is clearly shown in table 4.2. But with the addition of nanomaterials, electrical conductivity is noticeably visible. Also, by increasing the temperature in all weight concentrations, electrical conductivity increases. Increase in temperature causes electrons that exist in valence layer going to conductivity layer and participate in conductance [17].

IV. 4. 2 Scanning Electron Microscope (SEM)

In order to fully understand and know the properties of a material, it is necessary to characterize it. For this, various complementary techniques of surface and volume analysis are at our disposal. Among the techniques for the overall characterization of volume, we note the techniques of scanning and transmission electron microscopy, UV-Visible spectrophotometry. Scanning electron microscopy (SEM) was first developed in Germany in the 1930s in order to be able to observe ever smaller elements. Unlike optical microscopes, it is not photons but electrons that are collected. Most objects can be observed with SEM provided that their surface is conductive. If this condition is not met, it is possible to deposit a thin layer of a conductive metal or carbon on the surface of the object. In the field of chemistry, the scanning electron microscope makes it possible to control the morphology and the micrometric, even nanometric texture of a material, but also its surface composition.

The sample is analyzed using electrons accelerated by voltages of several tens of kV. When this beam of primary electrons comes into contact with the sample, several phenomena occur:

- The transmitted electrons are directed towards the mass.
- Backscattered, secondary and Auger electrons are selectively collected by detectors and then converted to display the topography of the sample on a display screen.
- X-rays are emitted by ionization of the deep layers of the sample by electrons.

Under the impact of the accelerated primary electron beam, the backscattered electrons and the secondary electrons emitted by the sample are selectively collected by detectors which transmit a signal to a cathode ray screen whose scanning is synchronized with the scanning of the object. In general, the role of the detector is to recover the signal induced by this probe to form an image, mapping the intensity of the signal. Secondary electrons are the most interesting for visualizing topology because they originate from the surface of the sample and provide high resolution images (around 5 nm).

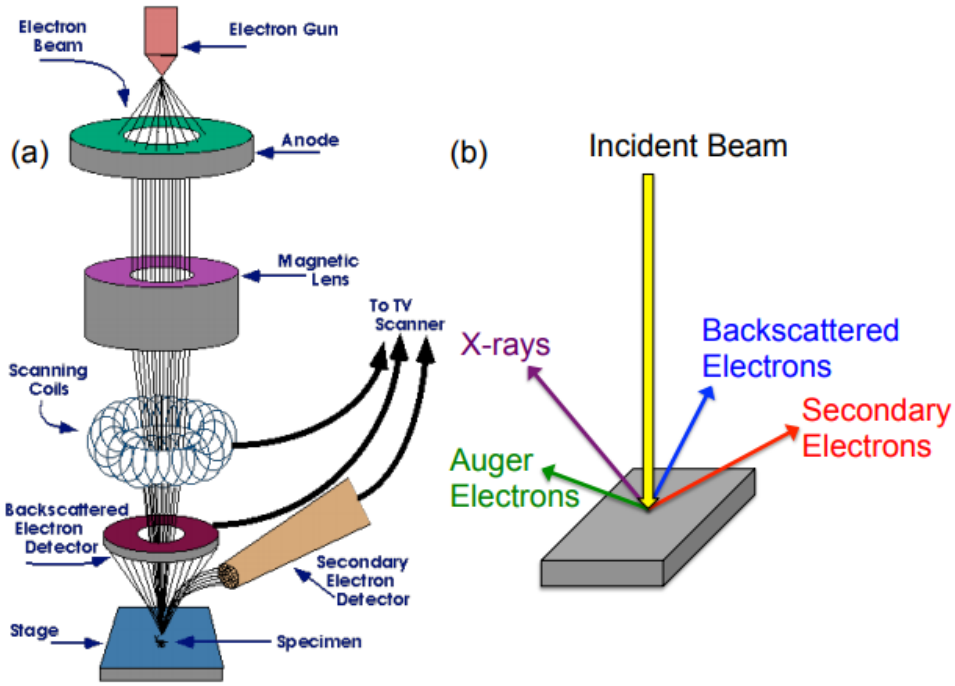

Figure 4.7: Schematic diagram of (a) the SEM [18]

Scanning Electron Microscopy is a technique that involves scanning the surface of a sample with electrons. (Fig. 4.8, 4.9 and 4.10) represent micrographs of a powder of Erbium $Er_2P_4O_{13}$ Tetrapolyphosphate obtained by this optical analysis technique

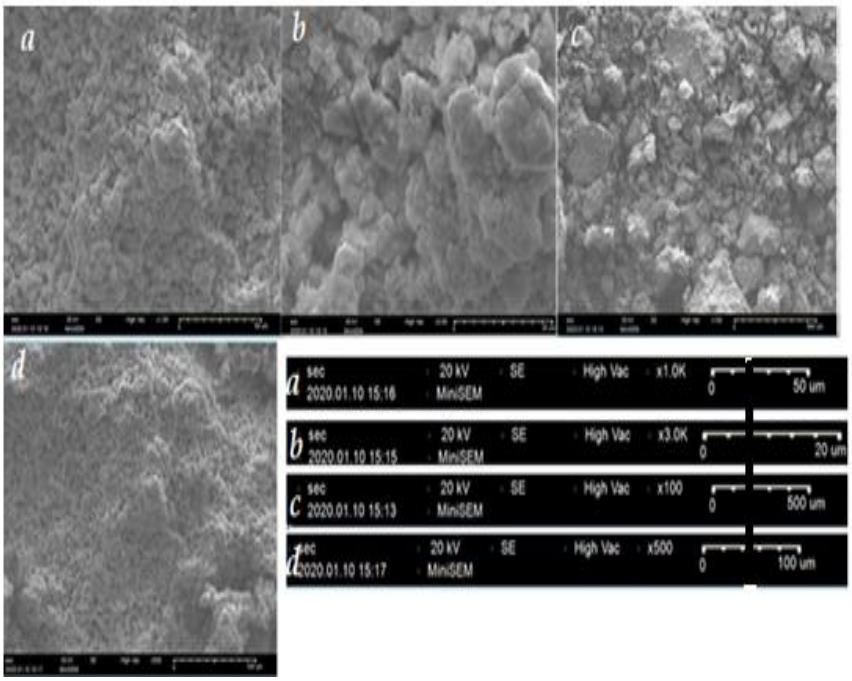

Figure 4.8: Micrographs of a powder of Erbium Er2P4O13 Tetrapolyphosphates at 650 °C obtained by SEM at four different magnifications

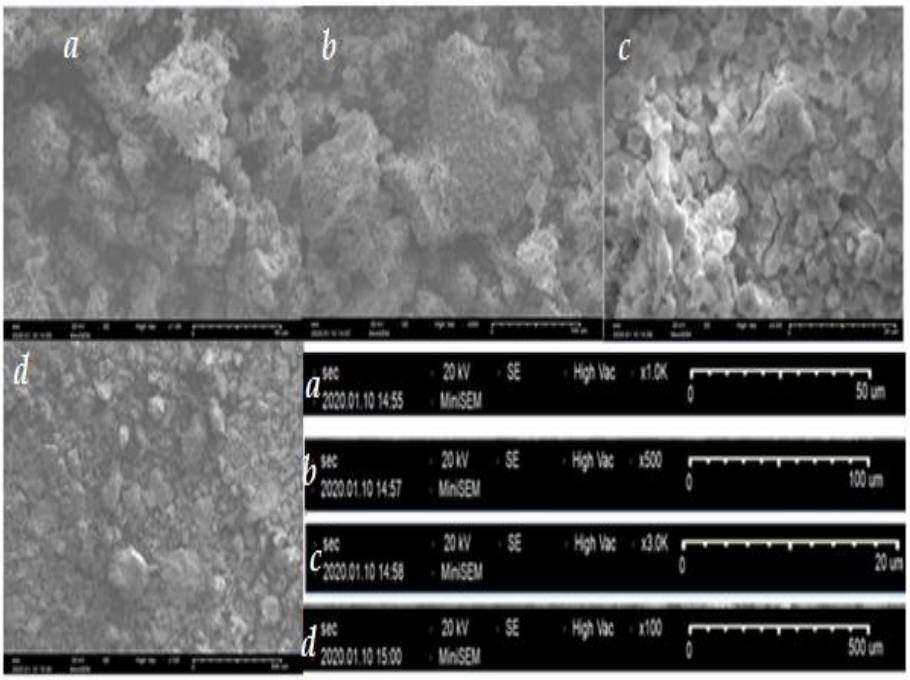

Figure 4.9: Micrographs of a powder of Erbium Er2P4O13 Tetrapolyphosphates at 850 °C obtained by SEM at four different magnifications

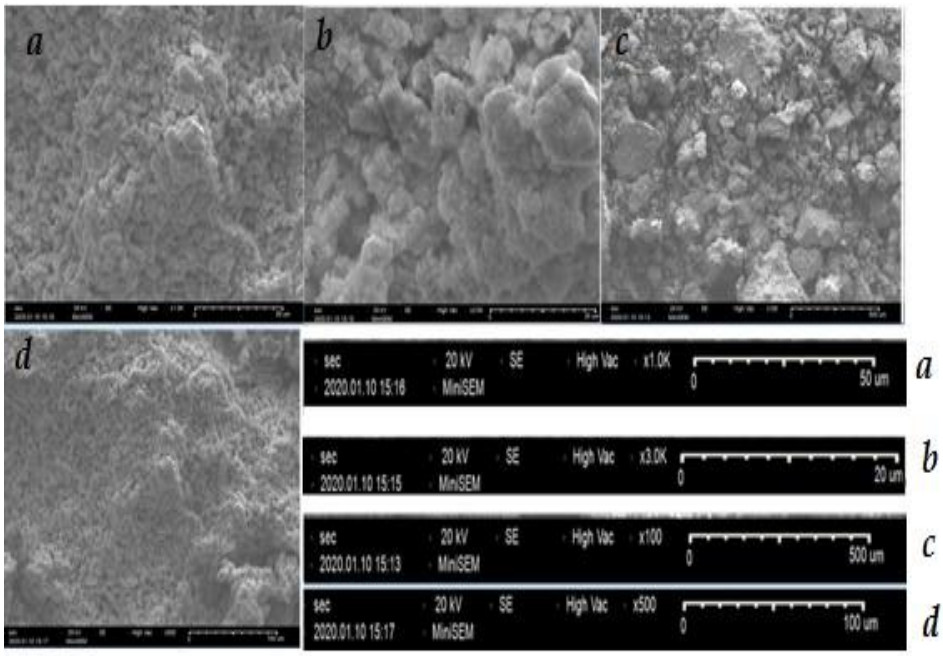

Figure 4.10: Micrographs of a powder of Erbium Er2P4O13 Tetrapolyphosphates at 1000 °C obtained by SEM at four different magnifications

Micrographs of the scanning electron microscope showed us nanoparticles of different shapes so their distribution was in a disorderly way; we saw a distribution of pore sizes well localized as shown in the figures (4.8, 4.9, 4.10). And SEM images have shown that the surface morphology of the various powder samples is quite different, cause of the effect of temperature.

The crystallites which are not similar but they are homogeneous so that the shapes of the layers are well organized and oriented in three dimensions. Textures presented in these figures have many layers with different thicknesses that showed white and black contrast, there are also deep pores. The size of these particles is on a microscopic scale 20-200µm. The morphology of these samples is not regular and panoramic. The distribution of the crystallites is poorly organized and periodic and it shows the atoms which constitute the material (Fig.4.8). The particles are not uniform with the appearance of a few orifices of medium size and well dispersed, and the size of the pores increased. The presence of pores is observed only on the periphery of the sample. We observe a big change in grain size. The pore has been changed in the middle of the temperature and the grains are tetragonal shape with very smooth surfaces. The arrangements are irregular and non-uniform. Some of these grains seem to be oriented perpendicular to the surface (Fig.4.9 - 4.10).

IV. 4. 3 Description of the structure Tetrapolyphosphate of Erbium $Er_2P_4O_{13}$

The projection of the structure on the ab plane shows that the basic structural unit of the $Er_2P_4O_{13}$ phase is composed of two phosphate chains. Each of them is formed by PO_4tetrahedra sharing vertices with a formula of $(PO_3)^{n-}$ (Fig.4.11 a). The chains $(PO_3)^{n-}$ (two per mesh) develop in direction a thus giving a zigzag shape. These phosphate chains are joined together by parallel chains of Erbium polyhedra forming a three-dimensional network. This stacking generates empty tunnels perpendicular to the plane bc (Fig.4.11b).

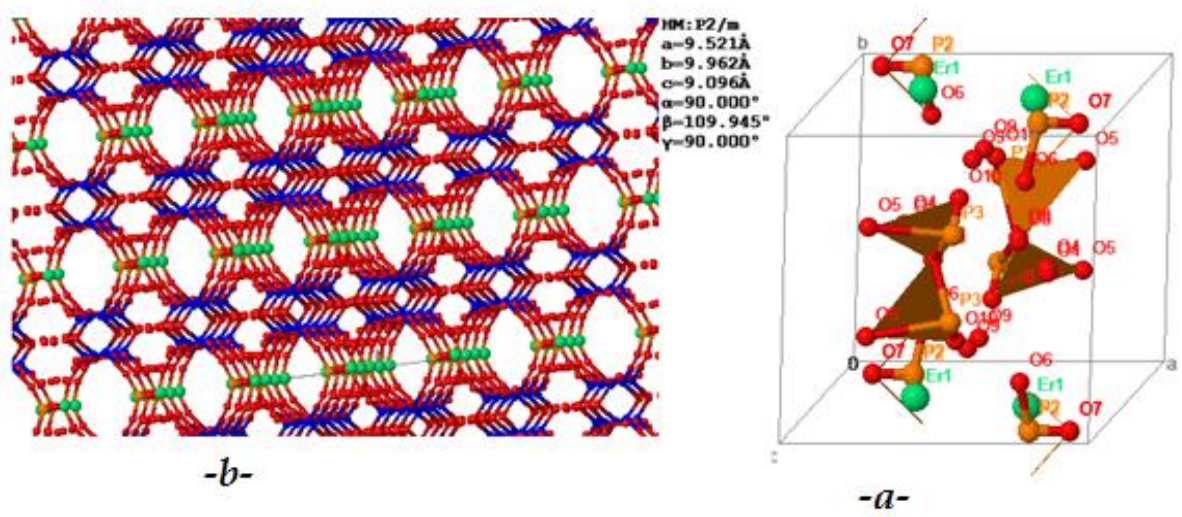

Figure 4.11: Projection of the structure $Er_2P_4O_{13}$ on the plane ab (Er^{3+}: green, P: Yellow and blue O^{2-}: red). - a- and Projection on the plane bc of the structure $Er_2P_4O_{13}$. Presence of tunnels parallel to the direction a. –b-

IV. 4. 4 The Spectroscopy Infra-Red (IR) for the analysis of nanofluids

The nano-systems prepared in this work were analyzed by the infrared type PerkinElmer Spectrum Version 10.4.2 FT-IR Spectrometer. FTIR studies were carried out in the range 400–4000 cm^{-1} in the transmittance mode in the fingerprint area. There is a strong absorption of the phosphate groups (PO_3) and the deformation (PO_3) [19]. It showed a shift of the most intense peaks of each compound thus the effect of MWCNT and TPE on Glycerol. We suggested that the nano-system is homogeneous and the particles were well separated. An increase in transmittance was observed when the matrix has been modified. This increase due of the absorption for MWCNT, the figure (4.12) shows the spectra of nano-system of Glycerol / $Er_2P_4O_{13}$ / MWCNT.

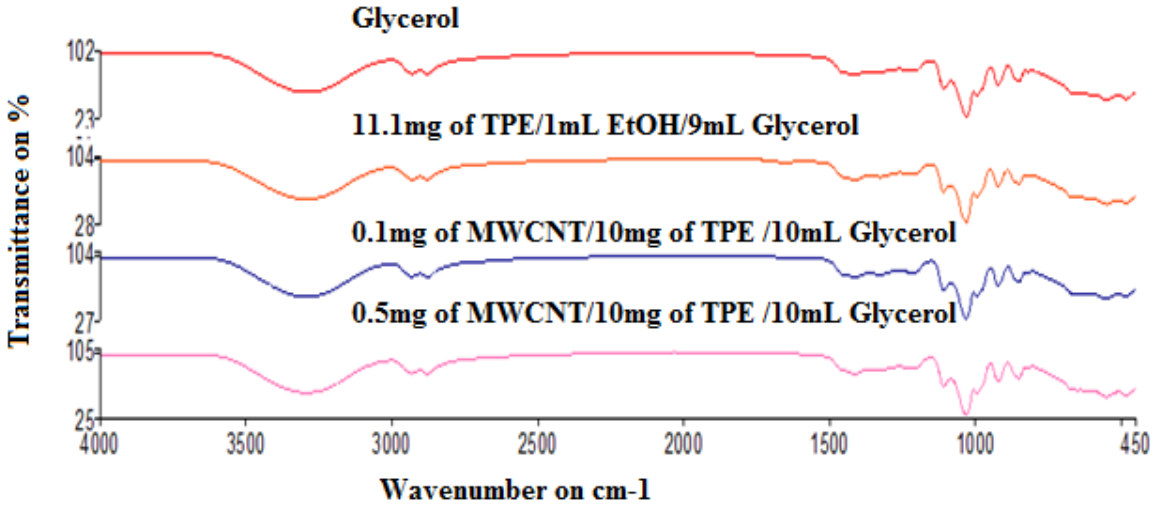

Figure 4.12: The infrared Spectra of nano-system of Glycerol / Er2P4O13 / MWCNT

IV. 4. 5 Glycerol anti-corrosive

With the increasingly serious environmental pollution and energy issues, Glycerol-based lubricating materials and Glycerol based MWCNT will gradually replace oil-based lubricating materials in some specific applications: in hydraulic fluid, cutting fluid, and the oil extraction industry due to their excellent properties, such as high thermal conductivity, good cooling performance, which has become a trend. Glycerol have the advantages of simple synthesis, good stability solubility, and excellent corrosion resistance properties, providing different methods to better solve the problems of traditional water-based additives**.**

In service, metallic materials are often in contact with an aggressive liquid or gaseous medium, so the corrosion phenomenon is a problem of the surface or more precisely of the interface between a metal and an aggressive liquid or gaseous medium; the corrosion process leads to destruction of metallic materials. This phenomenon has taken on considerable importance today. Metals are distinguished from other materials by a set of advantageous properties such as good ductility, high tensile strength, resistance to high temperatures, good electrical and thermal conductivity, great ease of processing, etc. Their drawbacks are their instability in contact with air and water, which reduces their resistance to corrosion and wear, ie their durability. However, in order to perform their function better during the expected service life, appropriate corrosion protection techniques are employed. The use of new corrosion resistant materials has been the subject of a great deal of research in recent years.

From an economic point of view corrosion is of prime importance. For example, it is estimated that each year a quarter of steel production is destroyed by corrosion, which corresponds to approximately 150 million tonnes / year or even 5 tonnes / second. These losses could be greater if there was no corrosion protection.

The replacement of corroded equipment and materials constitutes a very high financial burden for the industry, to which must be added the shortfall corresponding to the shutdown of the installations necessary to carry out the repairs. Corrosion is not limited to steel, but affects all metals as well as polymers and ceramics and it affects all areas of the economy from integrated circuit to Reinforced Concrete Bridge. The evaluation of losses due to corrosion must take into account:

- Direct losses: replacement of corroded materials and equipment.
- Indirect losses: repair, production losses.

Direct losses therefore only represent a part of the costs of corrosion. They are often lower than indirect losses. For example, if one has to stop a machine or an equipment of which one of the constituent elements is corroded, the price of the latter is derisory compared to the losses of gain due to the lack of production.

The causes of corrosion are multiple and complex and they result from chemical and / or physical interactions between the material and its environment. Corrosion to date is not completely clarified and this is explained by laboratory tests which do not allow to predict with certainty the behavior of a given metal or alloy when exposed to corrosion and in the same way there is no resistant metal, in general a metal resists corrosion under well defined conditions.

Corrosion problem has always been a problem to be solved urgently for steels and irons, which limits their applications. The corrosion properties were evaluated by immersion corrosion test of iron nail in Water, in Glycerol and in mixing Water/Glycerol at t=0 considered as reference, t= 2 months and t= 6 months, there exists much pitting corrosion pits on the iron nail surface immerged in Water and in mixing Water/Glycerol, the color of samples containing water is obviously blackened as shown in figure (4.13). Compared with reference sample, the participation of Glycerol can significantly improve its corrosion resistance that have the most obvious effects, following which, neither massive corrosion marks nor significant changes in color occurred on the iron nail surfaces immerged in pure Glycerol.

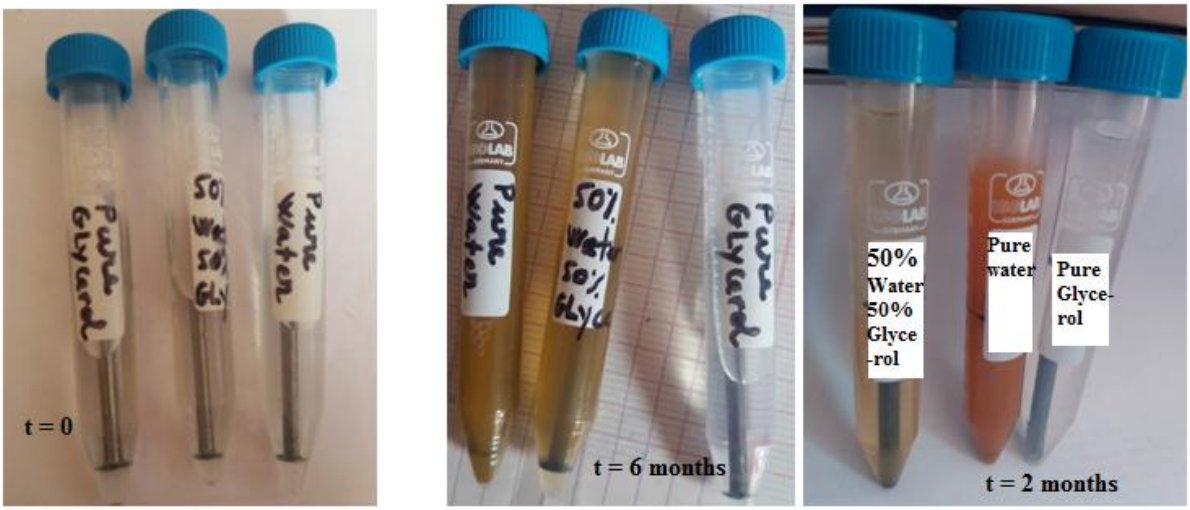

Figure 4.13: Iron nail in Water, in Glycerol and in mixing Water/Glycerol at t=0 considered as reference, t= 2 months and t= 6 months

We notice that Glycerol shows excellent anti-corrosive properties , this indicates new possibilities of usage of Glycerol it could be utilized as anticorrosive soap; this kind of application would only be possible for technical demands such as washing cars, tanks, lorries and trains, as well as external building surfaces. and also Glycerol can be evaluated as a corrosion inhibitor for steel specimen.

CONCLUSION 4

Experimental investigation of MWCNT/$Er_2P_4O_{13}$/Glycerol nanofluids in the Einstein concentration regime has been performed for electrical conductivity and electrical resistivity evolutions as functions of weight concentration and temperature in the region of 23–64°C. Sonicating for 30 mn, stable Glycerol nanofluids were prepared and investigated. The three solutions: Glycerol / $Er_2P_4O_{13}$ / MWCNT at various volume fractions, showed a great interest according to their conductivity and resistivity. Indeed, for three solutions at different temperatures, the results of conductivity and resistivity for nano-system are shown in the table 2. The results showed considerable enhancement in electrical conductivity and a decrease in electrical resistivity of nanofluids in all concentrations compared to pure Glycerol Owing to their sufficiently wide regions of applicability, this nanofluids are believed to represent an useful engineering tool for analysis and optimizing such ion condensation effects in nanofluids could potentially increase their applicability in nanotechnologies for which electrical conductivity is required and also Glycerol can be evaluated as a corrosion inhibitor for steel and iron specimen. In perspectives, we would like to highlight the stability of our

nano-system which can be described with the help of physico-chemical tests, but more coordinated research is needed.

References

[1] C.Duverger,M.Montagna,R.Rolli,S.Ronchin,L.Zampedri,et al.,Erbium¬activated silica xerogels:spectroscopic and optical properties. Journal of Non Crystalline Solids, 280(1$3): p.261$268. 2001.

[2] H. Bi, W. Cai, et L. Zhang,Reversible emission enhancement for Ce3+-doped silica nanoparticles dispersed within pores of mesoporous silica.Materials Research Bulletin, 35(9): p. 1495$ 1501. 2000.

[3] J.M.E.Vanagas,M.Mazilu,P.Riblet,B.Hönerlage,S.Juodkazis,F.Paille,J.C.Plenet,J. G.Dumas,M.PetrauskasandJ.Vaitkus,Dynamics of optical nonlinearties induced by strong light illumination in CdS nanocrystallites. Journal of AppliedPhysics, 81(8):p.3586$359,1997.

[4] W. J. Miniscalco, Erbium doped glasses for fiber amplifiers at 1500nm, J. Ligh.Tech. 9 234-250 (1991).

[5] S. O'Connor, Challenges and opportunities in commercializing a fermentation based production platform, World Congress on Industrial Biotechnology, April 20, 2016.

[6] J.V. Álvarez, MicroBioOil, World Bio Markets, Amsterdam, March 14 16, 2016.

[7] Gupta, S. S., Siva, M. V, Krishnan, S., Sreeprasad, T.S., Singh, P. K., Pradeep, T., and Das, S. K., Thermal Conductivity Enhancement of Nanofluids Containing Graphene Nanosheets, *Journal of Heat Transfer*, vol. 110, no. 084302, pp. 1–7, 2011

[8] Lee, S., Choi, U. S., and Li, S., Measuring Thermal Conductivity of Fluids Containing Oxide Nanoparticles, Journal of Heat Transfer, vol. 121, pp. 280–289, 1999.

[9] Hojjat, M., Etemad, S.G., Bagheri, R., and Thibault, J.,Thermal Conductivity of Non-Newtonian Nanofluids: Experimental Data and Modeling Using Neural Network, InternationalJournal of Heat and Mass Transfer, vol. 54,pp. 1017–1023, 2011.

[10] Choi, S. U. S., Enhancing Thermal Conductivity of Fluid With Nanoparticles, ASME, New York, NY, pp. 99–109,1995.

[11] Sarojini, K. G. K., Manoj, S. V., Singh, P. K., Pradeep, T., and Das, S. K., Electrical Conductivity of Ceramic and Metallic Nanofluids, Colloids and Surfaces A: Physicochemicaland Engineering Aspects, vol. 417, pp. 39–46, 2013.

[12] White, S. B., Shih, A. J., and Pipe, K. P., Investigation of the Electrical Conductivity of Propylene Glycol-Based ZnO Nanofluids, Nanoscale Research Letters, vol. 6, pp. 346–350, 2011.

[13] Wang, J. J., Zheng, R. T., Gao, J. W., and Chen, G., Heat Conduction Mechanisms in Nanofluids and Suspensions, Nano Today, vol. 7, no. 2, pp. 124–136, 2012.

[14] Bulavin L.A., Lebovka N.I., Kyslyi Y.A. et al. Microstructural, rheological, and conducto-metric studies of multiwalled carbon nanotube suspensions in glycerol, Ukr. J. Phys., 55 (2010).

[15] Sarojini, K. G. K., Manoj, S. V., Singh, P. K., Pradeep, T., and Das, S. K., Electrical Conductivity of Ceramic and Metallic Nanofluids, Colloids and Surfaces A: Physico- chemical and Engineering Aspects, vol. 417, pp. 39–46, 2013.

[16] White, S. B., Shih, A. J., and Pipe, K. P., Investigation of the Electrical Conductivity of Propylene Glycol-Based ZnO Nanofluids, Nanoscale Research Letters, vol. 6, pp. 346–350, 2011.

[17] H.R. Azimi, R. Taheri, Electrical conductivity of CuO nanofluids, International Journal of Nano Dimension 6 (Issue 1) 77–81, (2015)

[18] Schematic for scanning electron microscopy column, URL http://www-archive.mse.iastate.edu/microscopy/path2.html. (2003).

[19] B. Tbib, M. Eddya, and K. El-Hami, Phosphates based pigments for new anti-corrosion application: Synthesis and characterization, AIP Conference Proceedings 1932, 030042 (2018)

CHAPTER V:

EXPERIEMENTAL INVESTIGATION OF NOVEL SEMICONDUCTOR NANOFLUID BASED GLYCEROL/MWCNT

INTRODUCTION

Since the landmark discovery by Iijima in 1991 [1], carbon nanotubes (CNTs) have attracted significant interest for applications as fillers in composite materials due to their unique mechanical, electrical, and thermal properties [2-6]. In comparison with single-walled and double-walled carbon nanotubes, multi-walled carbon nanotubes (MWCNTs) have tremendous advantages in both scientific research and practical applications owing to their easy mass production, price competitiveness and convenient modification. Over the past decade, nanofluids, suspensions of solid, nanoparticles, have gained much interest and attention because of their remarkably enhanced electrical conductivity (EC) beyond the predictions of effective medium theory and the promising applications in energy transfer technologies [7-9]. Various types of nanoparticles such as metallic and nonmetallic, with different shapes and sizes were used to prepare nanofluids, and some inspiring results have been reported [10-13] The research on MWCNTs used as fillers for the nanofluids was pioneered by Choi et al. [10] Advances in nanotechnology have permitted nanofluids to be developed. Nanofluids are suspensions of nanometer-sized materials. Compared to the pure fluid, nanofluids have been shown to have higher thermal conductivities. Colloidal nanofluids, unlike suspensions of larger particles, are stable and do not clog even micron-sized channels. Nanofluids are readily prepared by dispersing nanomaterials into a pure heat-transfer base fluid. Suspensions filled with MWCNTs have been fulfilled. The researches were carried out in the intervals of temperature 296 K to 333 K and MWCNT volumetric fraction from Φ= 0.004% to 0.01%. The MWCNTs demonstrate a number of interesting mechanical, electrical, thermal, and other physical properties. Their potential applications became a focus of many experimental and theoretical researches, as well as industrial research programs in such branches as microelectronics, sensors, materials science, biotechnology, and medicine [11]. Important “biological” implementations of MWCNTs not only demand for them to be biocompatible, but also require that stable and well dispersed suspensions of MWCNTs in water or other biologically compatible liquid systems should be created [12]. This work aimed at carrying out the microstructural researches, as well as the study of electrophysical of suspensions created based on MWCNTs and Glycerol.

V. 1 UV-Visible Spectroscopy

V. 1. 1 Principle

Spectrophotometry is an analytical technique that measures the absorbance of a medium as a function of wavelength and studies its evolution over time. More the solution is

concentrated, or more the thickness of the medium traversed is significant, more radiation is absorbed. In the case of the study of a suspension, UV-Visible spectrophotometry is particularly interesting for monitoring the sedimentation of particles absorbing in these wavelength ranges. The medium must not diffuse the radiation.

A cell containing a thickness L of liquid is crossed by a beam with a wavelength ranging from ultraviolet to visible, that is to say between 200 and 800 nm (Figure 5.1). As a result of the absorption of part of the radiation by the liquid or suspended solid particles, the intensity of the transmitted beam is lower than that of the incident beam.

The measurements are corrected by the absorption of the reference liquid alone and the resulting signal is attributed to the absorption of suspended particles. Thus, a decrease in this absorption over time testifies to the sedimentation of the suspended particles. Diffusion phenomena must be low.

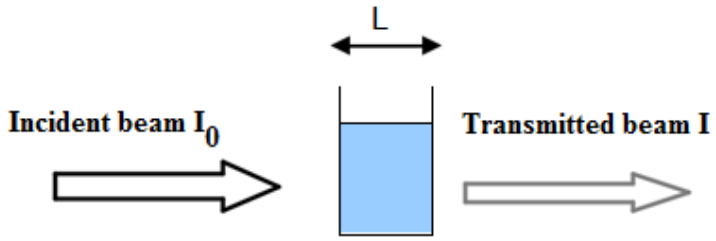

Figure 5.1: Principle of UV-Vis spectrophotometry

To measure the absorbance of the sample, the Beer-Lambert law is used:

$$\boldsymbol{A = \varepsilon . L . C} \qquad (5.1)$$

With:

$\boldsymbol{A}$: Absorbance

$\boldsymbol{\varepsilon}$: Molar extinction coefficient ($L.mol^{-1}.cm^{-1}$)

$\boldsymbol{L}$: Thickness of liquid crossed by the beam

$\boldsymbol{C}$: Molar concentration of the solution ($mol.L^{-1}$)

The measurement of the transmittance of the sample is also used in order to follow the evolution of a suspension over time. It is calculated using the following relation:

$$\boldsymbol{T = \frac{I}{I_0}} \qquad (5.2)$$

With:

T: Transmittance

I: Transmitted intensity

I_0: Intensity of the incident beam

The two relations of absorbance and transmittance are related by the following equation:

$$\boldsymbol{A = log\left(\frac{I_0}{I}\right) = log\left(\frac{1}{T}\right)} \qquad (5.3)$$

The principle of ultraviolet and visible absorption spectroscopy is based on the absorption of radiation by molecules in the range of 200 to 800 nm. This domain corresponds to energies between 1.55 eV to 6.2 eV which allow electronic transitions between an energy orbital E_1 and ahigher energy orbital E_2 of a molecule. However, as shown in Figure 5.2, there are also transitions in the fine and hyperfine structures, called vibrational and rotational, of the excited level, which generates not a line spectrum but a band spectrum which is the sum of all these transitions.In addition, in solution the molecules interact with the solvent which modifies the transition energy of the molecule and masks the fine structures. This is why, in UV-visible spectrometry, and in particular in solution, the absorption bands extend over a wavelength range from a few tens of nm to several hundred nm.

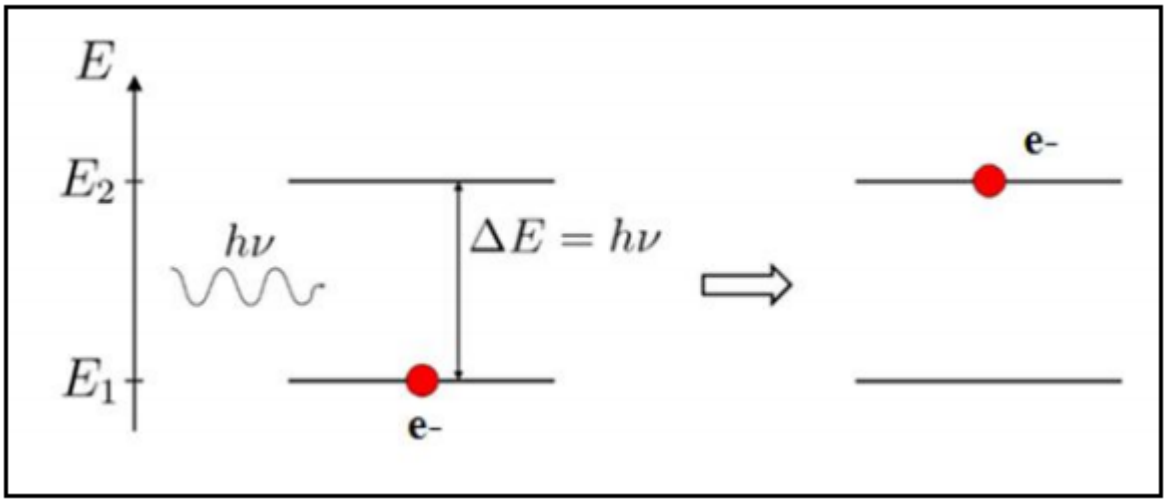

Figure 5.2: Phenomenon of absorption of light energy.

Ultraviolet-visible absorption spectroscopy is based on the phenomenon of absorption of light energy by matter. When the latter absorbs part of the energy of electromagnetic radiation, the absorption is accompanied by transition electronics (valence electrons) from a fundamental level to a higher energy level.This method provides information on the area of absorption of the compound to be studied.On the other hand, the electronic structure of the material provides information on its electrical properties and allows it to be classified among conductors, semiconductors or insulators.

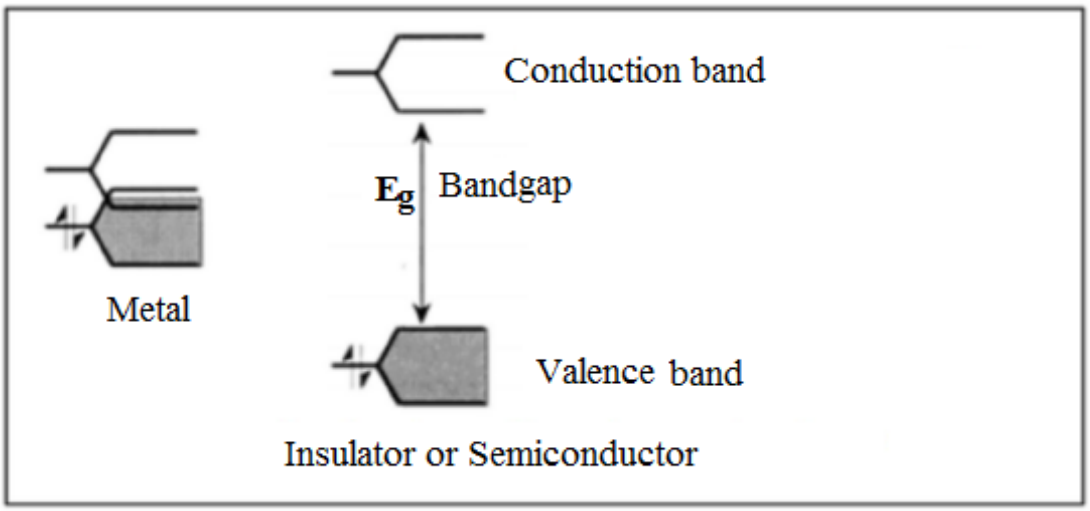

Figure 5.3: Representation of the band models of metals, semiconductors and insulators.

Metals are electron conductors because they have a partially filled conduction band (no bandgap) (Figure 5.3). Semiconductors have a filled valence band and an empty conduction band, separated by a forbidden band; the height in energy (Eg) of the latter must be less than bandgap is too large (from 4 eV) not allowing passage of an electron from the valence band to the conduction band. The highest occupied molecular orbital (HOMO) is assimilated from the top of the valence band (BV) and the lowest unoccupied molecular orbital (LUMO) from the bottom of the conduction band (BC).

By definition, gap energy (Eg) is the difference between HOMO and LUMO energy levels. It therefore corresponds to the first optical transition of lower energy that the material can absorb.

$$E_g = \Delta E = h\upsilon = \frac{hC}{\lambda_{max}} = \frac{1242}{\lambda_{max}} \qquad (5.4)$$

With: $h = 6.62607015 \times 10^{-34}\ J \cdot s$ **Planck's constant** is the quantum of electromagnetic action that relates a photon's energy to its frequencyυ and **C**is a Speed of light.

λ_{max} is easily determined from the absorption spectrum of the material by extrapolation of the linear parts of the spectrum at long wavelengths (Figure 5.4).

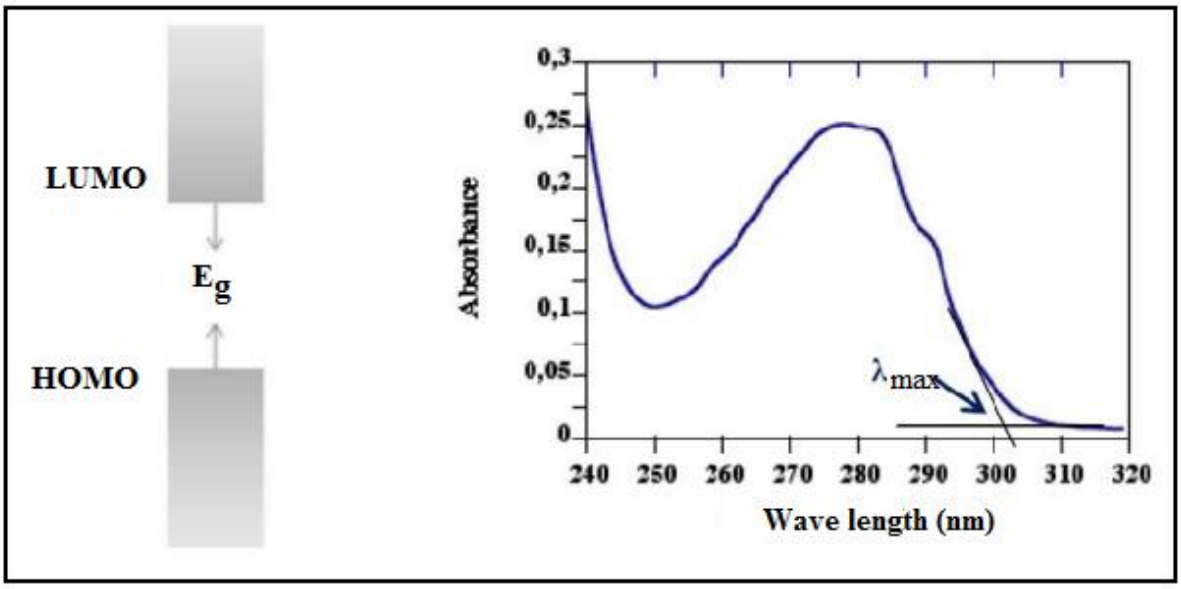

Figure 5.4: Determination of the optical gap from the UV-visible absorption spectrum

V. 1. 2 Apparatus and conditions for experimental analysis

The device used is a Perkin Elmer Instrument (Figure 5.5) double beam spectrophotometer with a variable spectral bandwidth from 0.1 to 5nm, selected by a continuous variable slit. The instrument is fitted and controlled by a microcomputer which ensures the acquisition of spectra and their mathematical treatment.

Figure 5.5: Photo of a UV-Visible spectrometer.

The interaction with infrared light causes molecules to undergo vibrational transitions in the UV (200-400 nm) and visible (400-800 nm) range of the electromagnetic spectrum. What this means is that when a molecule absorbs the energy from UV or visible light, one of its electrons jumps from a lower energy to a higher energy molecular orbital. UV-visible (UV-

Vis) absorption is the measurement of the attenuation of a beam of light after it passes through a sample or after reflection from a sample surface. Absorption measurements can be at a single wavelength or over an extended spectral range. The absorption of UV or visible radiation corresponds to the excitation of outer electrons.

V. 2 Fourier transform Infra-Red spectroscopy (FT-IR)

V. 2. 1 Principle

Infrared spectroscopy is widely used in chemistry to know the chemical functions present in a material. It is a non-destructive analytical technique easy to implement and can be used both on organic materials on inorganic materials. It is based on the absorption of infrared radiation by the material which leads to the vibration of the chemical bonds present when this radiation is of the same order of magnitude as the vibration frequency of the bond (elongation, deformation). The wavelengths at which the sample absorbs are characteristic of the chemical groups present in the material being analyzed. In our case, unlike UV-Visible spectrophotometry, infrared spectra are recorded in transmission and not in absorbance.Infrared spectraarerecorded using a measurement of frequency called the wavenumber (cm^{-1}), which is the inverse of the wavelength, most commonly used by physicists. The frequency domain studied is between 400 cm^{-1} and 4000 cm^{-1}(corresponding to 25 µm and 2.5µm). Infrared spectroscopy (IR spectroscopy) is an Optical technique that detects molecular bond vibrations and rotations upon absorption of infrared light. Because different chemical functional groups absorb IR light at different frequencies, IR spectroscopy can be used for chemical structure analysis, chemical fingerprinting and chemical imaging. This absorption has shown the existence of the bonds of certain samples, the infrared spectrum represents the transmittance T (%) on the ordinate; it is expressed as a percentage (%) according to the number of waves on the abscises, and is expressed in (cm^{-1}). We can see that the absorption strips are pointing downwards a low transmission value corresponds to a high absorption and each band is characterized by its position, width and intensity.In this scheme [13], sketched in Figure5.6, using a broadband source, typically a lamp, an interferometric pattern is recorded from the light interacting with the sample. By using the Fourier Transform approach, it is possible to reconstructthe transmittance spectrum of the substance under analysis.

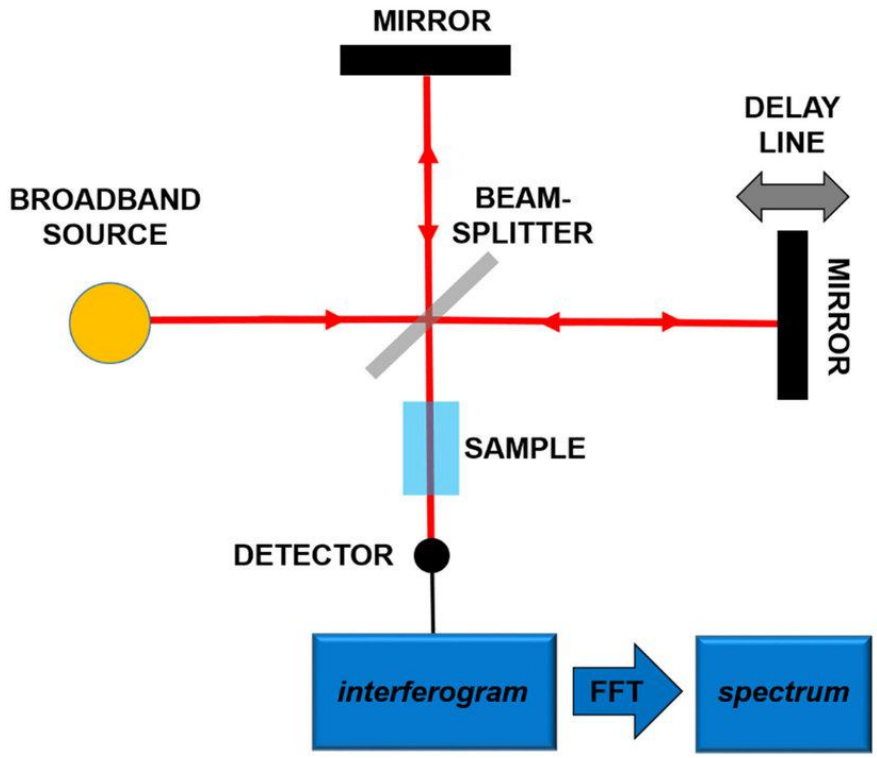

Figure 5.6: Principles of the Fourier-Transform Infrared Spectroscopy (FT-IR).

In the range of energies corresponding to the infrared domain, it is the energies of vibration of the atoms and of the movements of the electronic layer which are disturbed. The fact that the energy state of the molecule is described by discrete energy levels implies that the interaction between the incident wave and the molecule occurs only for specific energy values. IR absorption spectroscopy givesinformation on molecular vibrations that are characteristic of the local environment of chemical bonds and their nature.

In IR, a molecule is able to interact with the electromagnetic field and absorb a photon of frequency υ, if it has at least transiently, a dipole oscillating at this frequency. If one brings energy to the system by the intermediary of a light ray, it absorbs it provided that the energy of the radiation is equal to the energy step separating thefundamental level and the first excited level.

V. 2. 2 Instrumentation and working of FT-IR spectroscopy

In our study, this technique was used mainly in transmission to evaluate the transparency of the suspension containing multi-walled carbon nanotubes (MWCNT) in the wavelength ranges characteristic of the infrared lasers used.The device used is aPerkin Elmer Spectrum Version 10.4.2 FT-IR Spectrometer (Figure 5.7), Infrared spectroscopy is a chemical analysis method based on the absorption of infrared radiation by the material to be analyzed. The study of the radiation transmitted compared to the incident radiation makes it

possible to know the energies that have been supplied to the medium and hence the structure of the latter

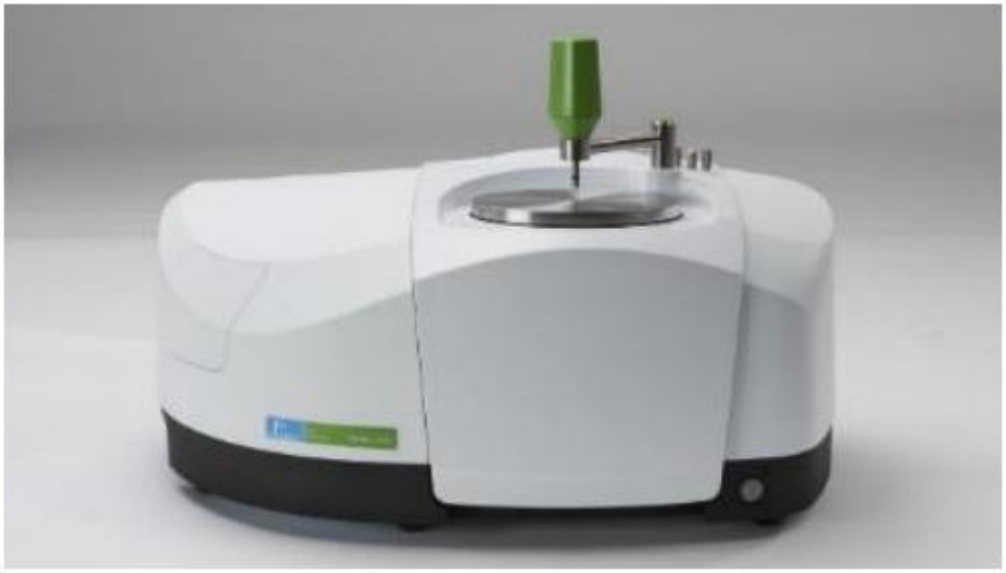

Figure 5.7: Perkin Elmer Spectrum Version 10.4.2 FT-IR Spectrometer

V. 3 Materials and Methods

As a liquid system, we used glycerol $C_3H_8O_3$ with purity of 99% to 101% purchased from Sigma-Aldrich, which was characterized by a molecular weight of 92.09, a melting point of 291.3 K, and a density of 1.261 g/cm^3 at the temperature of 293 K. The typical diameters of MWNTs used in this study, ranged from 50 to 120 nm while the lengths were mostly from 2µm to 50µm and the density is about 1.65g/cm^3. The nanofluids of Glycerol based MWCNT was prepared as follows: In this paper, a stable solution was obtained by dissolving 0.7mg;1mg; 1.7 mg of MWCNTs measured by METLLER TOLEDO XPE 26 balance (a display accuracy of 1 µg) in 1 ml of ethanol then it introduced respectively in 10 ml; 11ml; 9ml of Glycerol. Then, the nanofluid was exposed in the ultrasound for 30 minutes to prevent agglomeration of nanoparticles. We prepared a suspension of MWCNTs in Glycerol with a volumetric fraction of 0.004%; 0.005% and 0.01%. The electrical conductivities and resistivities of the nanofluids were measured by Seven Compact S230 Conductivity (conductivity accuracy 0.5%; temperature accuracy 0.1°C; conductivity measuring range 0.001µS/cm to 1000mS/cm). The FTIR spectra were recorded on Perkin Elmer Spectrum Version 10.4.2 FT-IR Spectrometer. FTIR studies were carried out in the range of 400–4000 cm^{-1} in the transmittance mode. The electrical conductivity and resistivity of different fluids was measured in a temperature range from ambient to 62 °C.

The UV-visible spectroscopy carried in the range of 200- 1000 cm^{-1} in absorbance mode for the three samples at different fractions. The UV-visible spectra were recorded on Perkin Elmer.

V. 4 Result and discussion

V. 4. 1 UV-Visible spectroscopy

Ultraviolet-visible absorption spectroscopy is based on the phenomenon absorption of light energy by matter. When the latter absorbs part of electromagnetic radiation energy, absorption is accompanied by transition electronics (valence electrons) from a fundamental level energy to the superior one. This method informs us about the absorption domain of the compound to be studied. On the other hand, the electronic structure of the material provides information on its electrical properties and allows classifying it among conductors, semiconductors or insulators. Metals are electron conductors because they have a conduction band partially filled (no band prohibited). Semiconductors have a filled valence band and an empty conduction band, separated by a band prohibited; the Gap energy (Eg) of the latter must be less than 3.5 eV. Insulators have a strip structure similar to that of semiconductors, but the width of the band gap is too large (from 4 eV) not allowing the passage of an electron from the valence band to the conduction band. The gap energy (Eg) corresponds to the first optical transition of lower energy than can absorb the material. it defined by this equation:

$$E_g = \frac{hC}{\lambda_{max}} \qquad (5.5)$$

This data is easily determined from the absorption spectrum of the material. λ_{max} is determined by extrapolation of the linear parts of the long-wavelength spectrum (Figure 5.8) determined by the extrapolation of the linear parts of the long-wavelength spectrum.

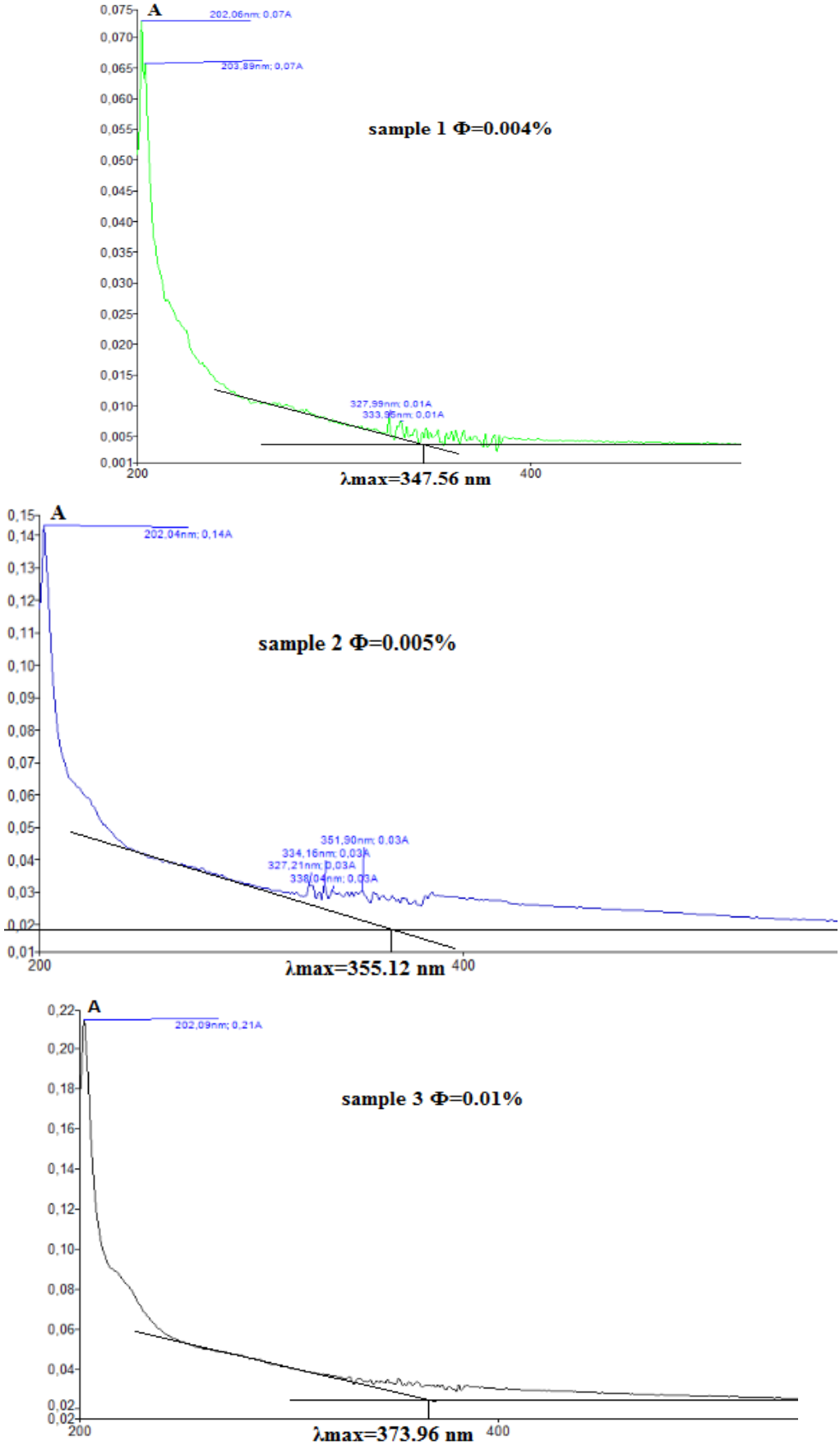

Figure 5.8: UV-visible absorption spectrum of the three samples various wavelength and determination of the λmax.

Figure 5.8 and 5.9 represent the absorption spectrum as a function of the wavelength (λ). The present spectrum shows the electronic absorption measured between 200 nm and 1000 nm using MWCNT in Glycerol. We notice that three simples have a strong absorption in the region of ultra violet region.

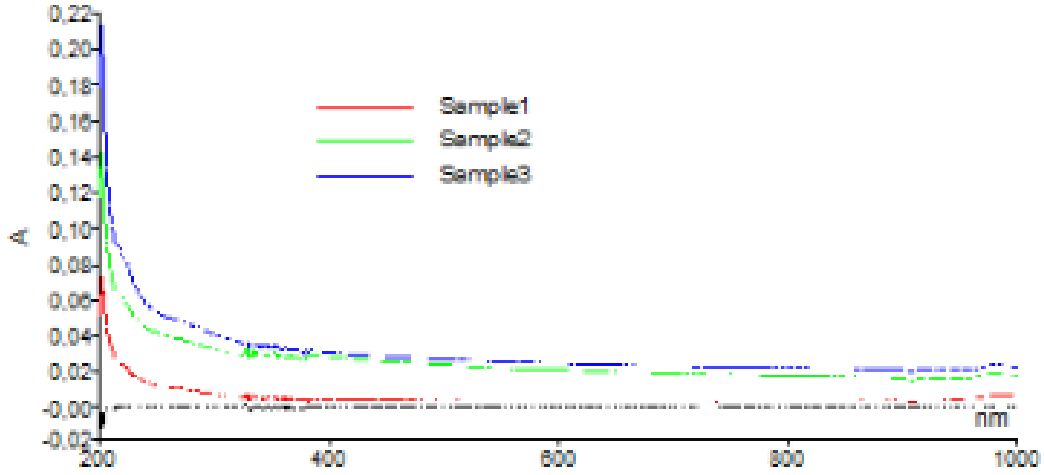

Figure 5.9: UV-visible absorption spectrum of the three samples

V. 4. 2 The optical Gap energy

We obtain the value of the optical gap energy (Eg) of nanofluid by increasing the percentage up to 0.01% as shown in table 5.1. Two curve tangents can be drawn till the intersection gives us the value of the wavelength λ_{max} values of the energy gap were reported in table 5.1.

Table 5.1: Values of λmax with the optical Gap energy calculated by precedent equation

Vol fraction (%)	0.004	0.005	0.01
Lambda(nm)	347.56	355.12	337.96
Gap energy(eV)	3.57	3.49	3.32

From table I, we have plotted the curve E_g as a function of the volume fraction (Figure 5.10). We notice that the gap energy decreases when the volume fraction of MWCNT increases. It reaches the value of 3.32 eV at ϕ=0.01%. This result confirmed that the present nanofluid can be used as semiconductors in photovoltaic and optoelectronic devices.

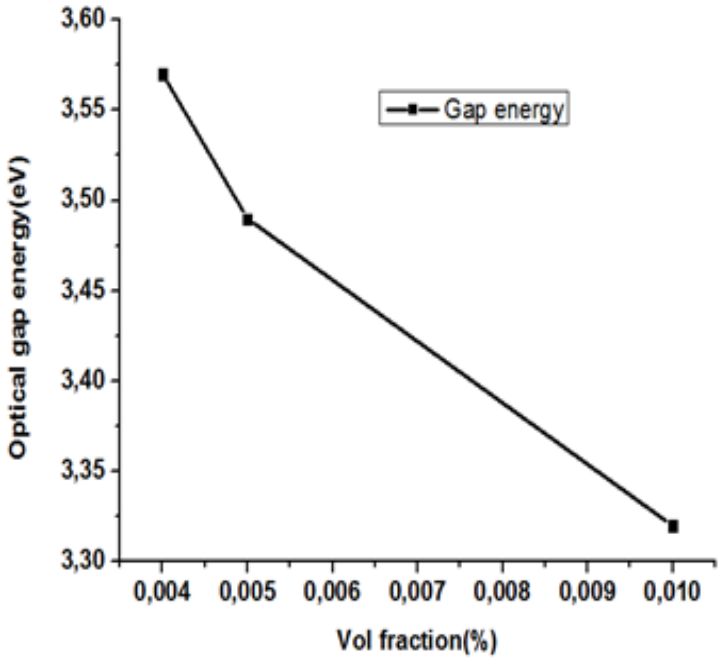

Figure 5.10: Dependence of the optical Gap energy on volume fraction for MWCNT suspensions in Glycerol

V. 4. 3 Electrical conductivity analysis

As we know, the conductivity of the solutions is the ability of a material or a solution to transport electrical charge unlikethe resistivity. In other words conductive material allows the passage of the electric current. The contribution of electrical properties in nanofluids is revealed in this work. There is a significant dependence on the dispersed particles and its concentration. A detailed study on electrical conductivity and resistivity of nanofluids with various parameters is analyzed. The electrical conductivity and resistivity of MWCNT/ Glycerol were also investigated to review the influence of MWCNT. The effect of temperature on the electrical conductivity and electrical resistivity of Glycerol/MWCNT nanofluids had been studied and the results were shown in figures 5.11, 5.12, 5.13 and 5.14. The conductivity was remarkably dependent on the content of MWCNT.

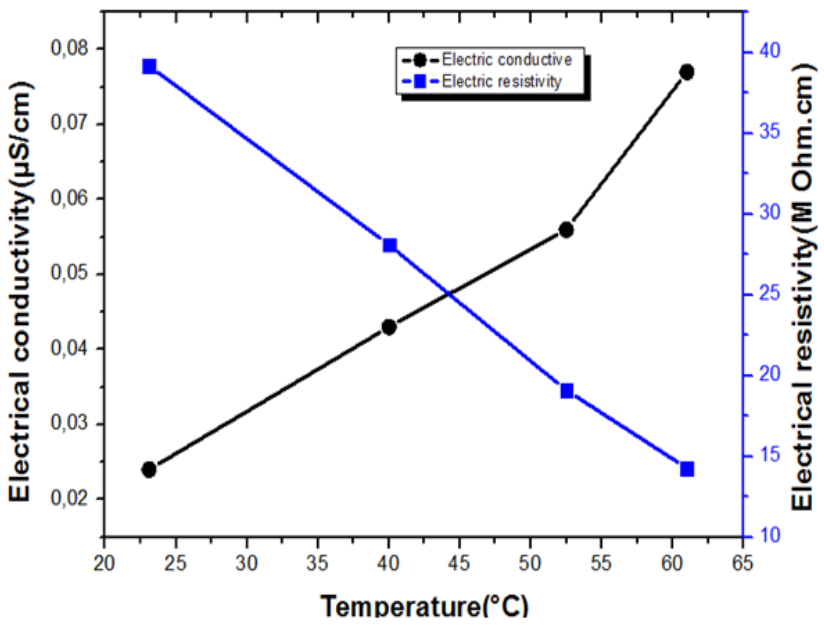

Figure 5.11: Dependences of the electrical conductivity and electrical resistivity on the temperature for MWCNT suspensions in glycerol at volume fraction (Φ=0.004%)

Figure (5.11) shows the evolution of both electrical conductivity and electrical resistivity experimentally measured on our sample according to the volume fraction of Φ=0.004%. We note that two parameters of electrical conductivity and electrical resistivity are inversely dependent with temperature from 23°C to 62°C: when the first one reaches its maximum the second reaches its minimum. This clearly confirms the close correlation between these two quantities. We may suggest that this finding is logically due to the presence of a density of MWCNT in Glycerol. For low percentage values, there is a large, steady and rapid increase in the electrical conductivity with temperature and volume fraction as shown in figures (5.12) and (5.13).

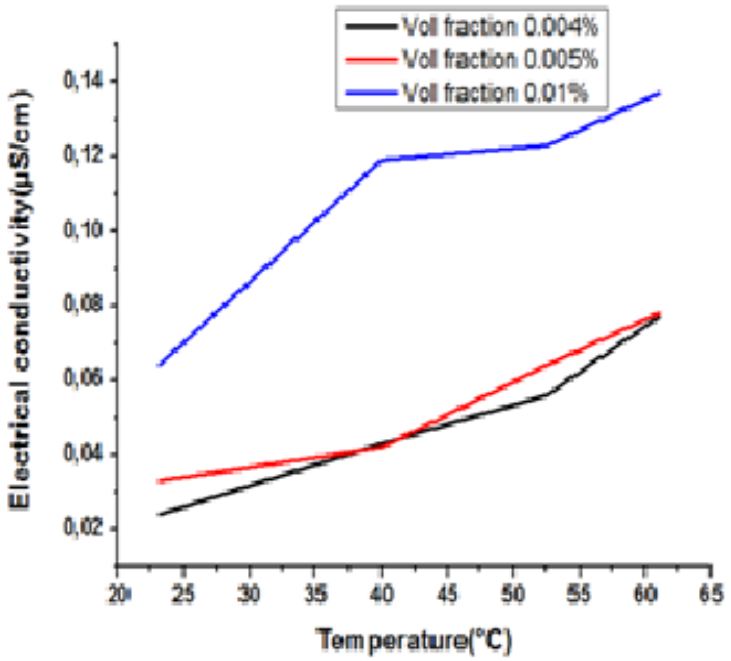

Figure 5.12: Dependence of the electrical conductivity on the temperature for MWCNT suspensions in glycerol at various fractions (Φ=0.004%, 0.005%, 0.01%)

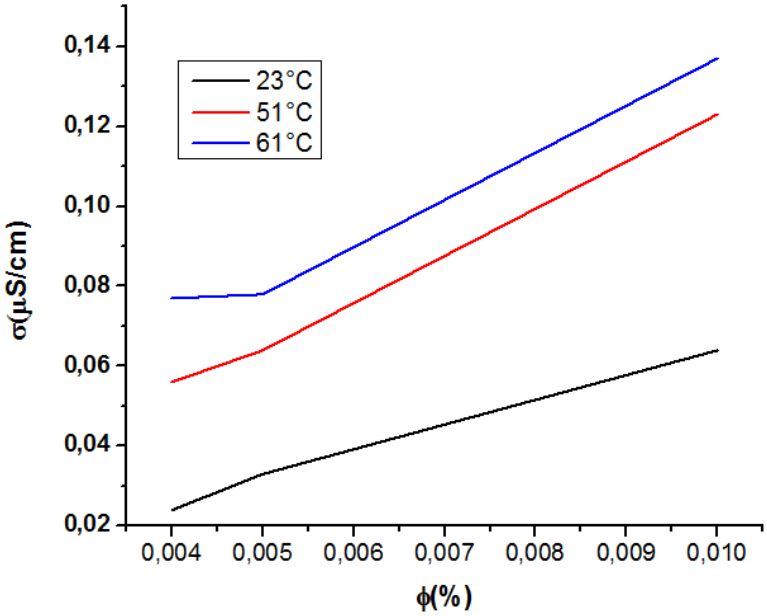

Figure 5.13: Dependence of the electrical conductivity on the volume fraction for MWCNT suspensions in Glycerol at different temperatures

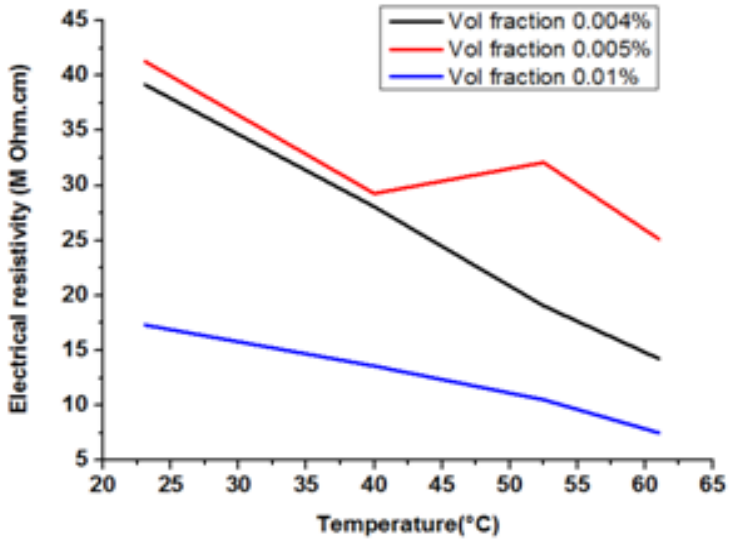

Figure 5.14: Dependences of the electrical resistivity on the temperature for MWCNT suspensions in Glycerol at various concentrations (Φ=0.004, 0.005, 0.01%)

Figures 5.12 and 5.14 us shown the Evolution of the electrical conductivity and the electrical resistivity changed with the temperature range 23 to 62°C, we observed that the electrical conductivity of nanofluidsincreases with temperature and volume fraction. We notice that the electrical resistivity's decreases when the temperature and volume fraction increase, the highest electrical conductivity was observed for the nanofluids due to high electrical conductivity of MWCNT.

V. 4. 4 Infrared analysis

In this section, we study the possible interactions between the surface of MWCNT nanoparticles and Glycerol molecules. The FTIR spectra of pure Glycerol and doped glycerol were recorded in figure 5.15. The x-axis represents the wave number in cm^{-1} while the axis is oriented from right to left by 400-4000 cm^{-1}. The ordinate axis is oriented upwards and represents the transmittance in percentage. Comparing both FTIR spectra of doped Glycerol by nanoparticles of MWCNT and the pure Glycerol as shown in figure 6, it has been found that many peaks obtained in the case of pure Glycerol spectrum were repeated in the FTIR spectrum in the presence of MWCNT nanoparticles with low changes in position as well as in intensity of transmission bands. The relatively broad transmission band, positioned at 3293 cm^{-1} in the pure Glycerol spectrum, which is attributed to the stretching vibrations of hydroxyl groups (-OH), became narrower with a decrease in band intensity in the spectrum of nanofluid. The peak observed at 1030 cm^{-1} which is attributed to the C-O stretching vibrations of the alcohol (Glycerol solvent), is displaced to 1032 cm^{-1} in the spectrum of the nanofluid

accompanied by a decrease in intensity. These results indicate that hydroxyl groups of Glycerol molecules are involved in the synthesis and stabilization of the nanofluid. We observed the bands that could be assigned to transmittance of C–H (1210–1413 cm^{-1}) [14]. The weak bands in the region of 1000–1150 cm^{-1} assigned to C–O, C–C is the characteristic feature of many carbon materials and of the materials of our interest. The strong bands at 2932 cm^{-1} and 2880 cm^{-1} are due to asymmetrical and symmetrical stretching group of –CH2– , respectively [15]. Associated with the bending vibration of –CH3, it also showed an important decrease but not eliminated. The existence of similarity between the four curves confirmed that nanofluids (MWCNT+ Glycerol) exhibited high stability

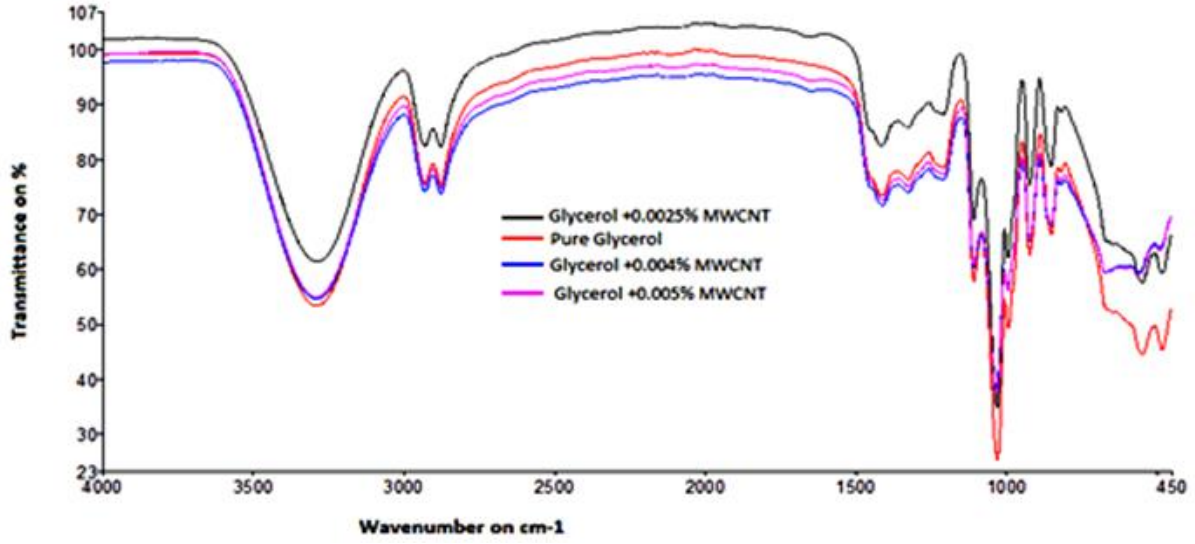

Figure 5.15: FTIR spectrum of Glycerol based MWCNT for different fraction

CONCLUSION 5

Experimental results allow us to conclude the effect of the incorporation of multi walled carbon nanotube (MWCNT) nanoparticles in Glycerol considered as a basic fluid in the electrical domain. In this work we notice that the electrical conductivity increased while the electrical resistivity decreased with temperature and volume fraction. The enhancement of the electrical conductivity was due to the synergistic effect of high electrical conductivity of MWCNT nanoparticles as well as their high surface area. Nanofluids show good stability due to the functional groups attached onsurfaces of MWCNT. This result confirmed that these nanofluids can be used as semiconductor in photovoltaic and optoelectronic devices for small fraction volumes ranging from 0.005% to 0.01% of MWCNT.

References

[1] G1 S. Iijima, Nature, 354, 56–58, 1991.

[2] Y. Breton, G. Desarmot, J. P. Salvetat, S. Delpeux, C. Sinturel, F. Beguin and S. Bonnamy, Carbon, 42, 1027–1030, 2004.

[3] F. Du, C. Guthy, T. Kashiwagi, J. E. Fischer and K. I. Winey, J. Polym. Sci., Part B: Polym. Phys., 44, 1513–1519, 2006.

[4] C. H. Liu, H. Huang, Y. Wu and S. S. Fan, Appl. Phys. Lett., 84, 4248–4250, 2004.

[5] Y. J. Zhang, Y. F. Shen, J. H. Li, L. Niu, S. J Dong and A. Ivaska, Langmuir, 2005, 21, 4797–4800.

[6] Y. J. Zhang, Y. F. Shen, D. X. Han, Z. J. Wang, J. X. Song andLi. Niu, J. Mater. Chem., 16, 4592 4597. 2006.

[7] S. Lee, S. U. S. Choi, S. Li and J. A. Eastman, J. Heat Transfer, 121, 280–289. 1999.

[8] S. Krishnamurthy, P. Lhattacharya, P. E. Phelan and R. S. Prasher, Nano Lett., 6, 419–423. 2006.

[9] L. Q. Wang and J. Fan, Nanoscale Res. Lett., 5, 1241–1252, 2010.

[10] S. U. S Choi, Z. G. Zhang, W. Yu, F. E. Lockwood and E. A. Grulke, Appl. Phys. Lett., 79, 2252–2254, 2001.

[11] P.J.F. Harris, Carbon Nanotubes and Related Structures. New Materials for the Twenty-First Century (CambridgeUniv. Press, Cambridge, 2000).

[12] Y. Lin, S. Taylor, H. Li, K.A.S. Fernando, L. Qu, W. Wang, L. Gu, B. Zhou, and Y-P. Sun, J. Mater. Chem. 14, 527 (2004).

[13] Smith, B. Fundamentals of Fourier Transform Infrared Spectroscopy (Second Edition). CRC Press: Boca Raton, doi:10.1201/b10777. USA 2011.

[14] H. Kong, C. Gao and D. Yan, Macromolecules, 37, 4022– 4030, 2004.

[15] L.Q. Jiang, L. Gao, J. Sun, Production of aqueous colloidal dispersions of carbon nanotubes, J. Colloids Interface Sci. 260 (2003)

GLOBAL CONCLUSIONS AND PERSPECTIVES

The work presented in this thesis focuses on the thermal and rheological characterization of a type of nanofluid that has never been studied to our knowledge: the system MWCNT/Glycerol. The characterization is made according to the temperature and the volume fraction of the particles put into suspension.This work required the design and production of a thermal characterization device using the 3ω method and finally the rheological and thermal characterization of these samples. An analysis of previous research was conductedin order to overcome the various parameters that can influence thermal and rheological behavior nanofluids whose parameters linked to the composition of the nanofluids, the temperature, the base fluid, etc. Following this study, we conducted an experimental study on the electrical and thermo-physical properties of the nanofluids tested (electrical conductivity, thermal conductivity, dynamic viscosity and density). The promising results of this study are very encouraging and show that the use of nanofluids containing carbon nanotubes clearly offers an improvement in thermal performance compared to the conventional base fluids. The results obtained with this new system are interesting because the increase in thermal conductivity reaches significant values: 85% and 50% respectively for volume fractions as low as 0.01% and 0.0025% of MWCNT/Glycerol. The results obtained are compared and discussed towards to existing classical models and we have found that Xue's model is the appropriate model to describe the thermal conductivity of the MWCNT/Glycerol nanofluid for low volume fractions. In particular, we observed that the effective thermal conductivity of this nanofluid increases with the concentration of nanoparticles and with the temperature. Nanofluids MWCNT/Glycerol show good stability due to the functional groups attached on surfaces of MWCNT.

The inclusion in Glycerol of carbon nanotubes in low proportions considerably modifies the viscosity of the Glycerol, increasing by almost 50% for a volume fraction $\Phi = 0.01\%$. The inclusion of nanoparticles does not change the law of behavior of the host fluid this observation can reflect the fact that nanotubes, in low concentration, do not significantly modify the interactions between Glycerol particles. The latter therefore imposes his law of behavior depending on the temperature. The results show that at low concentrations, less than 0.01% for MWCNT/Glycerol that the rheological behavior of nanofluids is Newtonian for a high shear rate and then we have proposed a new dynamic viscosity model inspired by Boboo's work and which incorporates the size and shape effect of carbon nanotubes. The density of the nanofluid depends on the density of the base fluid, that of the MWCNTs and

the volume fraction of the MWCNTs. The results show that at low concentrations, less than 0.01% for MWCNT/Glycerol that is a linear evolution in the relative density as a function of the volume fraction of the MWCNTs and also the classical mixing law makes it possible to estimate and correctly predict the evolution of the density of suspensions with a relative error of the order of 2, 4.10^{-4} %. This can be explained by the homogeneity and the stability of the nanofluids, in other hand the temperature does not have a significant effect on the evolution of the relative density. Experimental investigation of MWCNT/$Er_2P_4O_{13}$/Glycerol nanofluids in the Einstein concentration regime has been performed for electrical conductivity and electrical resistivity evolutions as functions of weight concentration and temperature in the region of 23–64°C. The results showed considerable enhancement in electrical conductivity and a decrease in electrical resistivity of nanofluids in all concentrations compared to pure Glycerol Owing to their sufficiently wide regions of applicability, this nanofluids are believed to represent an useful engineering tool for analysis and optimizing such ion condensation effects in nanofluids could potentially increase their applicability in nanotechnologies for which electrical conductivity is required and also Glycerol can be evaluated as a corrosion inhibitor for steel and iron specimen. Nanofluids show good stability due to the functional groups attached on surfaces of MWCNT. This result confirmed that these nanofluids can be used as semiconductor in photovoltaic and optoelectronic devices for small fraction volumes ranging from 0.005% to 0.01% of MWCNT. We note that the simulated platinum wire temperatures are close to those measured by the 3ω method for the determination of the thermal conductivity of our base fluid; these results are completely comparable with those obtained in the literature.

We propose to continue this work carried out at the macroscopic scale by a study at the molecular scale of the influence of carbon nanotubes on molecular dynamics of fluid to remedy the problem of the high viscosity of the MWCNT/Glycerol nanofluid. We also propose to improve our numerical modeling to take into account the 3ω method; this would make it possible to predict, depending on the temperature or the potential, the thermal conductivity of MWCNT/Glycerol nanofluids for different fractions. Finally, Glycerol is a model liquid for the study of glass transitions. It seems interesting to us, in a future work, to characterize the influence of nanoparticles on the glass transition of Glycerol.

Appendix A

1 Special Function "Exponential Integral"

The special function "Exponential Integral" Ei is defined by:

$$Ei(x) = -\int_{-x}^{\infty} \frac{e^{-u}}{u} du \qquad \text{(A.1)}$$

When x → 0, we can propose the following approximate form of $Ei(-x)$:

$$Ei(-x) \approx \gamma + ln\, x - x + \frac{1}{4}x^2 \qquad \text{(A.2)}$$

With γ ≈ 0.577216 the Euler constant. On the other hand, we recall that $\frac{dEi(x)}{dx} = \frac{e^x}{x}$

2 Special function "Modified Bessel function"

The modified Bessel function $K_0(z)$ verifies the integral:

$$\int_{-\infty}^{t} e^{i\omega u}\, e^{-\frac{r^2}{4\alpha(t-u)}} \frac{du}{t-u} = 2e^{i\omega t} K_0\left[\left(\frac{i\omega}{\alpha}\right)^{\frac{1}{2}} r\right] \qquad \text{(A.3)}$$

We also recall the following limit:

$$\lim_{x\to 0} K_0(x\sqrt{i}) = ln\frac{2}{x\sqrt{i}} - \gamma \qquad \text{(A.4)}$$

With **γ** the constant of Euler.